SPECTRAL VARIATIONS OF 12 LACERTAE

by

Andrea Mary-Anne Allison

B.Sc. , Loyola of Montreal, 1974

A THESIS SUBMITTED IN PARTIAL FULFILLMENT OF
THE REQUIREMENTS FOR THE DEGREE OF
MASTER OF SCIENCE

in the Department
of
GEOPHYSICS and ASTRONOMY

We accept this thesis as conforming to the
required standard

The University of British Columbia

April, 1976

In presenting this thesis in partial fulfilment of the requirements for an advanced degree at the University of British Columbia, I agree that the Library shall make it freely available for reference and study. I further agree that permission for extensive copying of this thesis for scholarly purposes may be granted by the Head of my Department or by his representatives. It is understood that copying or publication of this thesis for financial gain shall not be allowed without my written permission.

Department of GEOPHYSICS AND ASTRONOMY

The University of British Columbia
2075 Wesbrook Place
Vancouver, Canada
V6T 1W5

Date APRIL 23, 1976

Abstract

Observations of the β Cephei star 12 Lacertae have been made at both high time and spectral resolution with an Image Isocon television camera. The observations cover complete cycles of the pulsation on two consecutive nights in October 1972. The spectral region covered includes the two Si III lines at λ 4553 and λ 4568.

The line profile variations have been studied in detail; in particular the line doubling at certain phases of the pulsation. Wavelength shifts of the separate components were measured and a discontinuous radial velocity curve was obtained.

Table of Contents

List of Tables

List of Figures

Acknowledgments

I would like to thank my supervisor Gordon Walker for his patience and support. I would very much like to thank John Glaspey and Greg Fahlman for taking part in many helpful discussions. Drs. Fahlman and Glaspey also wrote many of the computer programs used and I thank them for making them available. I would also like to thank Tad Ulrych for his assistance with part of the data analysis. I thank the National Research Council for support from a postgraduate scolarship. I thank Graham Hill of the Dominion Astrophysical Observatory for allowing me to use data he originally obtained. Finally I would like to thank the graduate students of the department who were always willing to answer my many questions.

Introduction

12 Lacertae, also known as the variable star DD Lacertae, is a member of the β Cephei class of variables. These are a group of stars which show short period variations in both light and radial velocity. The light variations Δm are usually only a few hundredths of a magnitude and the radial velocity amplitudes $2K$ range from 5 km/sec to 150 km/sec giving a large $2K/\Delta m$ ratio. The β Cephei stars range in spectral type from B0.5-B2 and have luminosity classes II-III-IV. The light and radial velocity curves are approximately sinusoidal but many of the stars show multiple periodicity and some show a beat phenomenon. General review articles have been written by Struve (1955), Underhill (1966), and Percy (1967) as well as others.

The pulsation properties and spectral variations of the β Cephei variables are quite different from the other intrinsic variables. Whereas the pulsational modes and excitation mechanisms of such stars as the Classical Cepheids and RR Lyrae stars are well understood, those of the β Cephei stars are not yet known with any certainty.

The suspected cause of pulsation for some of the cooler variables is envelope ionization. The flux modulation brought about by regions in the stellar envelope containing abundant elements such as hydrogen and helium in various stages of ionization can have the proper phasing for driving of pulsations, and under the proper conditions can induce

pulsational instability in a star. The β Cephei stars are very hot (Te 20,000-25,000 $^{\circ}$K) and so this would not apply. There is no H ionization zone and the He^{+} ionization zone lies too close to the stellar surface to be effective (Cox, 1974).

A good discussion of β Cephei stars and their location in the theoretical H-R diagram is given in Lesh and Aizenman (1973a). They find that the β Cephei stars occupy a very narrow strip in the H-R diagram and by model calculations they find that this region is traversed in an S-shaped manner in the course of post-main sequence evolution: once in the core hydrogen burning phase, once in the secondary contraction phase, and once in the shell hydrogen burning phase. It is not known definitely in which of these 3 stages the β Cephei stars are, but it is suspected that the pulsation is connected with the structural changes caused by one of these stages of evolution.

It has sometimes been thought that the β Cephei stars were a 'peculiar' type of star but both Watson (1972) and Lesh and Aizenman (1973b) attempt to show that the β Cephei stars are normal B type stars. Watson (1972) uses the (θe, log g) plane to define the β Cephei instability strip. He concludes as do Lesh and Aizenman (1973b) that the β Cephei stars differ from the nonvariable stars only in their state of evolution.

Various attempts have been made towards understanding the nature of the pulsation. A brief summary of this work can be found in Cox (1974). Radial and non-radial modes have been

examined as well as interactions between the two to explain the observed phenomenon.

Two recently proposed excitation mechanisms are found in Aizenman, Cox and Lesh (1975) and Osaki (1974). Aizenman et al. conclude that in model calculations for a 10 $M_\odot$ star, the lower gravity (g^+) modes are unstable against non-radial oscillations in the early shell hydrogen burning stages. (Considering only the adiabatic case, the equations of motion for the non-radial case reduce to a fourth order problem where the eigenvalue σ^2 enters non-linearly in the coefficients. This results in two distinct spectra for σ^2. For σ^2 large the solutions correspond to accoustical or pressure (p) modes. All these p modes have discrete positive eigenvalues ($\sigma^2 > 0$). For σ^2 small, there are two possibilities which arise. If there is convective stability, the solutions correspond to gravity or g^+ modes. The σ^2 are all positive and thus the star is dynamically stable. If there is not convective stabiliy, the solutions correspond to unstable convective modes g^-; σ^2 becomes negative. There is in addition an intermediate fundamental or f mode with a positive eigenvalue σ_f^2 separating σ_p^2 and σ_g^2). Non-linear mode coupling is suggested whereby the long period g^+ modes can excite a shorter period stable mode: f, p, or radial harmonic modes which have been shown to agree with observations. Osaki (1974) assumes that the β Cephei stars are massive stars in the late stages of core hydrogen burning. The basic mechanism is this: if the large-scale convective motion in the core (described as unstable g^- modes) is oscillatory and if the

frequency of one of the convective modes happens to coincide with the eigen-frequency of a non-radial oscillation of the whole star, then this resonance may excite a non-radial oscillation of the star, which may be observable at the stellar surface.

A few properties of 12 Lac are mentioned in Table I. The symbols P1 and P2 correspond to the primary period 4h 38m and secondary period 4h 44m respectively. It was first thought to be a spectroscopic binary (Adams, 1912) because of the broadening of the lines at certain phases. It was found that the absorption lines are double at maximum and minimum radial velocity but the effect is measurable only when the variable amplitude 2K is large (Struve, 1950). In my work I will just consider the variations over one cycle of the pulsation (of duration 4h 38m). The whole question of the multiple periodicity of 12 Lac will be reviewed in the discussion section. Most of the work done on 12 Lac has been photometric, including an International Campaign in 1952. These efforts have mainly been directed towards more accurate period determinations. Among these are Fath (1938), Opolski and Ciurla (1961), De Jager (1962), Barning (1962), Opolski and Ciurla (1962), Jerzykewicz (1963), Ciurla (1973), and Sato (1973). Some spectroscopic work has been done by Struve (1950), Struve and Zebergs (1955), De Jager (1957), Grabowski (1966), Opolski and Grabowski (1966), Beres (1965), Grabowski (1969) and Heard et al (1976).

Table I. Observed Properties of 12 Lac.

	SYMBOL		REF
MK Spectral Type		B1.5 III	1
		B2 III	2,3,4
Visual Magnitude	V	5.25	2
		5.18	4
Absolute Magnitude	M	-3.61	1
		-4.0	2
		-4.15	4
Log of Period(days)	log P1	-.705	4
Radial Velocity Range	2K	36 (P1)	2
(km/sec)		15 (P2)	2
B-V Colour Index	B-V	-.135	4
		-.140	2
Amplitude of Light Curve	Δ m	.074 (P1)	2
		.042 (P2)	2
Effective Temperature	θ_{eff}	.214	1
Parameter=5040/T K			
Ultra-Violet Colour	U-B	-.945	4
Index			
Apparent Rotational	v sini	79	4
Broadening (km/sec)		29	2

References

1. Lesh and Aizenman (1973)
2. Percy (1967)
3. Opolski and Grabowski (1966)
4. Hill (1967)

The primary aim of my investigation was to look at high dispersion, high time and high spectral resolution observations of 12 Lacertae and examine the line doubling feature in much more detail than had previously been done. Observations of BW Vul and β Cephei, two other β Cephei stars obtained with the same detection system were analyzed by Goldberg (1973). As in 12 Lac, rapid spectral variations occurring at certain phases of the pulsation cycle were detected in both stars.

The Observations

The observations were taken using a refrigerated image Isocon television camera as a detector. The spectrum is imaged onto the photocathode of the Isocon tube and integrated for a predetermined time. An electron reading beam then scans the target normal to the spectrum. The data is digitized by means of a 12 bit analog-to-digital converter and stored on magnetic tape. Each scan gives 840 data points over 70 mm of the cathode. The system is monitored by an Interdata Model 4 computer which displays the spectrum on an oscilloscope. Short period observations of the dark current over the same integration period are taken after the star data. A more detailed description of the system is given by Walker et al. (1972).

The observations were taken using the coude spectrograph of the 48 inch telescope of the Dominion Astrophysical Observatory, Victoria. The 96 inch camera with a mosaic of four 800 line/mm gratings was used in the second order. In addition a transfer lens which magnifies a small region of the spectrum and matches the curvature of the focal plane to the curvature of the the photocathode (Richardson, 1973) was used giving a dispersion of 0.5 A/mm. The useable area of the tube face between the fiducial marks gives a spectral coverage of $\simeq$25 A.

The integration time for 12 Lac was 30.87 secs. 576 individual frames were obtained on October 15,1972 U.T. and 688

on October 16, 1972 U.T. The total time of observations was 4h55m and 5h53m respectively. The primary period of 12 Lac is 4h38m. Thus the observations cover more than one cycle of the pulsation. The wavelength region examined showed the two Si III lines λ 4553 and λ 4568.

Preprocessing of the Data

The average of the dark current for each night was smoothed by an 11 point (an arbitrary number) running mean. This was then subtracted from all of the spectra. The mean spectra for the two nights are shown in Figures 1(a) and 1(b). A 5-point running mean smoothing was applied to the data. The two dips at either end of the spectra are fiducial markers on the face of the tube. These are pieces of black tape which serve as reference markers to monitor any changes in the scanning raster pattern. The numbers on the wavelength axis correspond to the 840 data points in the spectrum. The tiny blips at points $\simeq$290 and 430 also show up on the spectrum of a calibration lamp. They are most likely due to "dust" specks on the face of the tube.

In order to see the line profile changes during a cycle, the time-series spectra were grouped into blocks of equal time duration. The spectra in each block were added together and the final sum was normalized such that the sum within a specified data point interval was 1000. This interval was chosen away from the spectral lines to prevent any variations in line intensity from affecting the normalization. In addition each block was divided by the average of the calibration lamp spectrum. A 5 point running mean smoothing was also applied to the data to improve the signal to noise ratio.

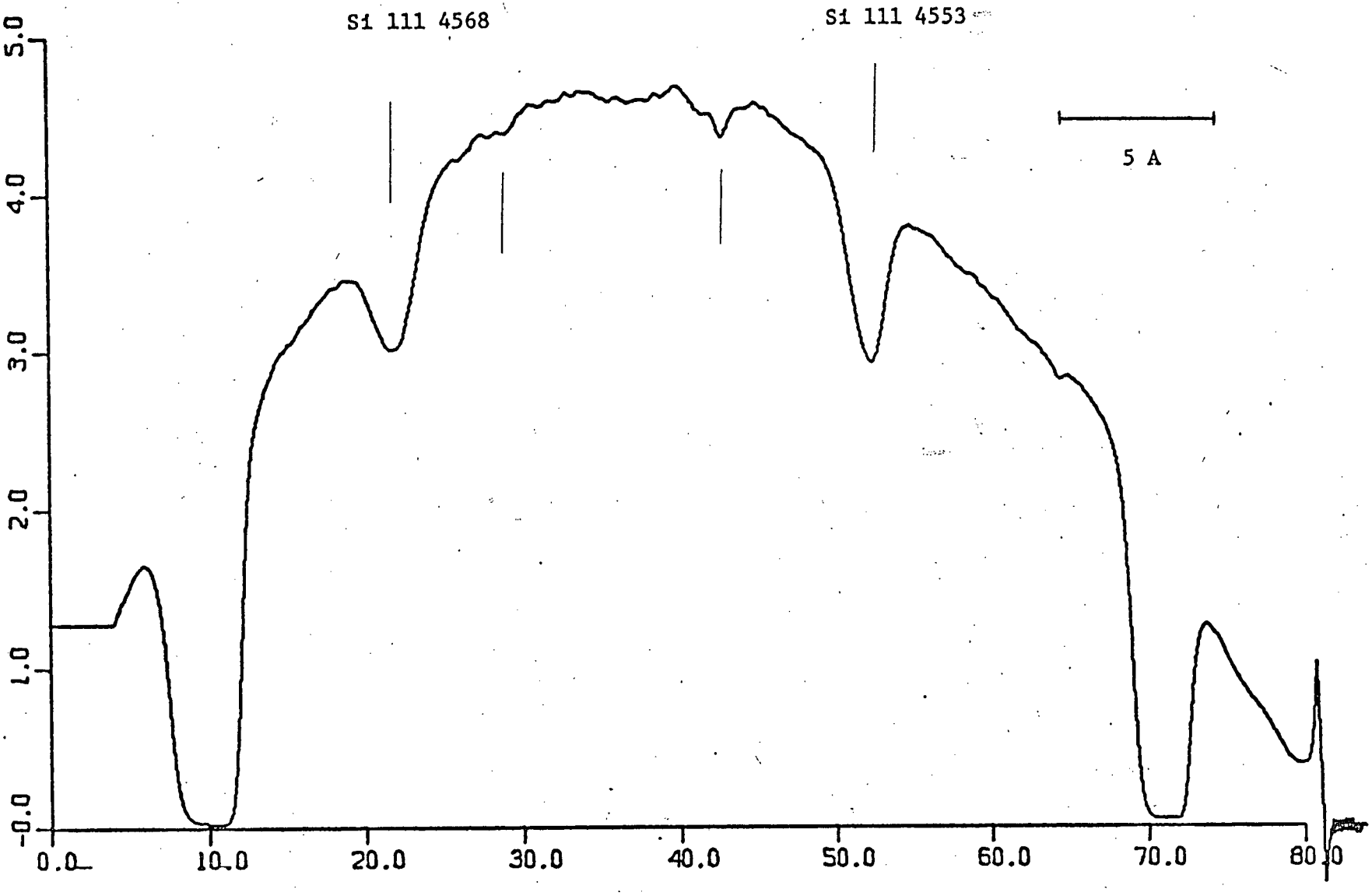

Figure 1(a). Mean Spectrum for October 15 data.

Figure 1(b). Mean Spectrum for October 16 data.

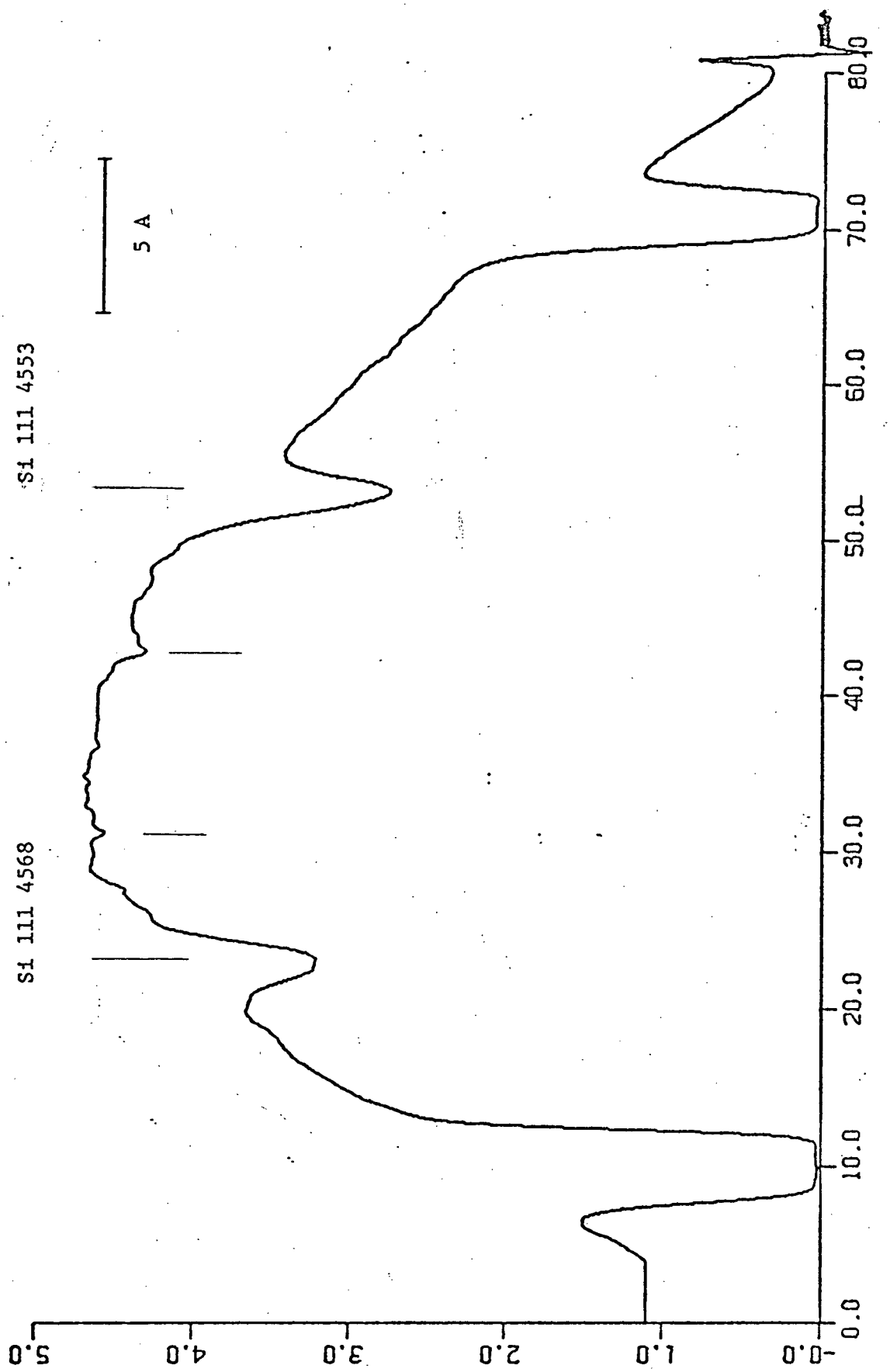

12 LACERTAE

The sequence of spectra for each night are shown in Figures 2(a) and 2(b). Each spectrum is a 20.6 minute mean of 40 individual exposures. The signal to noise ratio is $\tilde{}$75:1.

The signal to noise characteristics of the image isocon have been discussed for the U.B.C. system by Buchholz et al (1973). They found that there is a linear signal to noise relationship from spectra with strong absorption lines. This relationship is shown to hold for the 12 Lac spectra as indicated in Figures 3(a) and 3(b). For the variance analysis, signal values were selected from a limited data point interval. Thus the addition of N frames of data gives a $\sqrt{N}$ improvement in the signal to noise.

The scanning pattern of the camera reading beam is known to vary with time (Fahlman and Glaspey, 1973). This can produce an artificial wavelength shift in the spectrum. It is important to have some estimate of this shift for measures of radial velocity. The fiducial marks mentioned previously are used for this purpose. A two-dimensional (wavelength,time) presentation in contour form of the area around the fiducial marks is shown in Figures 4(a), 4(b), 4(c) and 4(d). The data is quantized into 20 minute blocks as for Figure 2 and the intensity distribution of the lines is mapped. The labels on the contour lines are a measure of intensity; smaller numbers indicating lower intensity, ie. absorption. From these figures one can see clearly the raster shift during the period of observation.

Figure 2(a). Time series sequence of spectra for October 15 data.

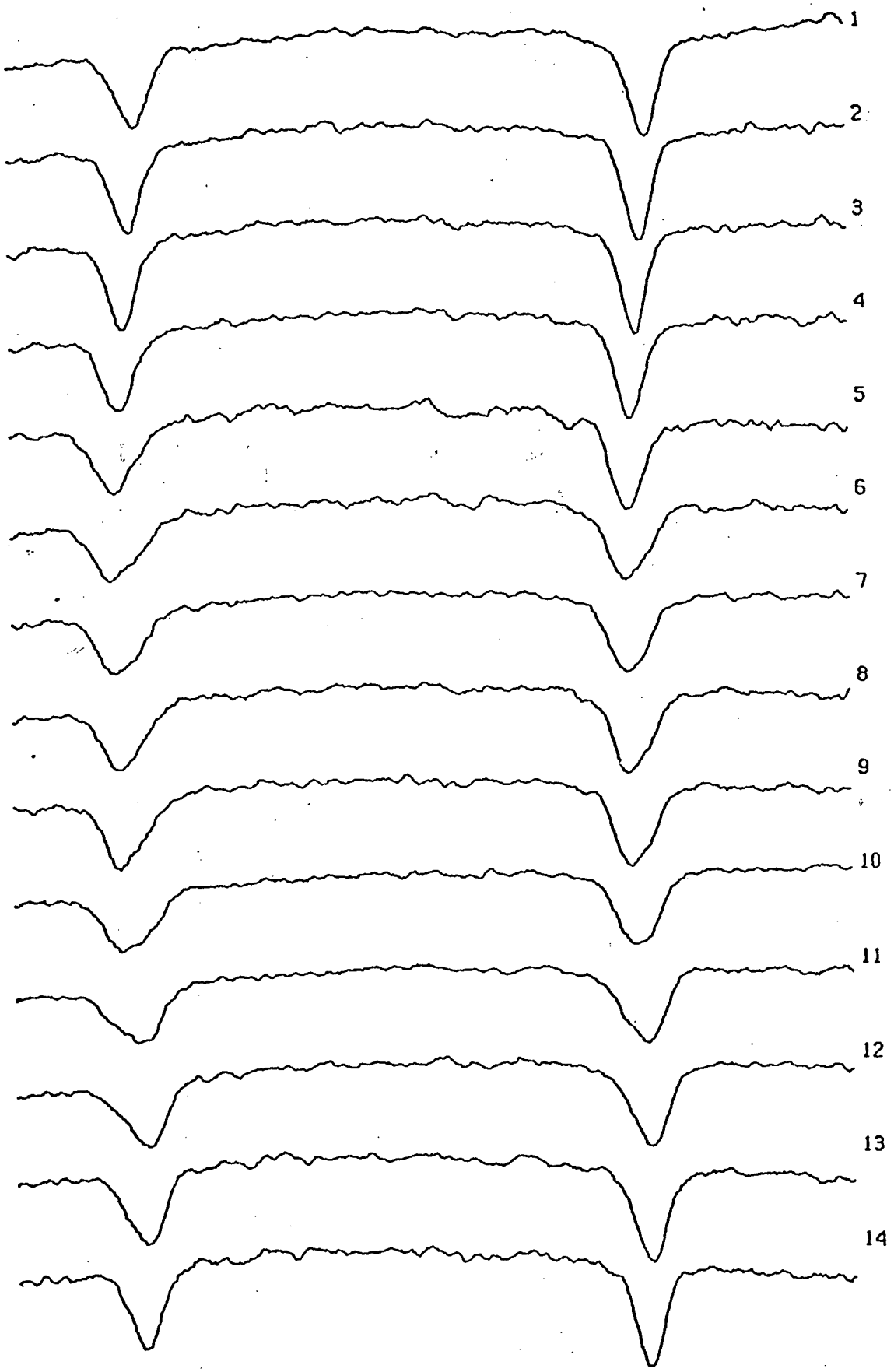

Figure 2(b). Time series sequence of spectra for October 16 data.

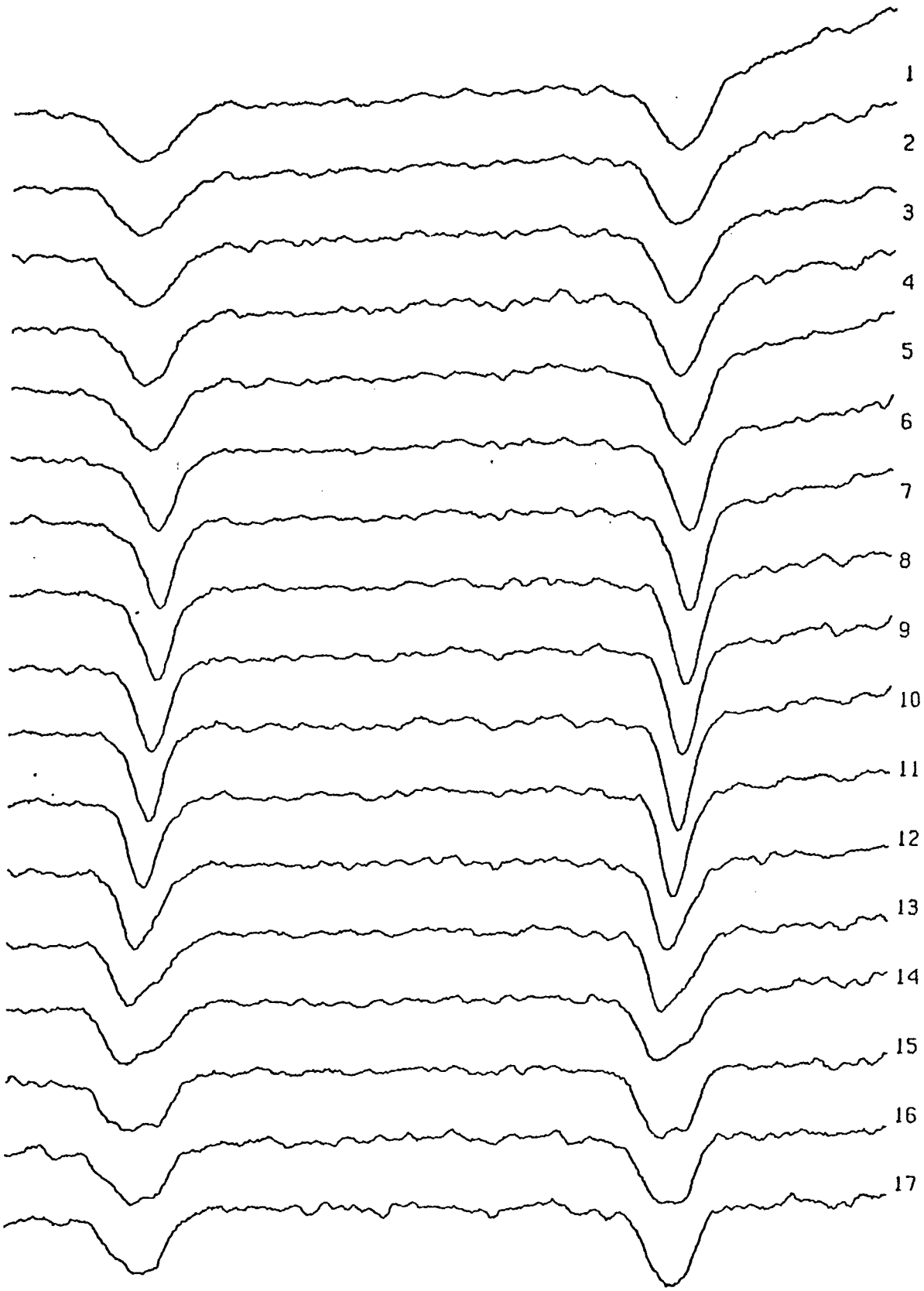

Figure 3(a). Variance vs. signal for October 15 data.

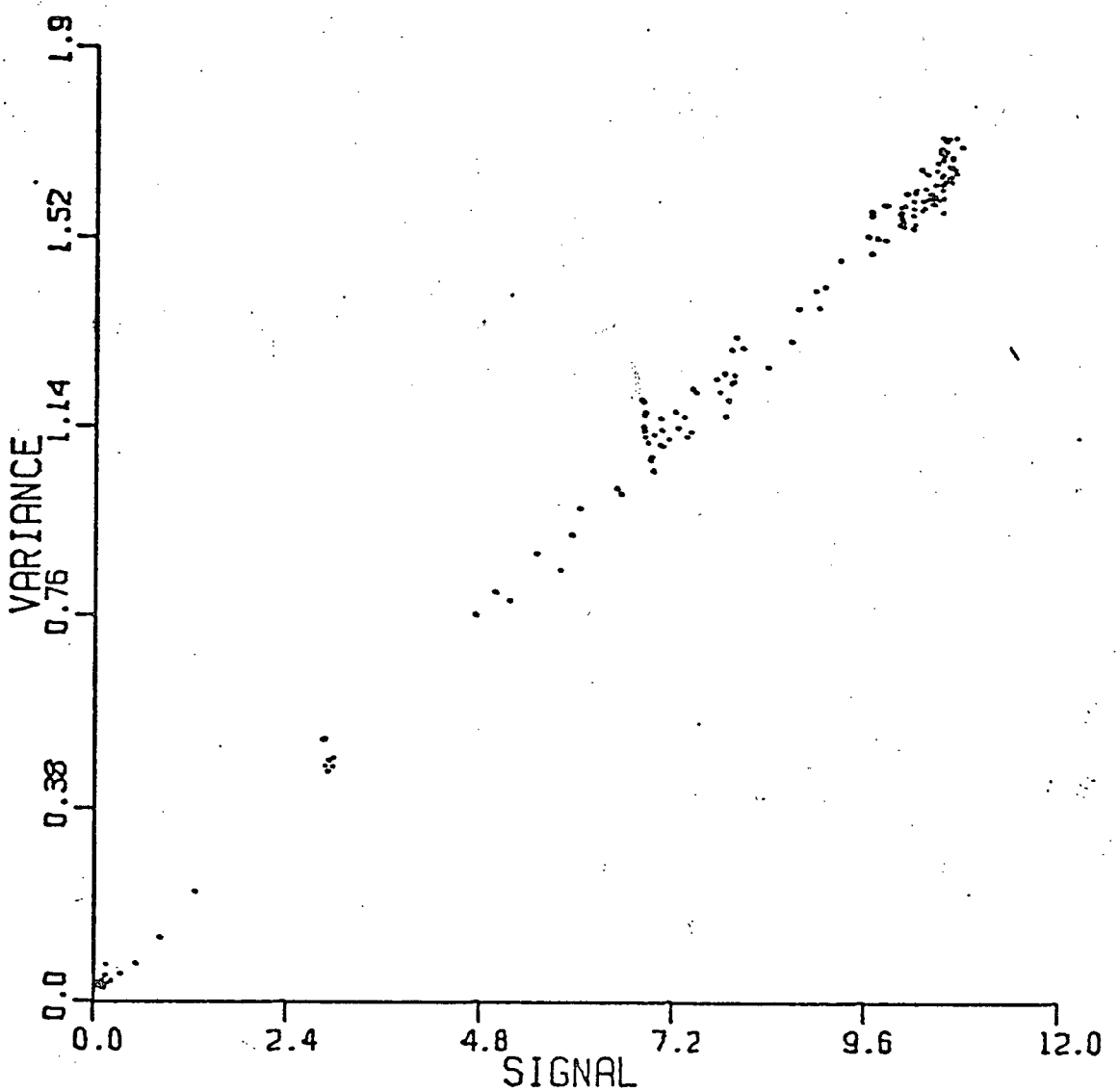

Figure 3(b). Variance vs. signal for October 16 data.

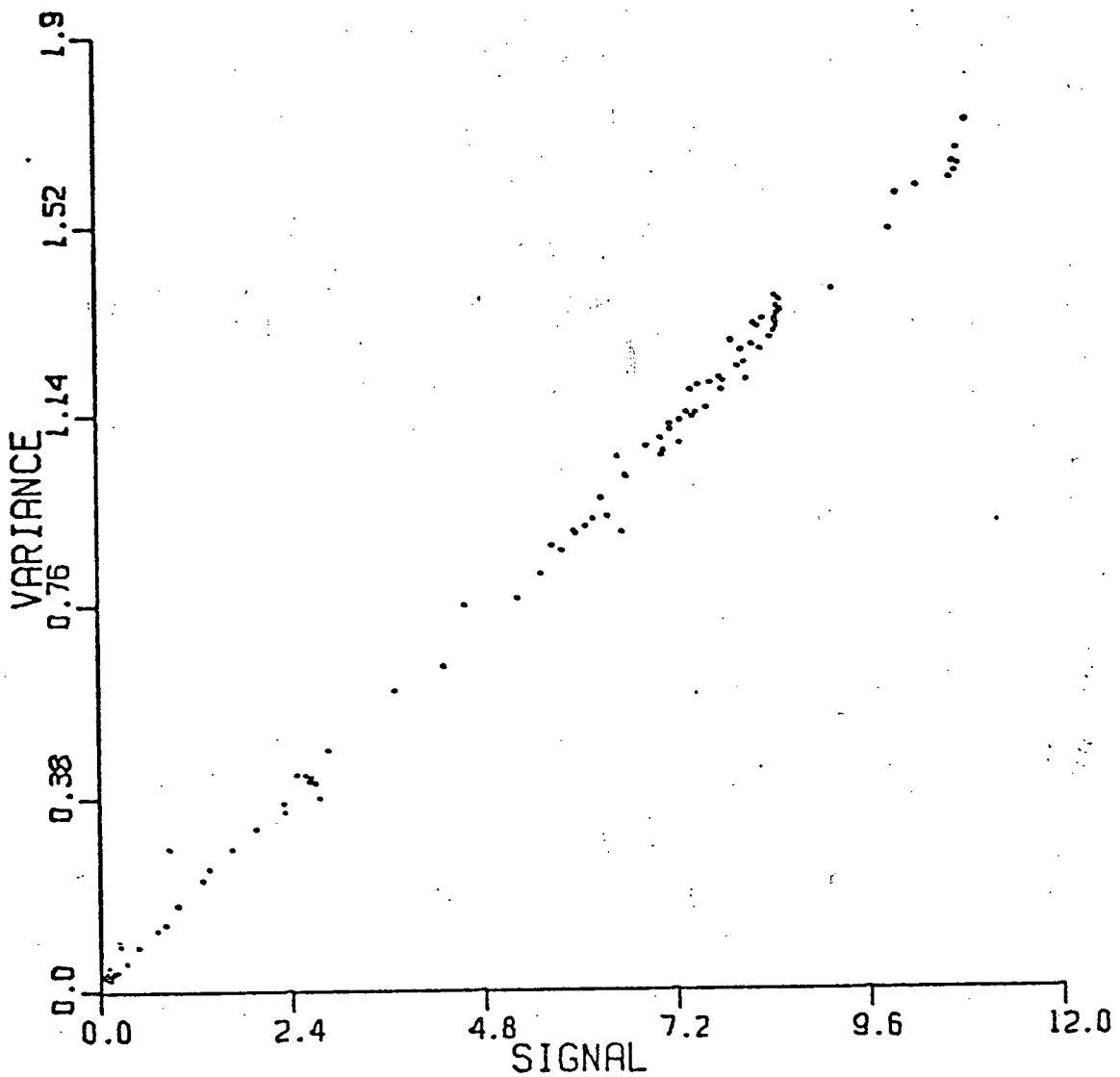

Figure 4(a). Contour plot of left Fiducial mark for October 15 data.

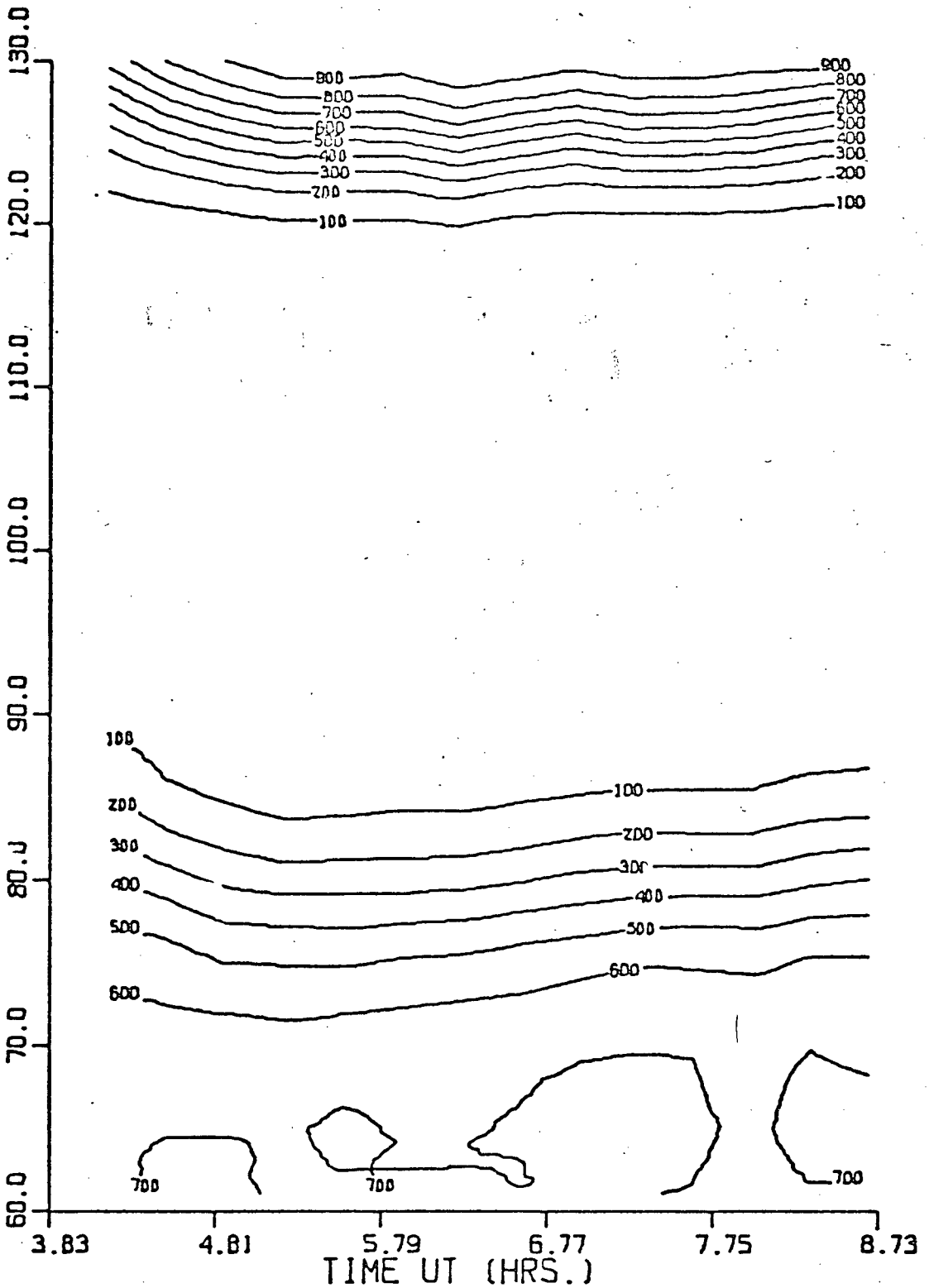

Figure 4(b). Contour plot of right Fiducial mark for October 15 data.

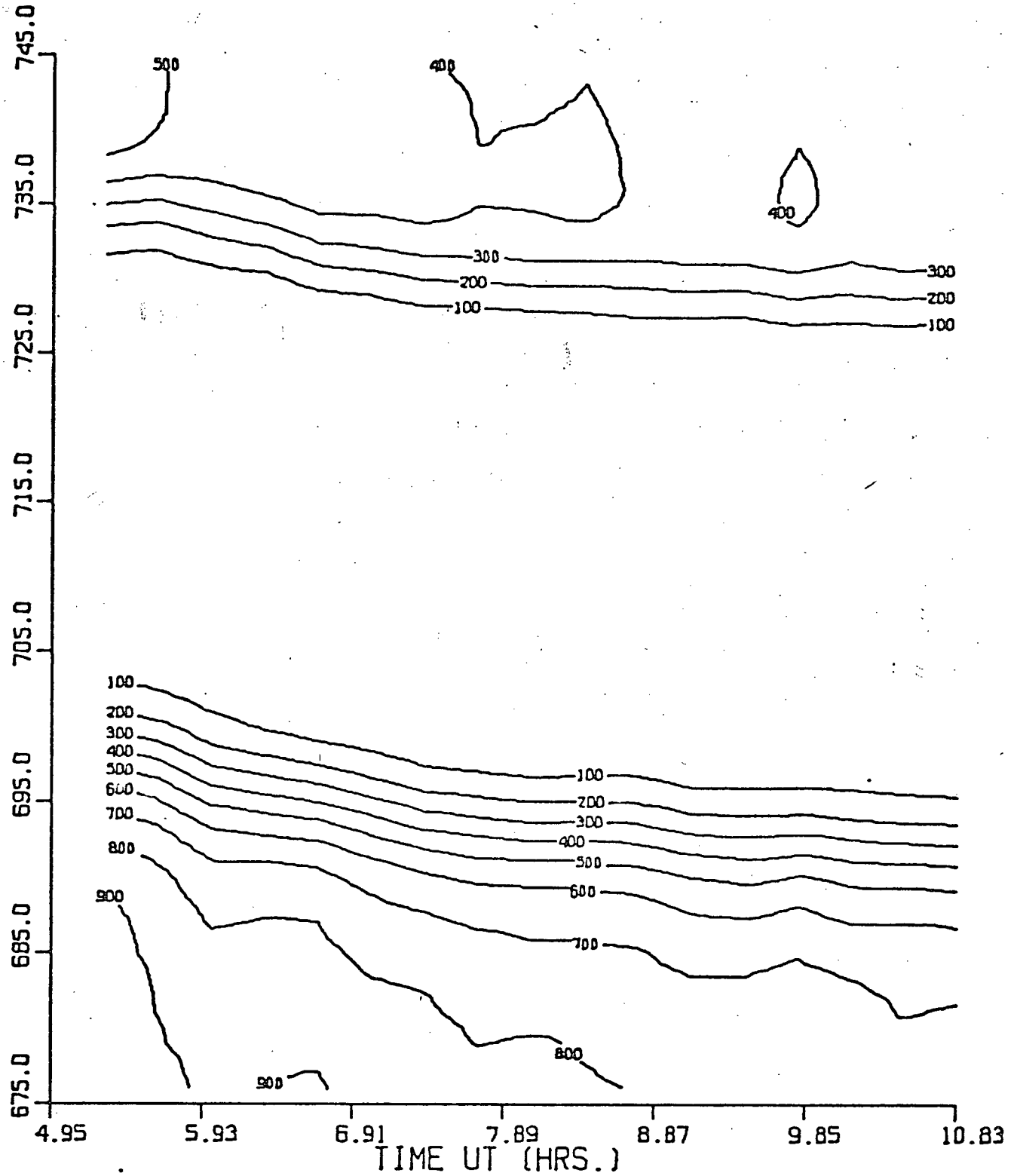

Figure 4(c). Contour plot of left Fiducial mark for October 16 data.

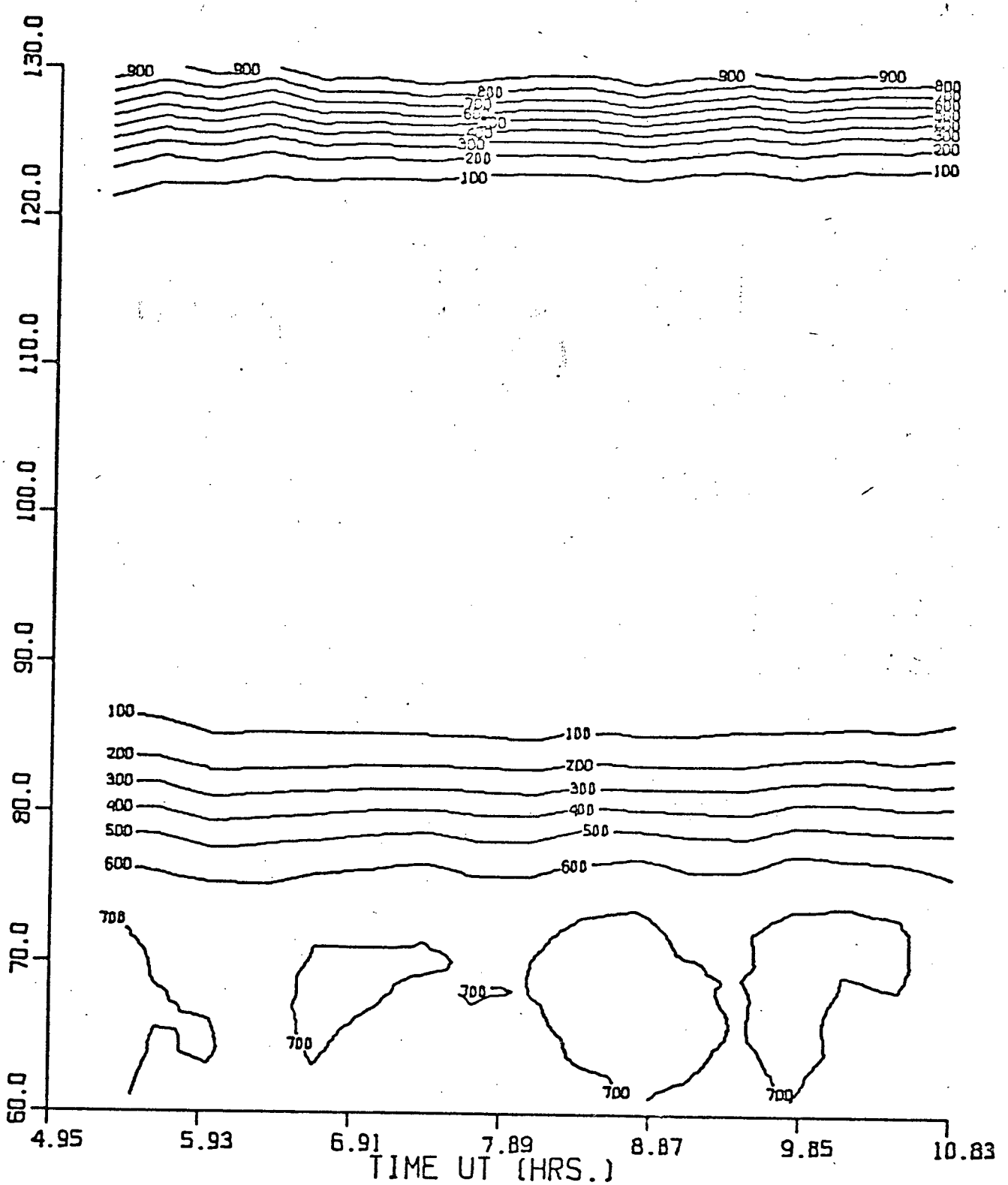

Figure 4(d). Contour plot of right Fiducial mark for October 16 data.

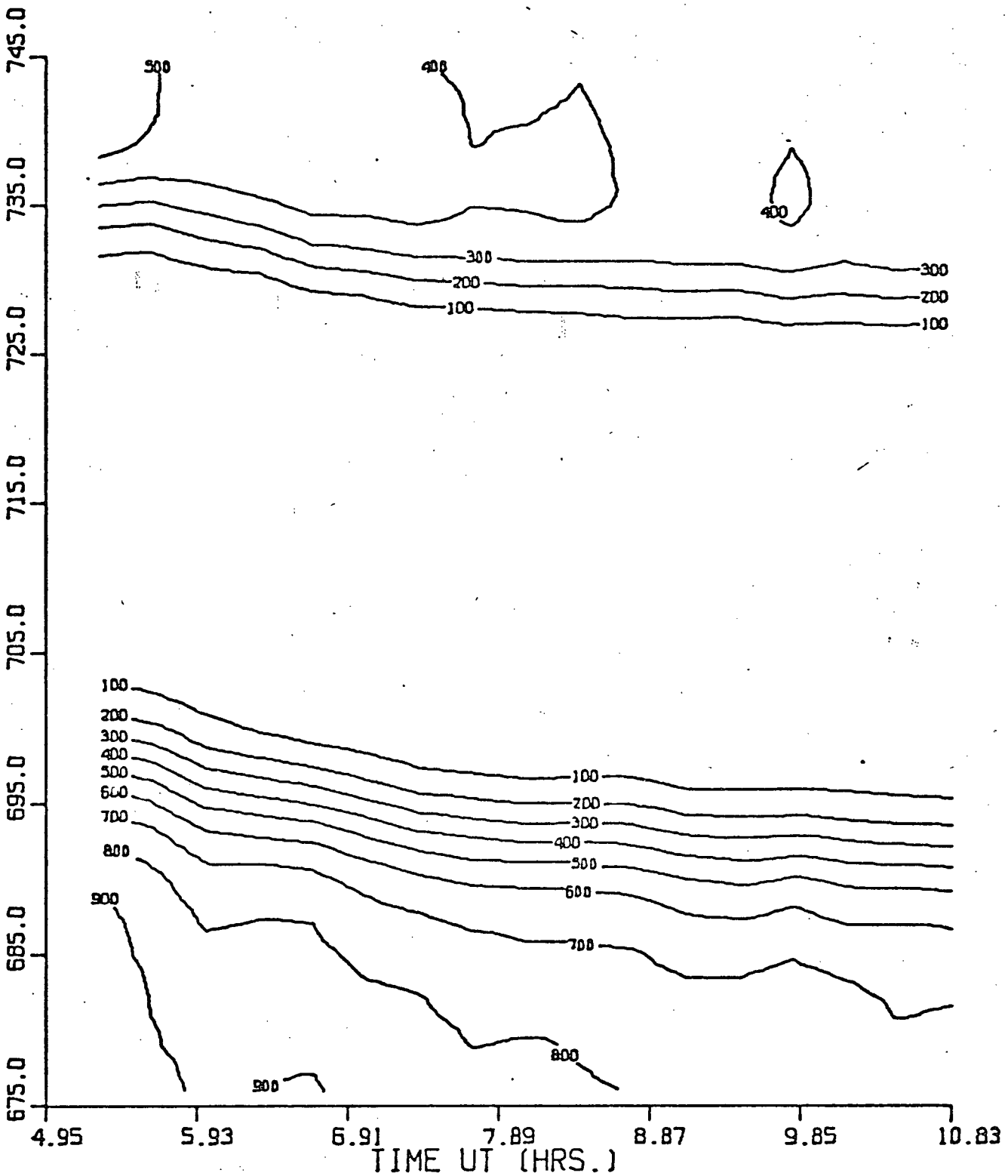

The displacements are calculated using a program described by Fahlman and Glaspey (1973). The spectrum to be measured is systematically shifted relative to a reference spectrum in order to find that shift which minimizes, in a least squares sense, the differences between the two spectra. The shifting and differencing is done in the Fourier domain. The correction to be applied to the absorption line is found by linear interpolation between the measured shifts of the fiducials. The mean spectrum was used as the standard. The shifts of the right and left fiducial marks as well as the slope of the straight line fitted through the shifts are given in Tables II(a) and II (b). The values of the shifts are given to three decimal points, however the accuracy of the technique can only be guaranteed to $\simeq$0.1 of a sample point. It is necessary to assume a linear shift across the face of the tube since we only have two reference points. Thompson (1974) found an apparent non-linear expansion of the camera reading beam which necessitated putting upper limits to the radial velocity variations. This point will be returned to later in the radial velocity discussion. The shift corrections were not applied until the actual radial velocity measures were made.

Another instrumental problem associated with isocon data is what appears to be microphonics. The glass target is only $\simeq 2\mu m$ thick, and it is suspected that the scanning by the reading beam could cause the target to vibrate. What results is a sinusoidal variation imposed on the spectrum. Unfortunately the frequency of the microphonic variation is roughly the same as

Table II a. Fiducial Shift Corrections for Oct. 15.

Block No.	Fiducial Shift Left (70-124)	Fiducial Shift Right (685-730)	Slope (Shift/Pt)
1.	-2.472	-6.064	-0.0059
2.	-0.833	-4.287	-0.0057
3.	0.269	-2.743	-0.0049
4.	0.791	-1.907	-0.0044
5.	0.683	-0.396	-0.0018
6.	0.653	-0.252	-0.0015
7.	1.032	0.008	-0.0017
8.	0.492	0.539	0.0001
9.	-0.016	1.255	0.0021
10.	0.239	1.429	0.0020
11.	0.207	1.739	0.0025
12.	0.085	2.033	0.0032
13.	-0.521	2.635	0.0052
14.	-1.165	2.819	0.0065

Table II b. Fiducial Shift Corrections for Oct. 16.

Block No.	Fiducial Shift Left (70-124)	Fiducial Shift Right (685-730)	Slope (Shift/Pt)
1.	.320	-4.000	-0.0071
2.	.035	-3.500	-0.0058
3.	.287	-2.220	-0.0041
4.	.187	-1.360	-0.0025
5.	.212	-0.760	-0.0016
6.	.183	0.182	0.0000
7.	.300	0.820	0.0008
8.	.162	1.100	0.0015
9.	.020	1.380	0.0022
10.	-.061	1.300	0.0022
11.	.131	1.586	0.0024
12.	-.041	2.110	0.0035
13.	-.232	2.180	0.0040
14.	-.315	2.240	0.0042
15.	-.500	2.400	0.0048
16.	-.417	2.620	0.0050
17.	-.842	2.655	0.0057

that of the spectral lines and so cannot be filtered out. A visual inspection of the data was carried out and those frames which showed a marked sinusoidal pattern were rejected. It was difficult to determine an objective criteria for rejection as the amplitude of the effect was often hard to establish, but the volume of data prohibited any other approach. The sequence of spectra as in Figure 2 were recomputed with the rejected records omitted. No significant change was noted other than a decrease in the signal to noise ratio where lesser numbers of records were averaged together, and so it was decided to use the original data intact.

For further analysis of the data, it was decided to filter the data using a bandpass filter truncated with a Lanczos window instead of using the running mean smoothing. The high frequency cutoff point of the filter was chosen as the frequency where the power spectrum of a single block of data fell below -32 db. For the data of Oct. 15 this was 25 per cent of the Nyquist frequency, and for Oct. 16 it was 28 per cent. The low frequency cutoff was set at zero.

The instrumental response is removed from the spectra by a rectification procedure. The spectra were rectified to a continuum by a least squares fit of 4th order polynomials to points in the spectrum which represent real continuum. A new continuum fit using the same points was determined for each of the 20 minute blocks to compensate for any fluctuations in the instrumental response. The sequence of rectified spectra for

the two nights are shown in Figures 5(a) and 5(b).

Figure 5(a). Time series of Rectified spectra for Oct. 15.

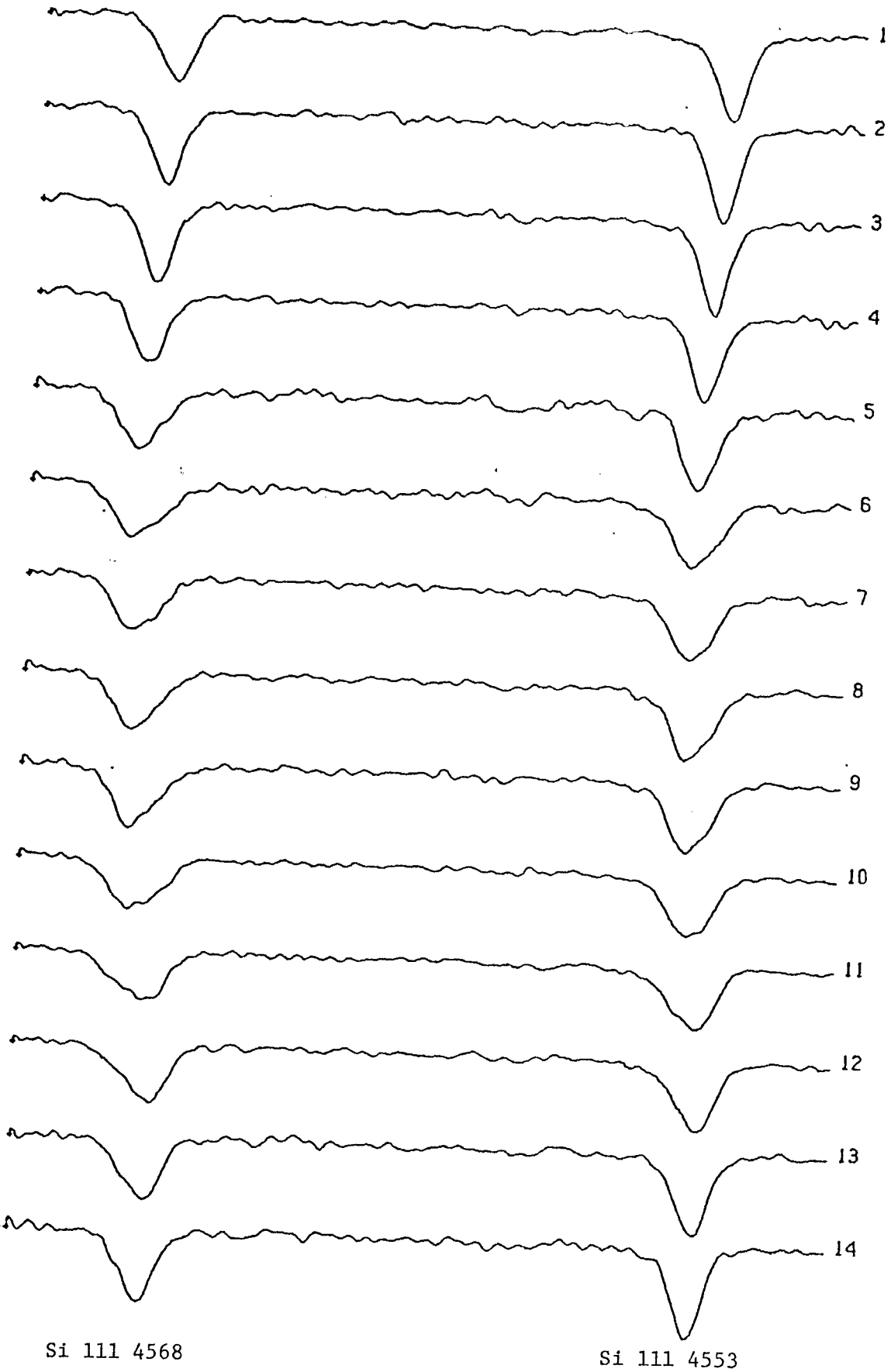

Figure 5(b). Time series of Rectified spectra for Oct. 16.

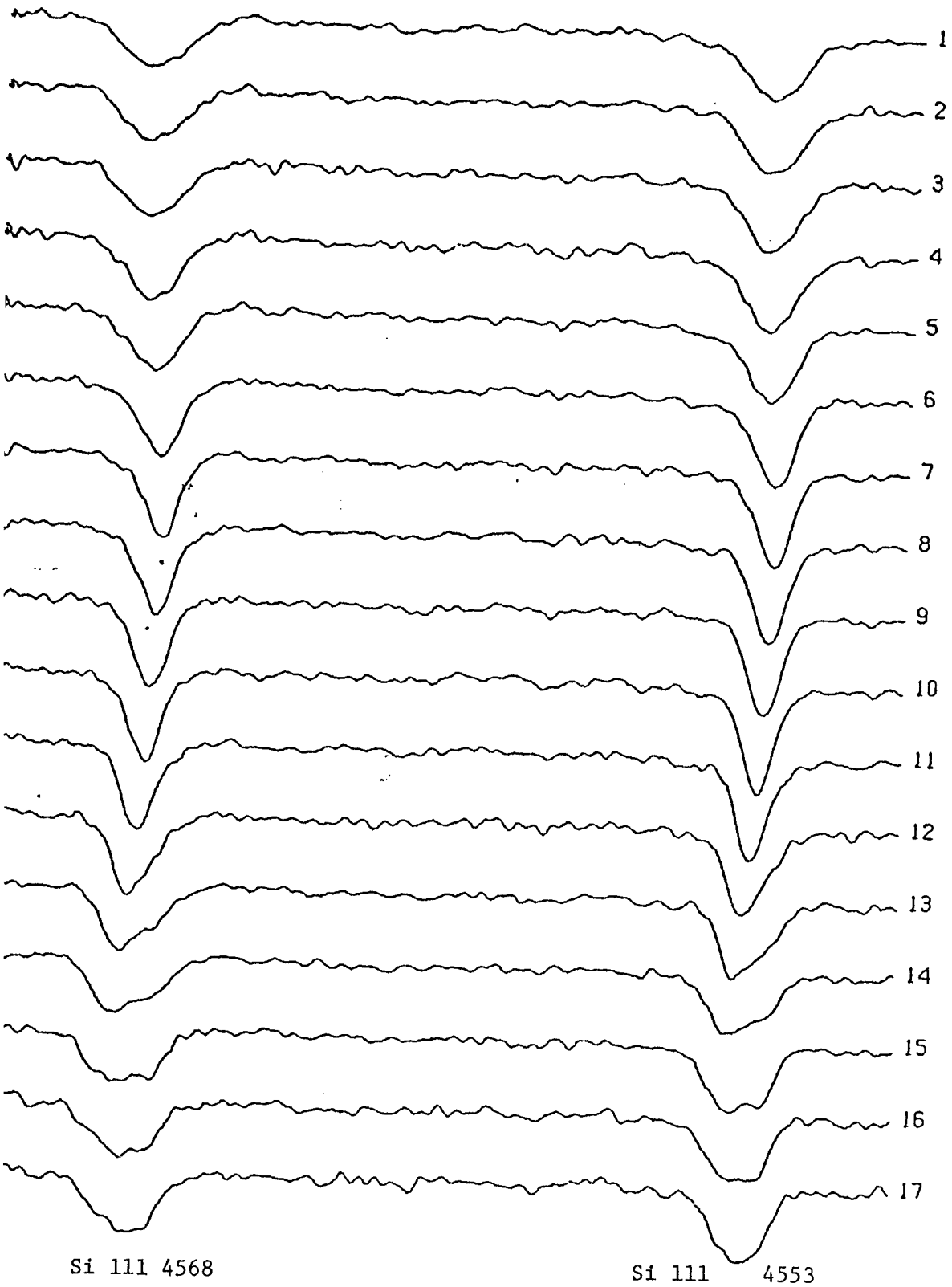

Line Profile Variations

The line profile variations over a cycle are quite remarkable. The digitized form of the data allows much freedom in presentation. What we have essentially is a two-dimensional set of data: a certain wavelength region is sampled at discrete time intervals - resulting in a "time series" of wavelength blocks. If the spectral features are changing with time as is the case here, it is often a problem to correctly visualize what is really going on.

To aid in overcoming this difficulty, I have chosen a number of ways of illustrating the line profile variations, both qualitative and quantitative. These are the following:

1) The "Time Series" Plot.- An example of this is shown in Figures 5(a) and 5(b). Such a diagram is useful in giving a true "picture" of the spectral lines.

2) The Contour Plot.- A preliminary description of this technique has already been given for the fiducial marks. This is a particularly effective method of showing immediately the wavelength shifts and intensity changes.

3) The Difference Plot.- From each block of data is subtracted the mean spectrum of all the data and the result is given in the form of a time series plot. This is very useful in showing the differences between individual blocks.

4) The Second Derivative.- The second derivative of each block of the time series is taken. This "line sharpening" technique has the important character of sometimes being able to resolve

individual components from blended lines.

5) Finally a quantitative description of the line profile changes can be given in terms of measures of line depth, half-width, asymmetry and equivalent width.

1) The Time Series Plot.

As stated in the previous section Figures 5(a) and 5(b) are a series of rectified spectra: each spectrum a 20 minute mean of 40 individual exposures. In order to obtain better time resolution, a smaller time sampling interval was considered. Figures 6 and 7 are a series of rectified spectra: each block a 6 minute mean of 12 individual exposures. Because lesser numbers of records are averaged together, there is a corresponding decrease in signal to noise. Unfortunately when one averages this few number of records, evidence for microphonics is present in some of the blocks (eg. #28 Fig. 6, and #48 Fig. 7.) nevertheless one sees clearly the development from sharp line to broad line phase. In particular, the presence of two components at certain phases is very clearly indicated. It is also possible to monitor the relative growth and decline of the components.

From looking at these line profiles one sees that the line at λ4568 appears broader than that at λ4553. This is due to a slight non-linearity in dispersion across the face of the tube. This is probably due to the use of the transfer lens. Around λ4568 the dispersion is $\simeq$.045 A/pt. ; at λ4553 it is closer to .051 A/pt.

Figure 6(a). Time series of rectified spectra for Oct. 15.

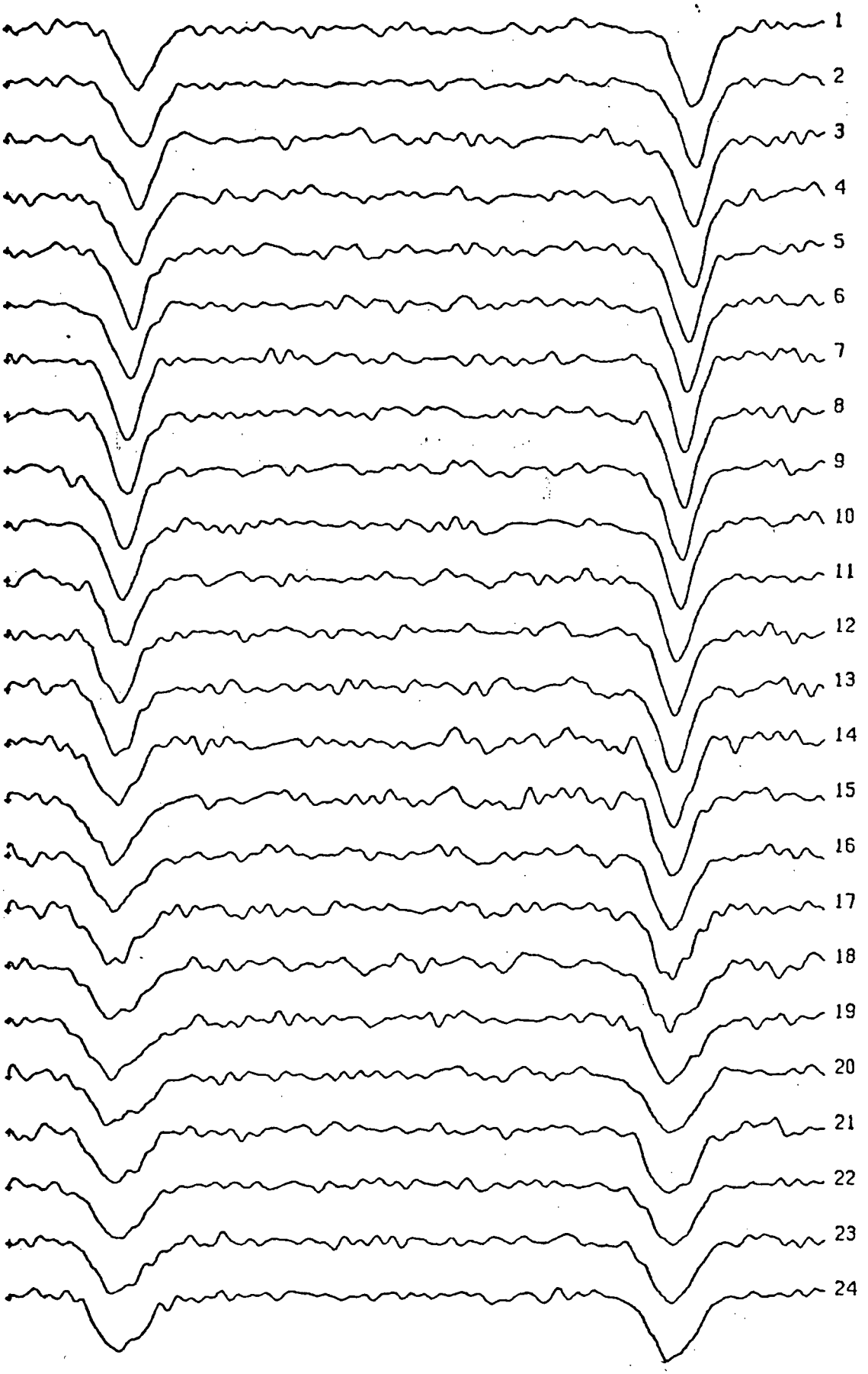

Figure 6(b). Time series of rectified spectra for Oct. 15.

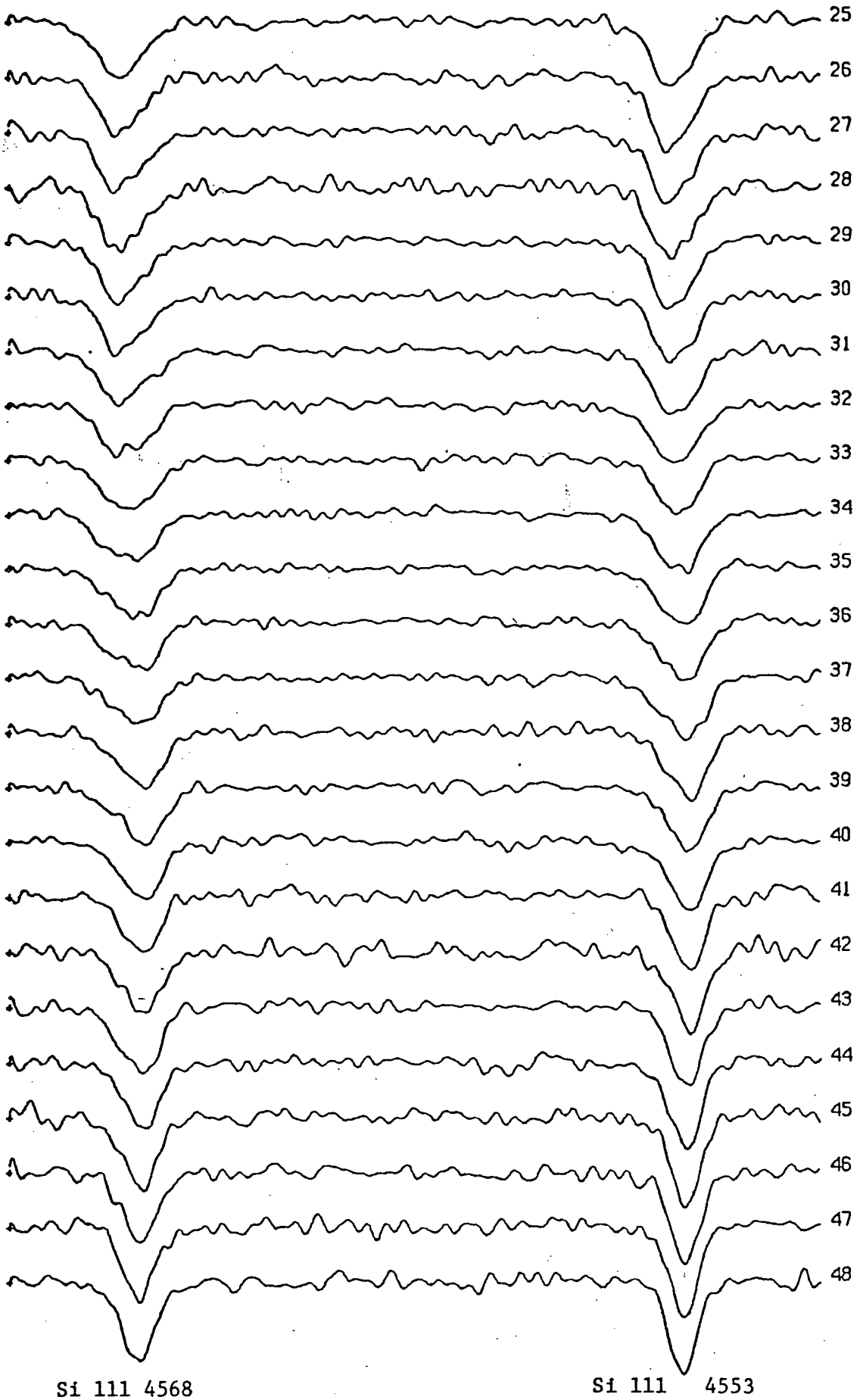

Figure 7(a). Time series of rectified spectra for Oct. 16.

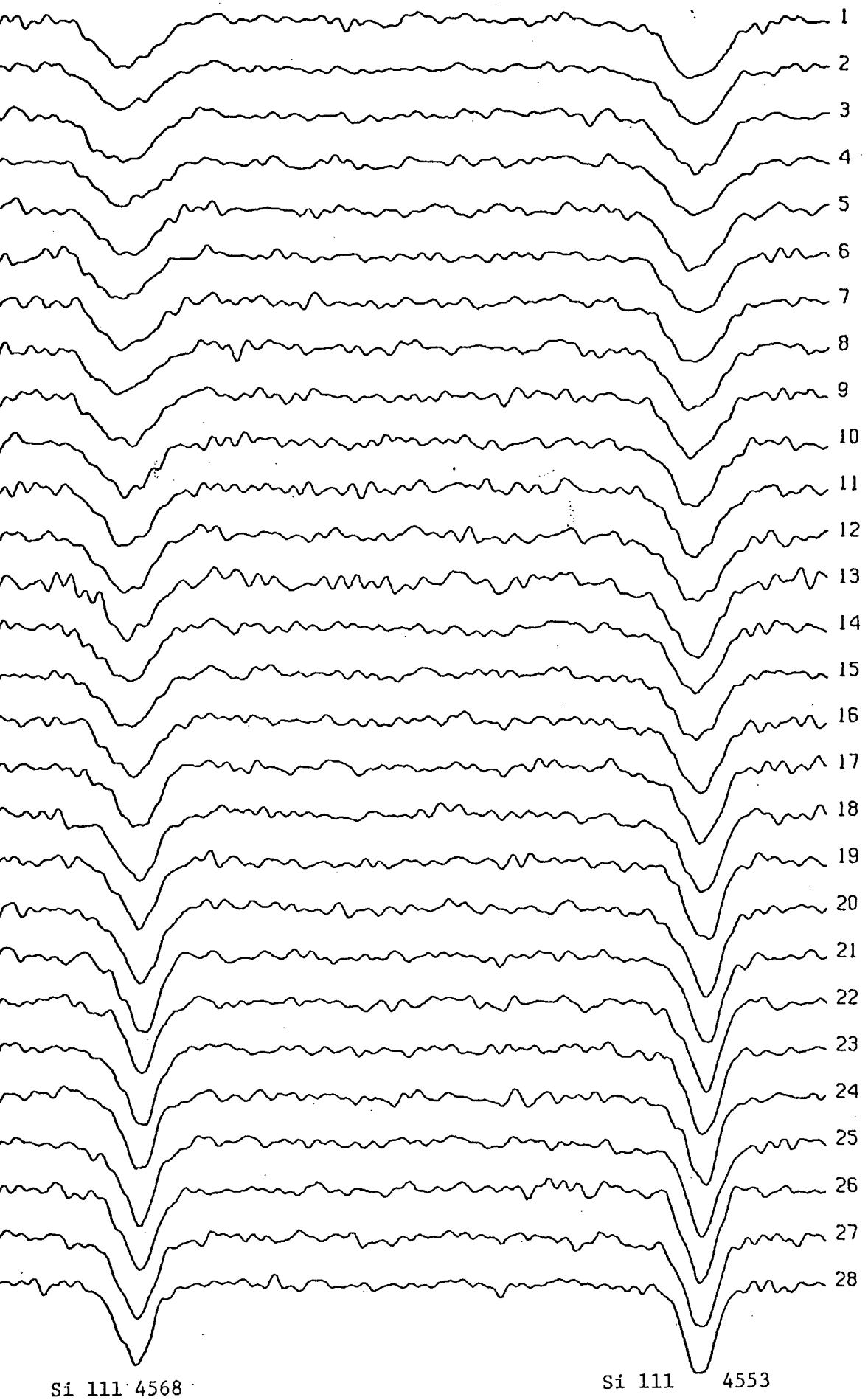

Figure 7(b). Time series of rectified spectra for Oct. 16.

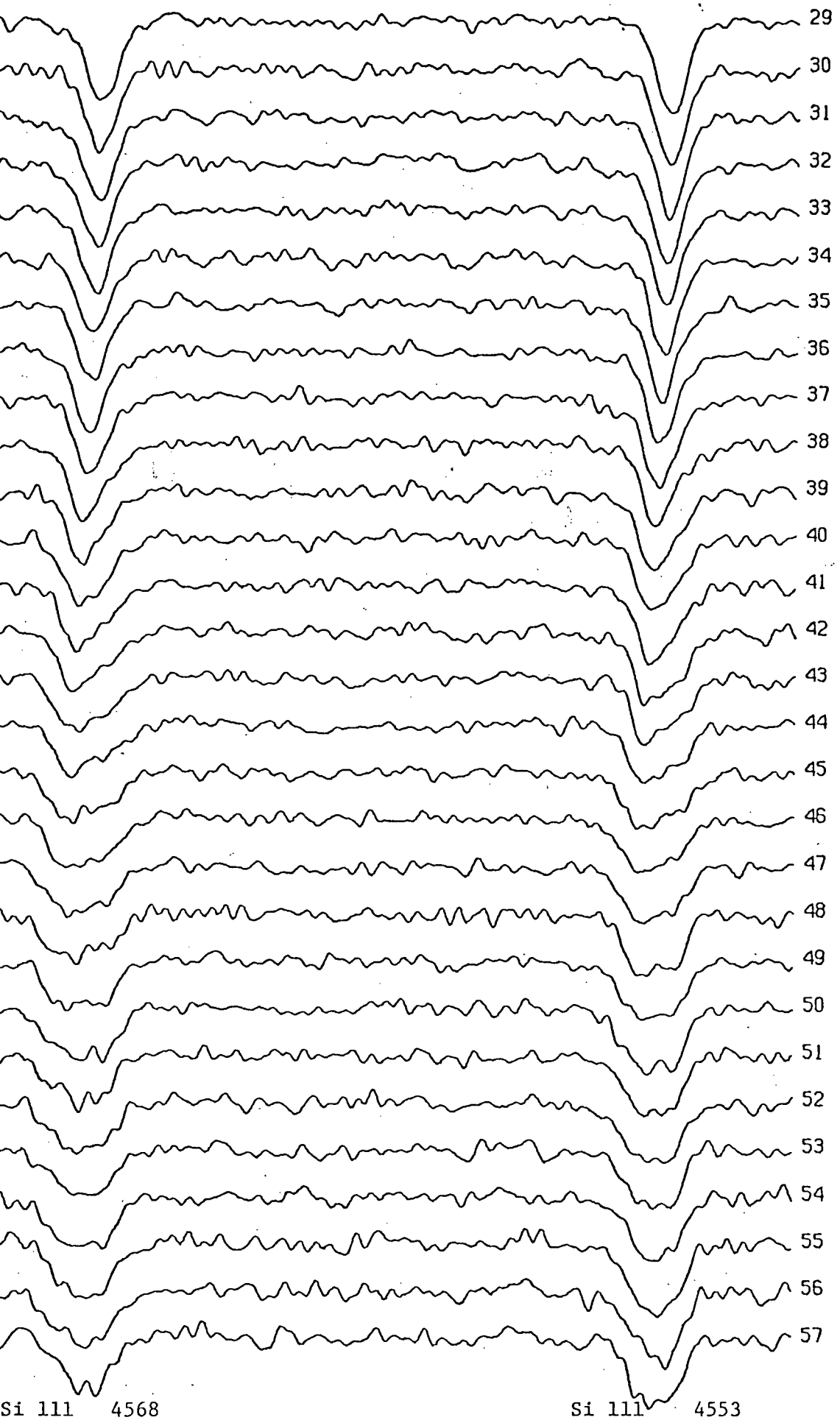

2) The Contour Plot.

Contour plots of the data blocks of Figure 5 are shown in Figure 8. Each spectral line is contoured separately. A great amount of information can be gathered from such a two-dimensional display. Consider Figure 8(a):

A) At the beginning of observation the line is sharp and symmetric. This is indicated by the symmetric distribution of the contour lines on both sides of the minimum contour line of 100.

B) As the cycle progresses, the line becomes broader--shown by a greater spread in the equal intensity contour lines.

C) The nature of the asymmetry can also be seen from these plots. Around $\sim$6 hrs. U.T. the contour lines on the blue side of the absorption peak are more widely separated than those on the red side. Thus there is an asymmetry with an extended wing to the blue. This is confirmed from Figure 5(a) by looking at block numbers 5,6,7, and 8. Towards the end of observation the asymmetry reverses itself showing an extended wing to the red.

D) The wavelength shifts are obvious from looking at the vertical displacement of the contour lines.

E) A rough idea of the variations in line depth can also be obtained. Take for example Figure 8(d). The path of line minima is indicated very approximately by the dashed line. In the first half it crosses successively lower valued contour lines- ie. the line gets deeper. As the cycle progresses the line gets shallower again.

Figure 8(a). Contour plot of Si III 4553 line for Oct. 15.

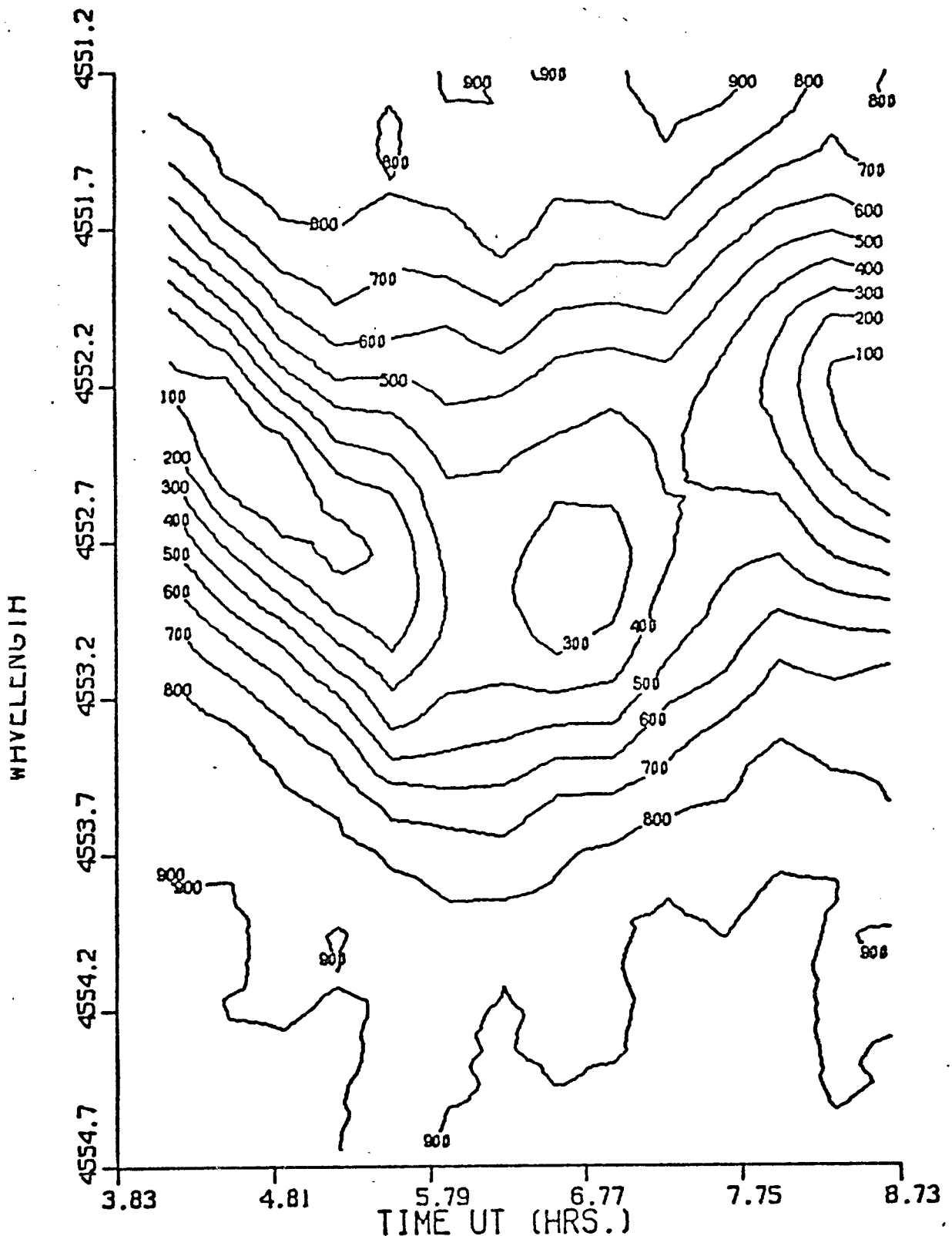

Figure 8(b). Contour plot of Si III 4568 line for Oct. 15.

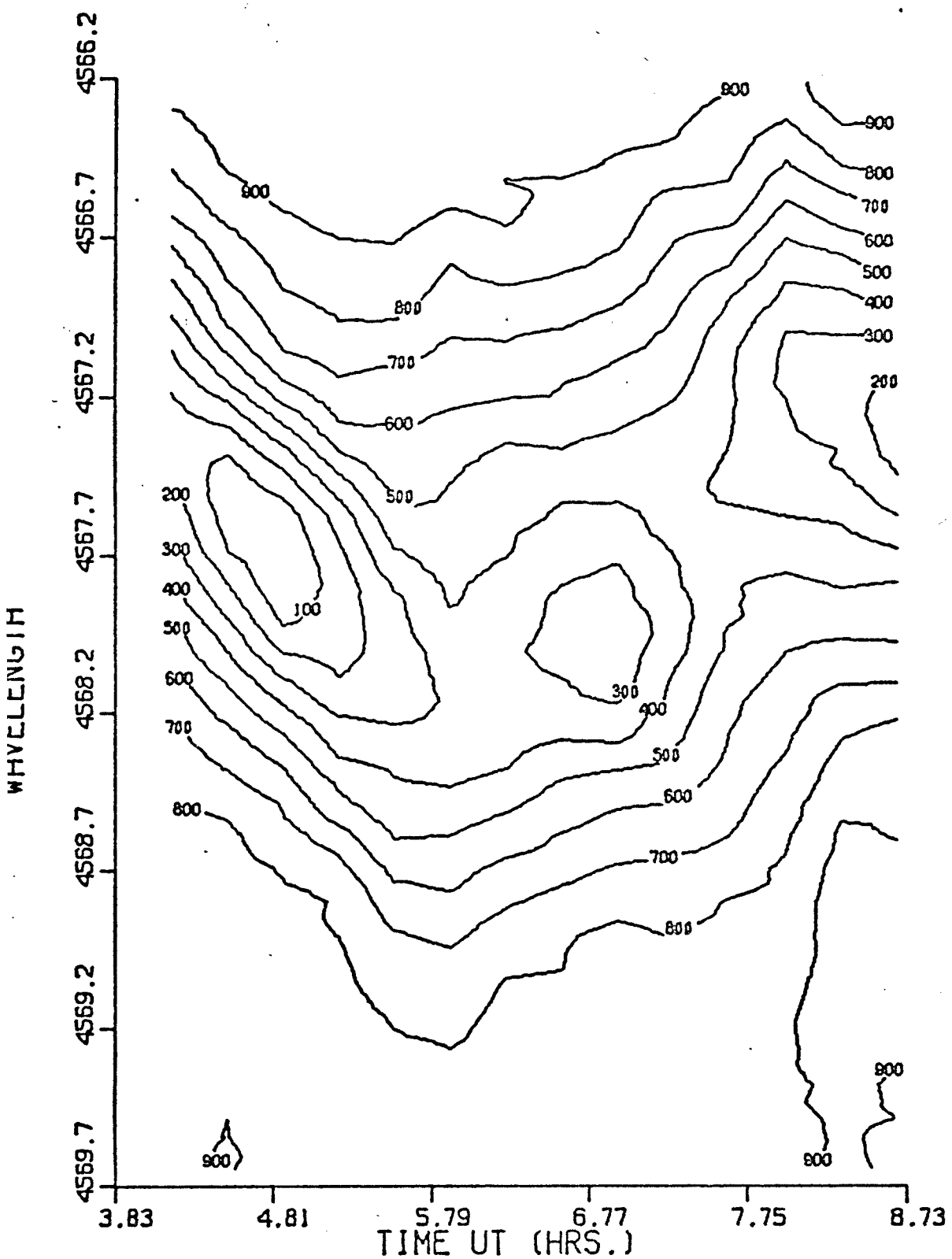

Figure 8(c). Contour plot of Si III 4553 for Oct. 16.

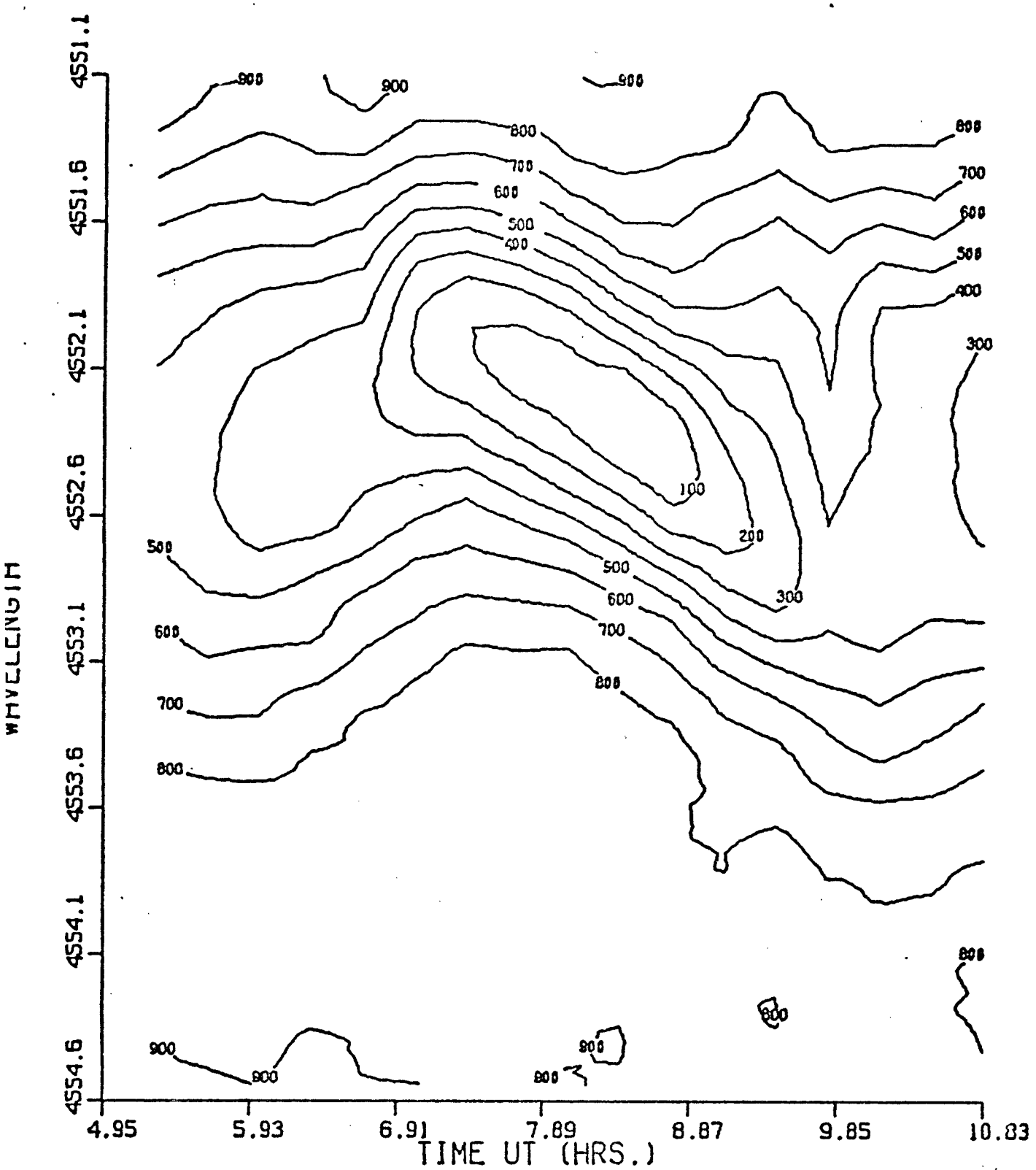

Figure 8(d). Contour plot of Si 111 4568 for Oct. 16.

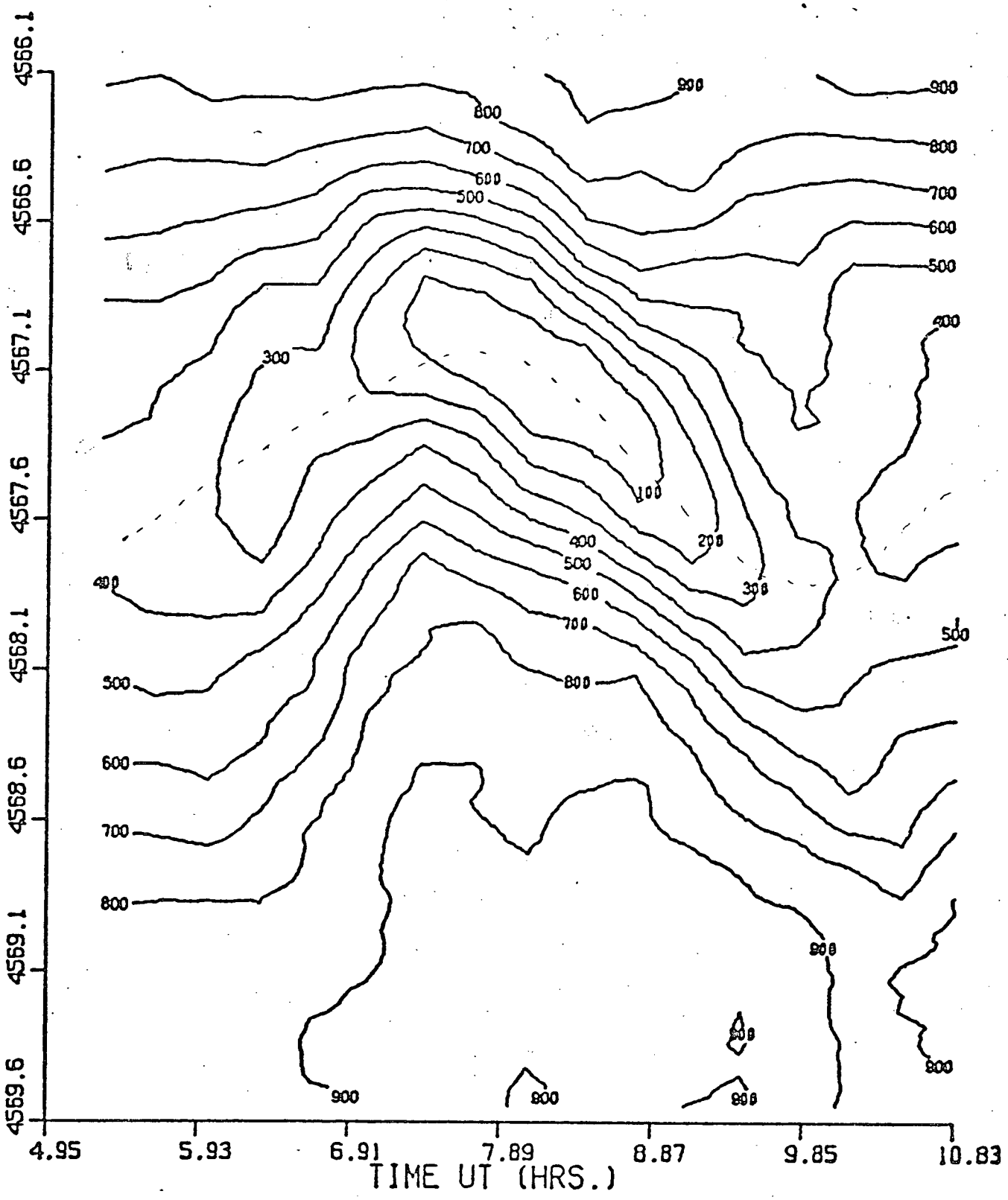

3) The Difference Plot.

Difference plots for the blocks of Figure 5 are given in Figure 9. The mean spectrum subtracted from each block is essentially that of Figure 1 with the instrumental response removed. The difference spectrum of a displaced spectral line is essentially an S shaped curve. It resembles a sinusoid whose wavelength is equal to the width of the line. These diagrams show more clearly than any of the others, the individual block changes at discrete time intervals. The difference plots are basically first derivative plots which are very sensitive to position changes. The second derivative plots described below are more sensitive to profile changes.

4) The Second Derivative.

The second derivative plots of the data blocks of Figure 5 are shown in Figures 10 and 11. One modification was necessary. The data was first 5 point smoothed instead of filtered to 25 or 28 per cent of the Nyquist. When you apply the second derivative to a set of data each slight change in slope becomes greatly amplified. The noisier the data the worse the problem. It was found that a 5 point smoothing gave the best compromise between resolution and noise level. The 2nd derivative was in addition filtered to 20% of the Nyquist.

From looking at the plots one sees immediately the growth and development of the two components. Consider for example in Figure 10(a) λ 4553:

a) In the first 4 blocks only one component is present.

Figure 9(a). Difference plots of rectified spectra for Oct. 15.

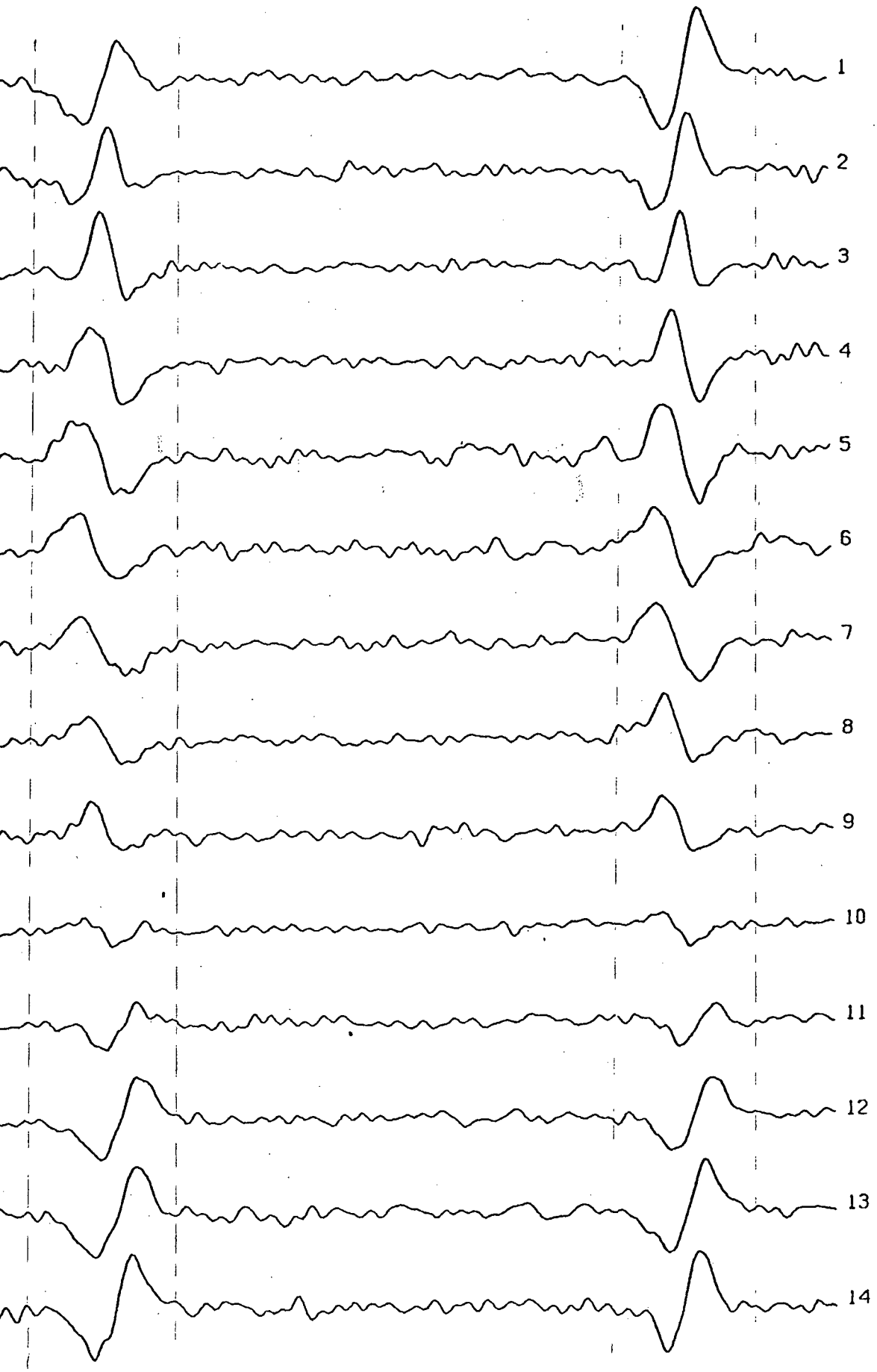

Figure 9(b). Difference plots of rectified spectra for Oct. 16.

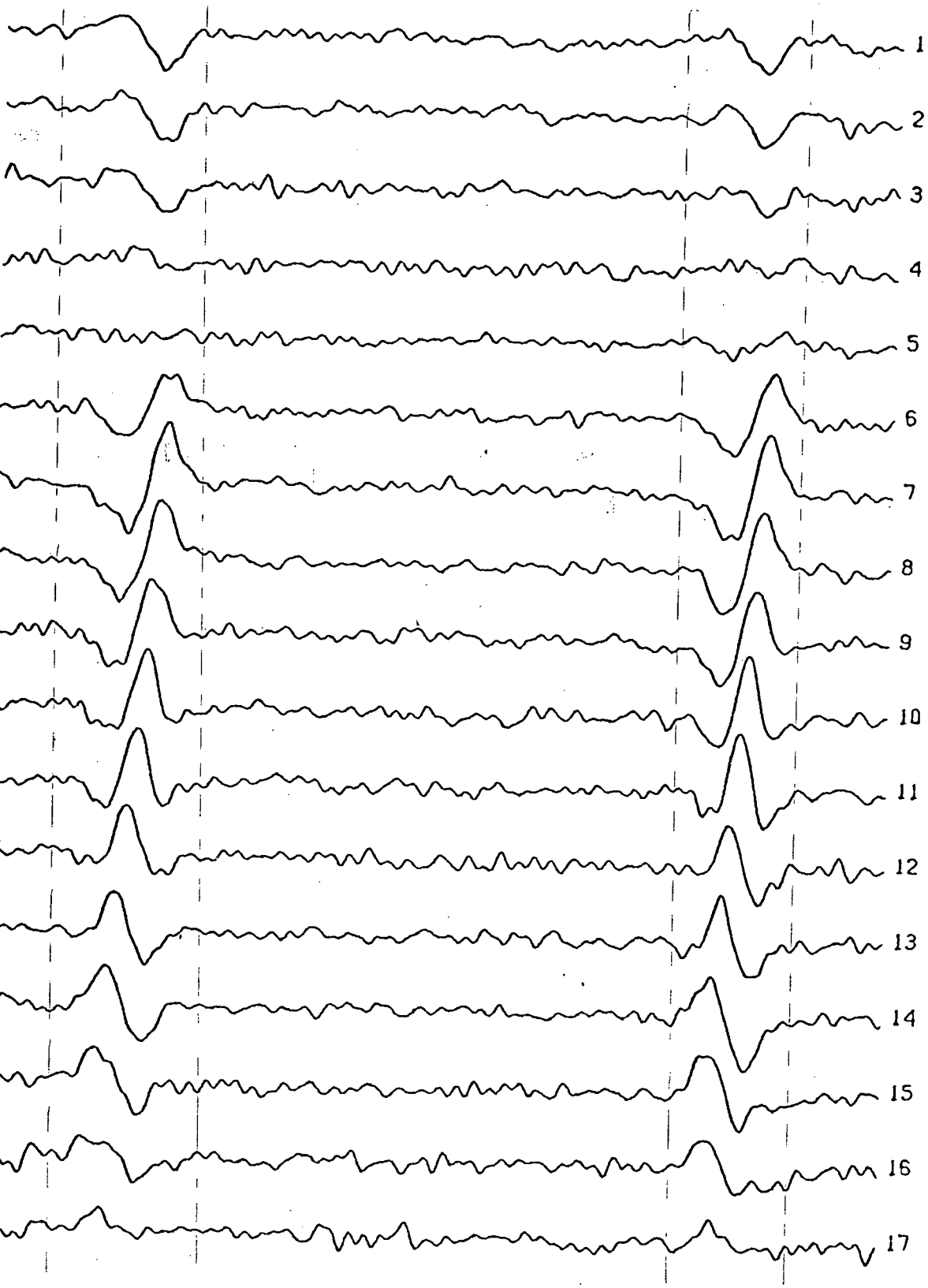

Figure 10(a). Second derivative plots for the data of October 15.

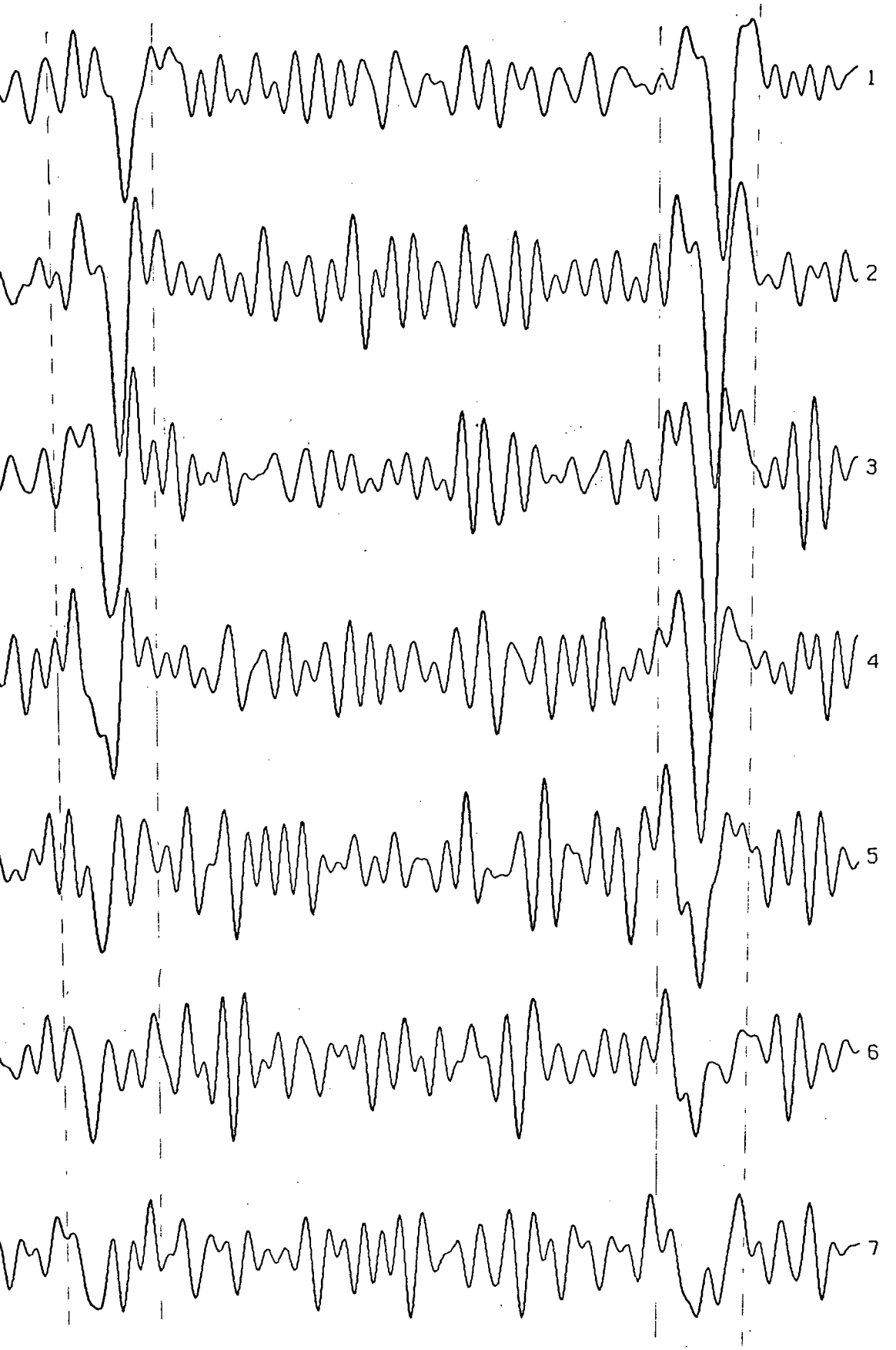

Figure 10(b). Second derivative plots for the data of October 15.

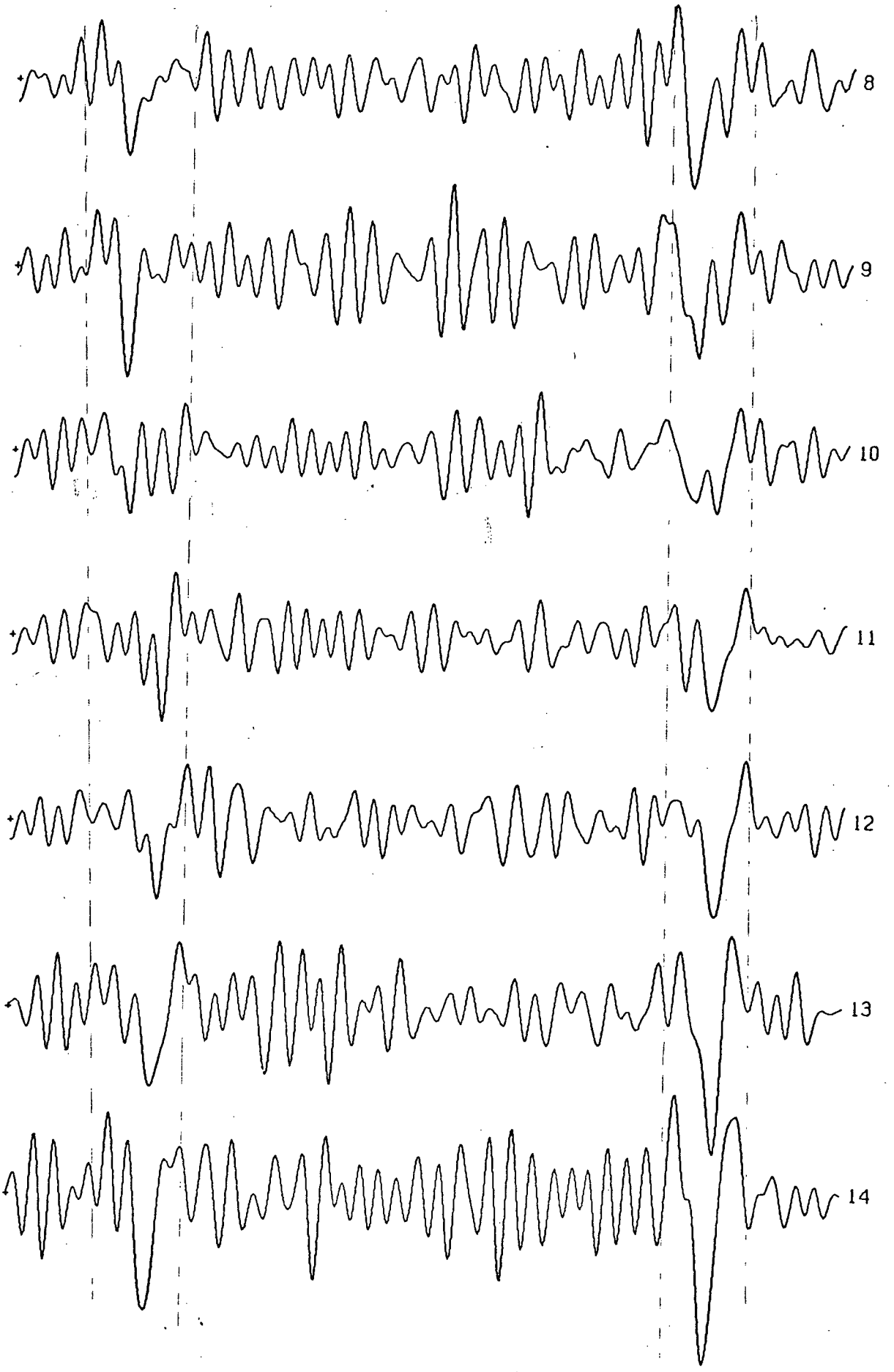

Figure 11(a). Second derivative plots for the data of Oct. 16.

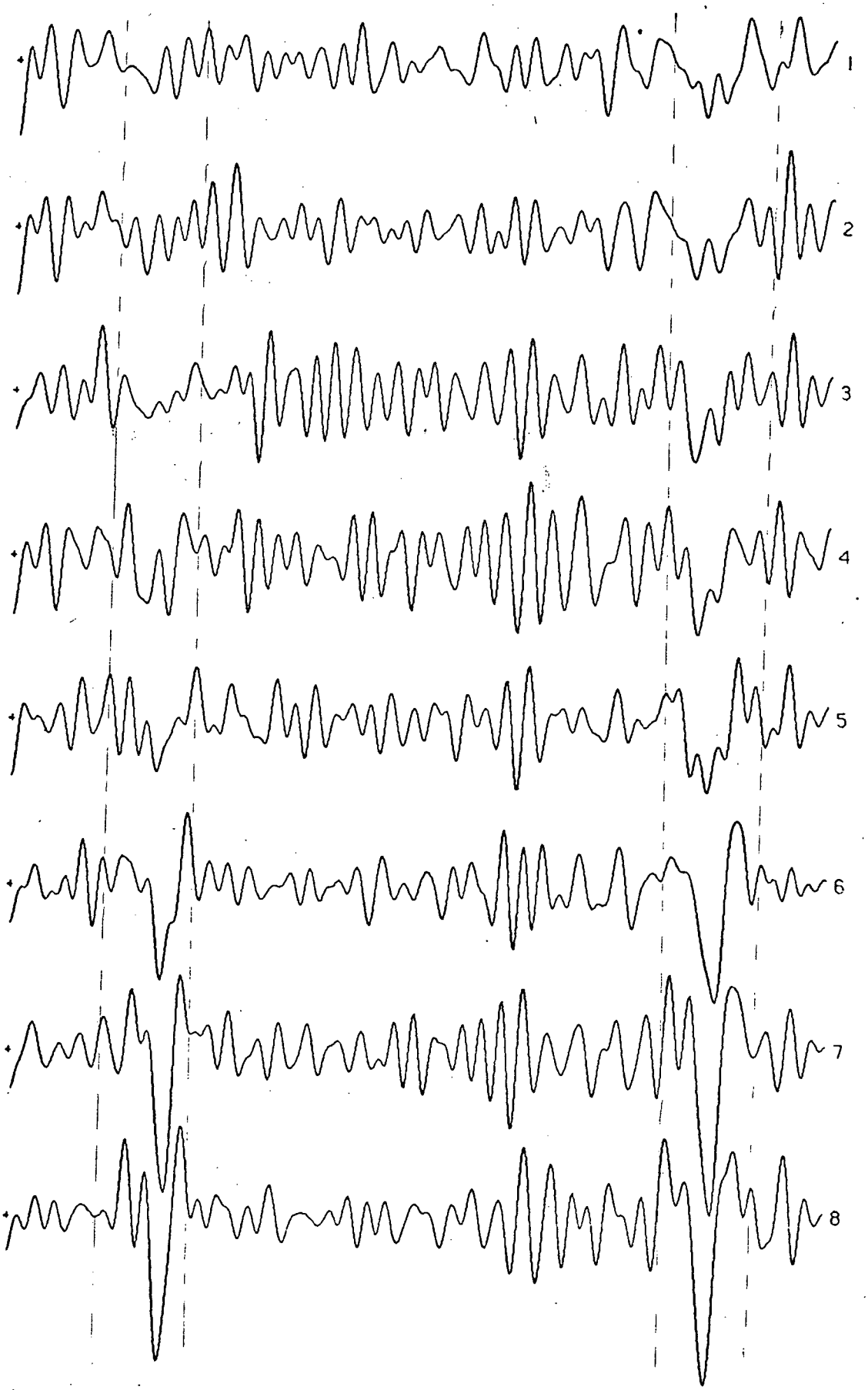

Figure 11(b). Second derivative plots for the data of Oct. 16.

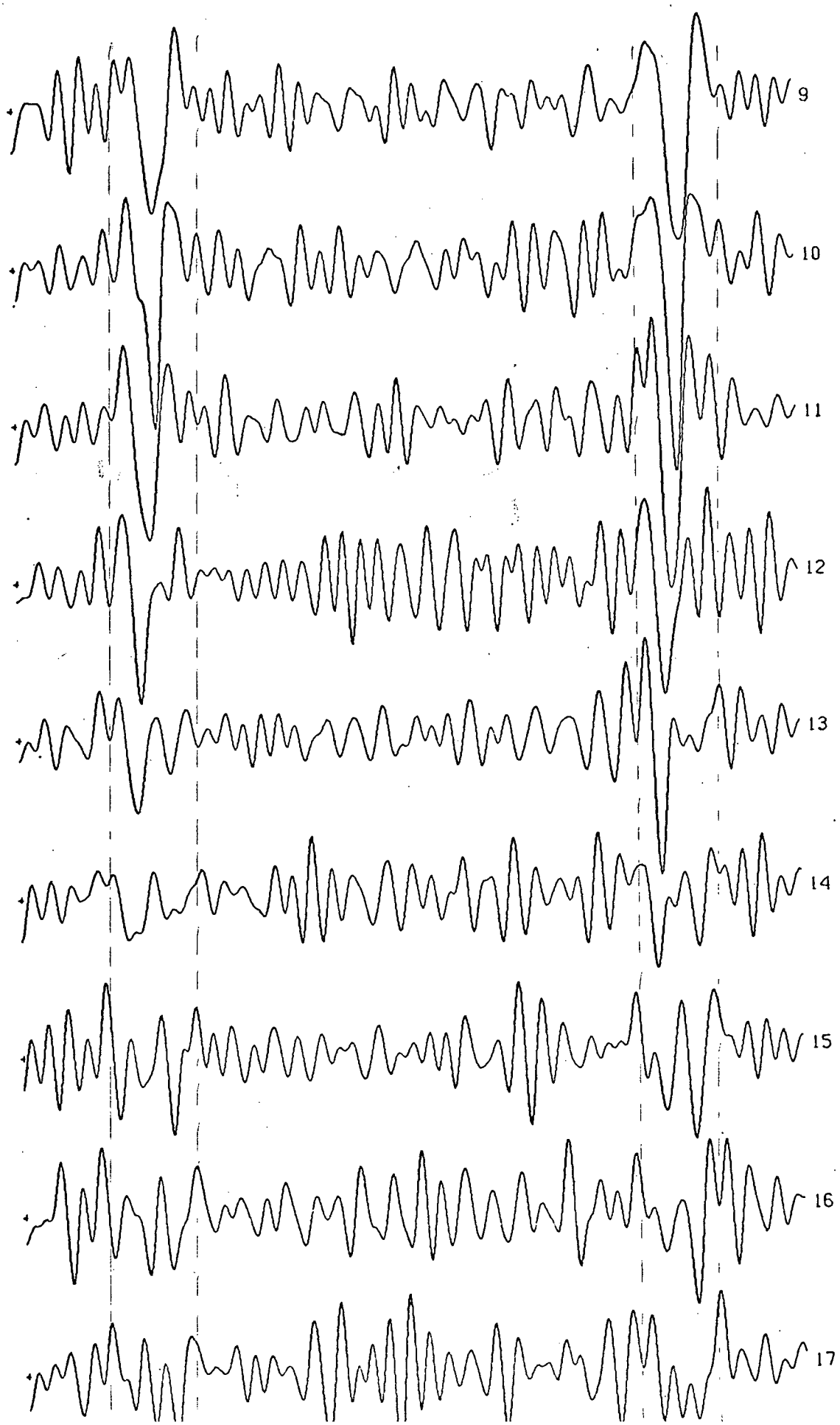

B) In the fifth block a component is beginning to develop on the blue side.

C) In blocks 7,8, and 9 this blue component continues to grow and increase in amplitude.

D) In block 10 the redward component begins its decline and continues to decrease in amplitude in blocks 11,12, and 13.

E) In block 14 you have essentially only one component present.

The situation is a little more confused when you look at λ4568. At times three components actually seem to be present. This is suspected to be more a character of the second derivative technique than any real spectral feature.

5) Quantitative Measurements.

The equivalent width, line depth, half-width and an indication of the degree of asymmetry were measured from the line profiles. The blocks of Figures 6 and 7 were used to give a more detailed analysis of the variations.

Equivalent widths for the lines were determined by area integration between continuum and line from the rectified spectra. This result will be influenced by inaccuracies in the continuum fit. Nevertheless, relative measures of equivalent width can be made to a very good approximation. For the two nights of observation, the equivalent widths of the lines appears to remain constant over the entire cycle. The equivalent width did not vary by more than ≃ 1 % on the average during the observation period. This is in agreement with

Huang's (1955) result for ν Sco ($2K \sim 80$-120 km/sec) and Goldberg's (1973) result for BW Vul ($2K \sim 150$ km/sec).

The line depth was defined as the difference between minimum intensity and the continuum intensity set equal to 1. The results are shown in Figure 12. Again, as for the equivalent widths, absolute measures are not possible but the internal consistency of the continuum fitting procedure allows very good relative comparisons. The extent of one period is shown by the dotted lines in Figure 12.

The half-width was defined as the full width of the line at the half-peak intensity level. What is plotted in Figure 12 is the half-width normalized to the mean half-width for all the blocks of data. The mean half-width $\bar{W}$ for the Si III λ 4553 line was 1.21 A and 1.36 A for Oct. 15 and Oct. 16 respectively. $\bar{W}$ for Si III λ 4568 was 1.16 A and 1.32 A for Oct. 15 and Oct. 16 respectively.

The asymmetry is defined as in the paper by Heard et al (1976). It is taken as the displacement of the core from the midpoint of the width at half-depth. The result is again normalized by the mean width at half depth. A positive measure of asymmetry means that the core is to the red and a negative value means the core is to the violet. The position of the core was taken to be that of minimum intensity. Naturally at those times when there are actually two components present the core position is not really meaningful and this shows up as increased

scatter in the points as shown most clearly in Figures 12(c) and 12(d).

Figure 12(a). Line depth, half-width, and asymmetry vs. time for Oct. 15.

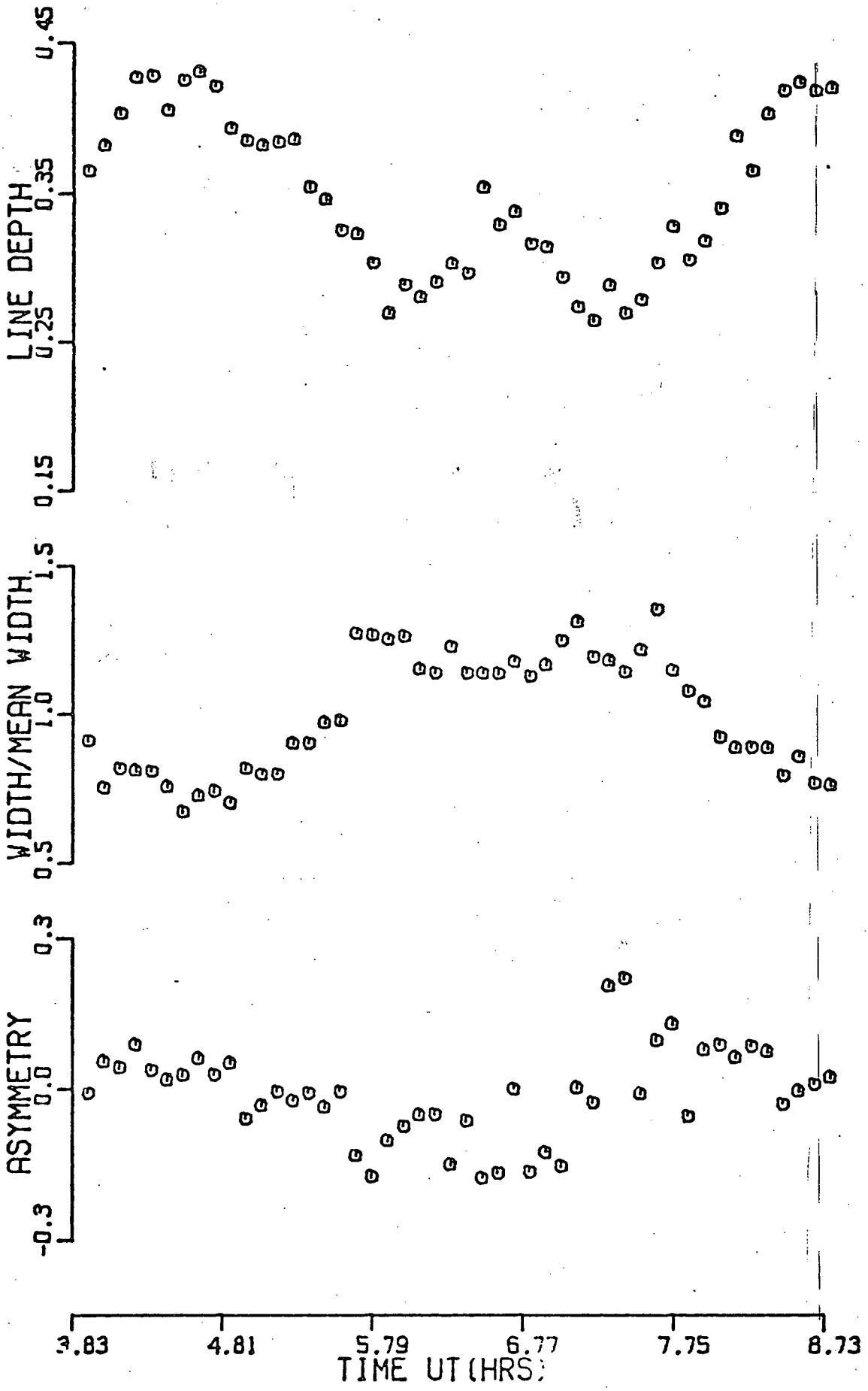

Figure 12(b). Line depth, half-width, and asymmetry vs. time for Oct. 15.

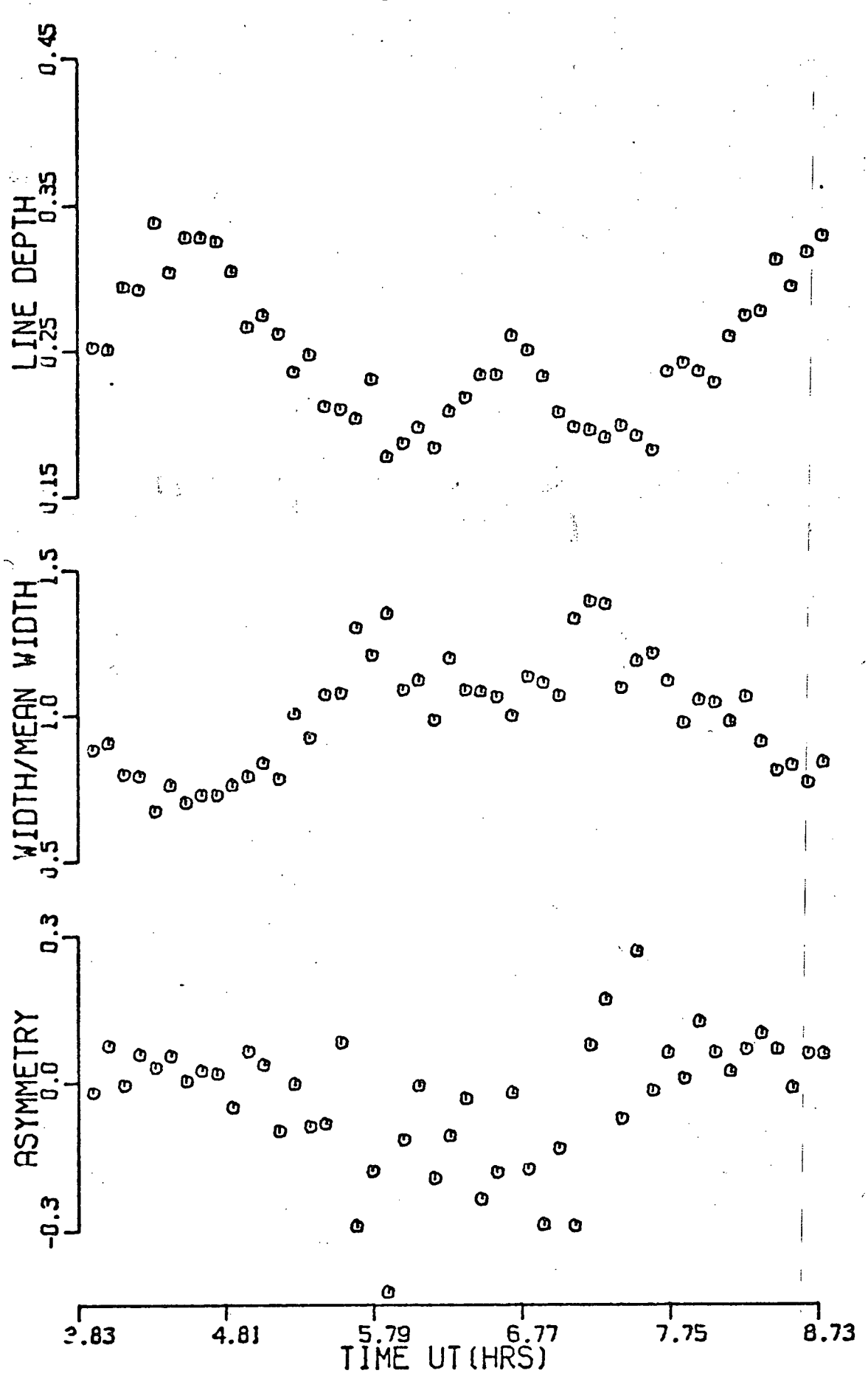

Figure 12(c). Line depth, half-width, and asymmetry vs. time for Oct. 16.

Si III 4553

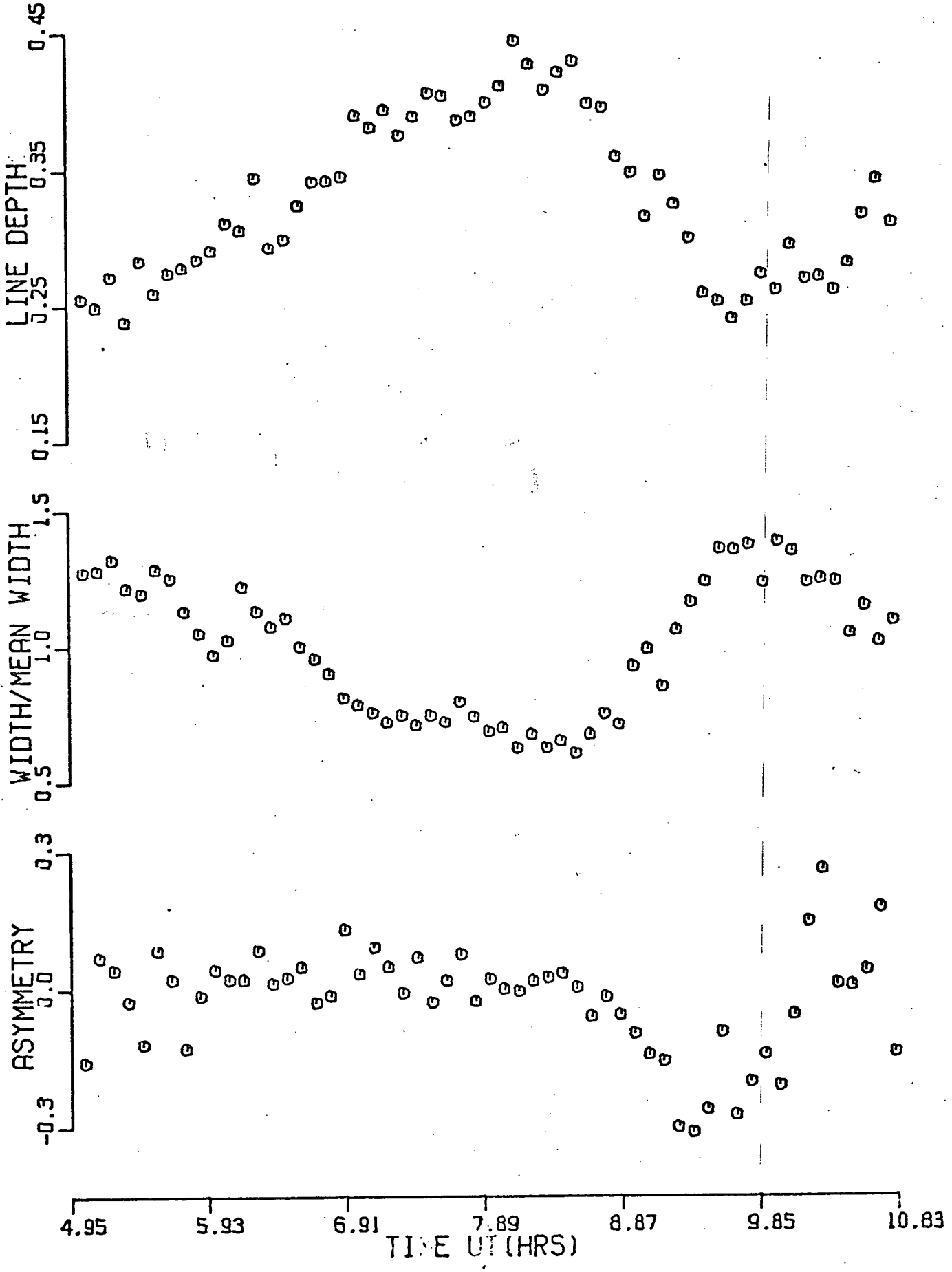

Figure 12(d). Line depth, half-width, and asymmetry vs. time for Oct. 16.

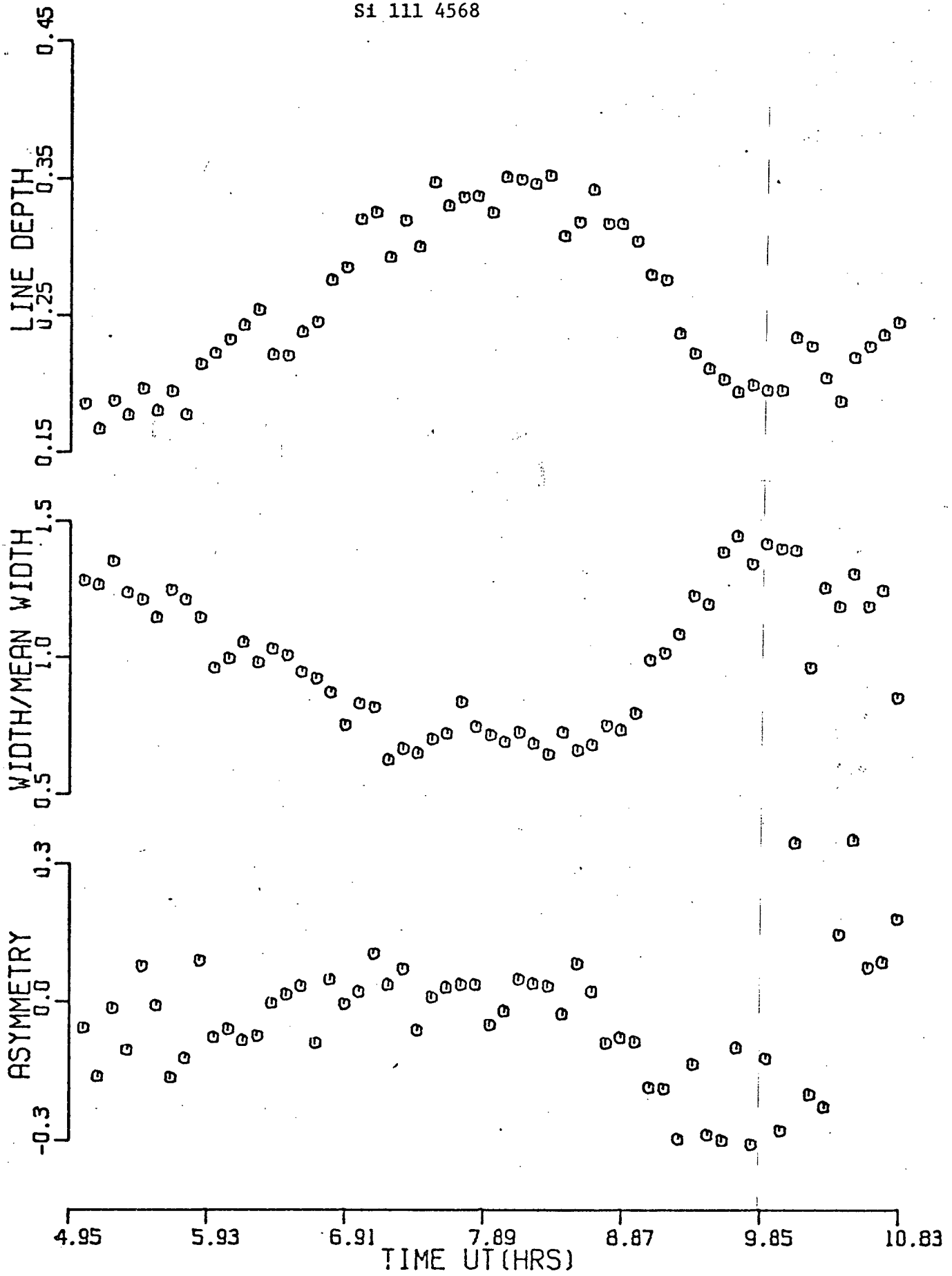

It is important to have some idea of the error associated with the points plotted in Figure 12. This can be obtained a number of ways; one is from a consideration of the equivalent widths. I have said before that the equivalent width remains approximately constant throughout the cycle. There are of course small block to block variations and it is these that one can use to estimate the errors of the points in Figure 12. The error bars are $\simeq$ 2 to 3 times the diameter of the symbols used in the plot.

The Radial Velocity Measures

The broadening of the lines at certain phases is assumed to be due to the presence of two unresolved components. In BW Vul the radial velocity amplitude is on the order of 150 km/sec. The double nature of the spectral lines at certain phases is very evident in this star (Goldberg, 1973). In 12 Lac the radial velocity amplitude is considerably less. Radial velocity curves obtained by various authors are all continuous. One would usually measure the wavelength shift from the position of line minimum. The observations described here however, have improved spectral and time resolution. In light of the discontinuous velocity curve obtained by Bruce Goldberg for BW Vul an attempt was made to measure the radial velocities of the separate components.

A new method of deconvolution developed by Rob Clayton and Tad Ulrych (Clayton and Ulrych, 1976) was applied to the data. A brief description of this method and diagrams showing examples of the deconvolved spectra are given in Appendix A. The results are quite amazing.

The wavelength shifts for each component were measured from the positions of line minimum from the deconvolved spectra. This technique was applied to the blocks of Figures 6 and 7. Corrections for shifts and non-linearities in the scanning raster discussed in a previous section were applied to the data. A reference velocity of -20 km/sec was somewhat arbitrarily

taken as the stillstand velocity (the term 'stillstand' is further described in the Discussion section). One must therefore view the actual numbers with caution and consider instead the amplitude changes. A wavelength calibration spectrum was taken but was not used since our primary interest is in motion within the framework of the star. Also, large raster shifts in the calibration spectrum were found which would limit the accuracy in any case.

The resulting radial velocity curves are plotted in Figure 13. Each line was considered separately. In the radial velocity measures line positions were determined only to the nearest instrumental channel. From a consideration of the raster shift and the discrete sampling interval mentioned above, the errors in velocity are estimated to be $\simeq$ 7 km/sec. It should be noted that the errors will be larger where there are two components present; the scatter is very small when there is only one component present. Because of the scatter in the points there is some question as to the exact location of the stillstand velocity. For this reason an average velocity curve for the two lines (λ4553 and λ4568) was not obtained. Further remarks on the velocity curve are reserved till the next section.

The deconvolution technique used to separate the two components uses the Maximum Entropy method of spectral analysis (a very brief description of this is given in Appendix A). This gives quite accurate position measurements but does not

provide true values for the intensities of the components.

A synthetic profile fitting method developed by John Glaspey was used to determine the intensities of the components. Details of the technique can be found in Glaspey et al (1976). Each line profile was reconstructed by adding two Voigt components, both of the same width but with different velocities and amplitudes, and convolving their sum with the Modulation Transfer Function of the isocon. The width of the Voigt components was chosen as that which gave the best fit when compared to a line profile at sharp line phase. A Gaussian profile gave a satisfactory fit. The doppler width of the components was taken to be constant throughout the cycle. The velocities used were those obtained from the deconvolved spectra. Only two parameters, the amplitudes of the components, were then permitted to vary in order to obtain a 'good' fit. Because of the large volume of data to be analyzed an automatic fitting procedure was used. The method of least squares consists of determining the values of the amplitude parameters A1 and A2 which yield a minimum for the function χ^2 (where χ^2 is essentially the sum of squares of the difference between the input data profile and the fitting profile). The grid search method described by Bevington (1969) was used.

The line depths of the separate components are shown in the upper plots of Figure 13. The symbols used in the line depth plots correspond to the two components in the velocity curves. Examples of the Gaussian profile fit to the input data are shown

in Figures 14(a) and 14(b). The Gaussian curve is indicated by the plus(+) signs. The resulting difference curve (observed-Gaussian) is shown below the line profile. The position of the component(s) is marked by the arrows.

In order to be able to more readily compare my velocity curve with that obtained by other observers, I have plotted the velocity curve as obtained by measuring the wavelength shift from the centroid of the line ($\lambda_c = (A1\lambda_1 + A2\lambda_2)/(A1+A2)$; λ_1 and λ_2 are the wavelength positions of the two components). The resulting curves for λ 4553 are shown in Figures 15(a) and 15(b) for Oct. 15 and Oct. 16 respectively.

Figure 13(a). Radial velocity curve for Si III 4553 for Oct. 15.

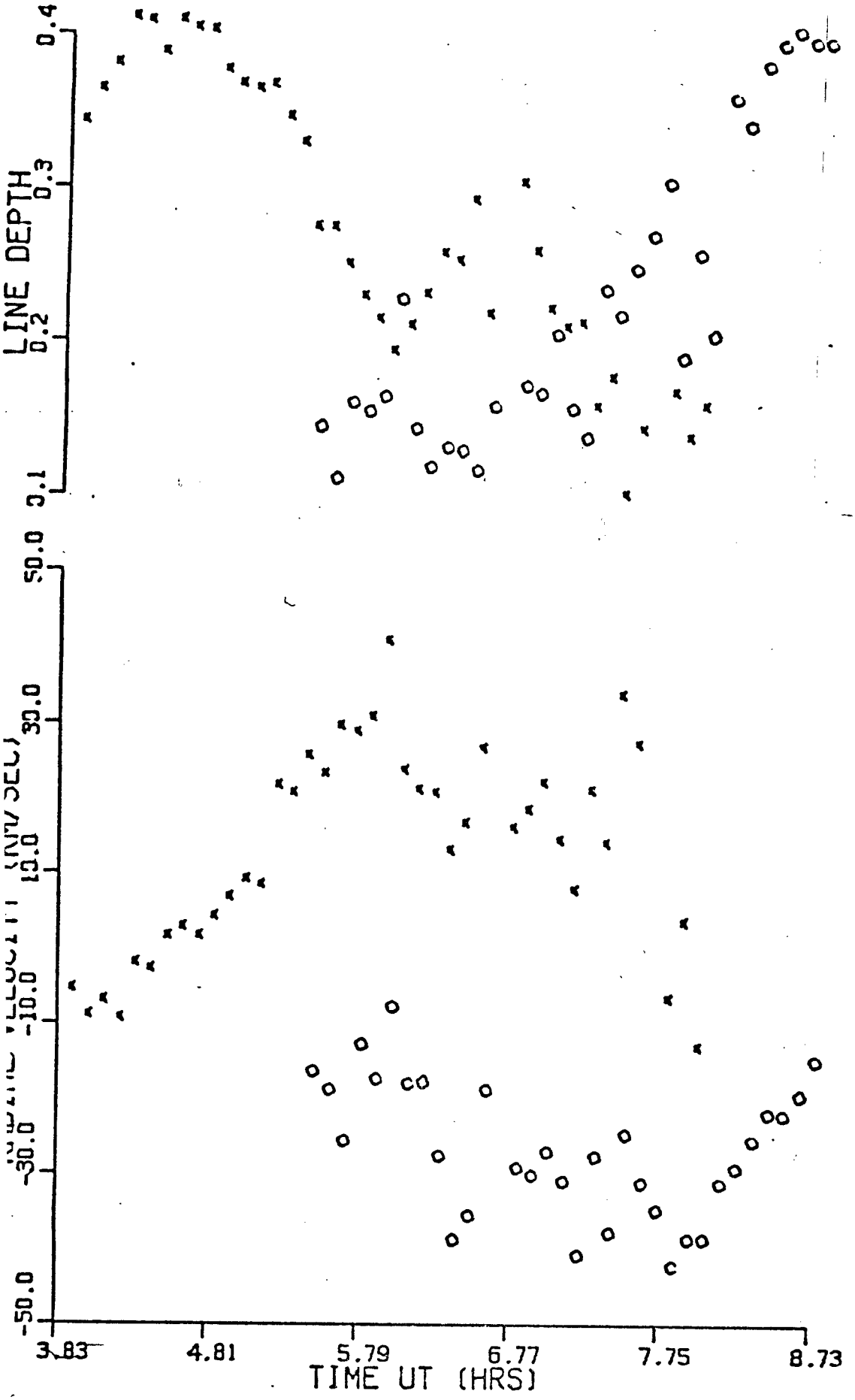

Figure 13(b). Radial velocity curve for Si III 4568 for Oct. 15.

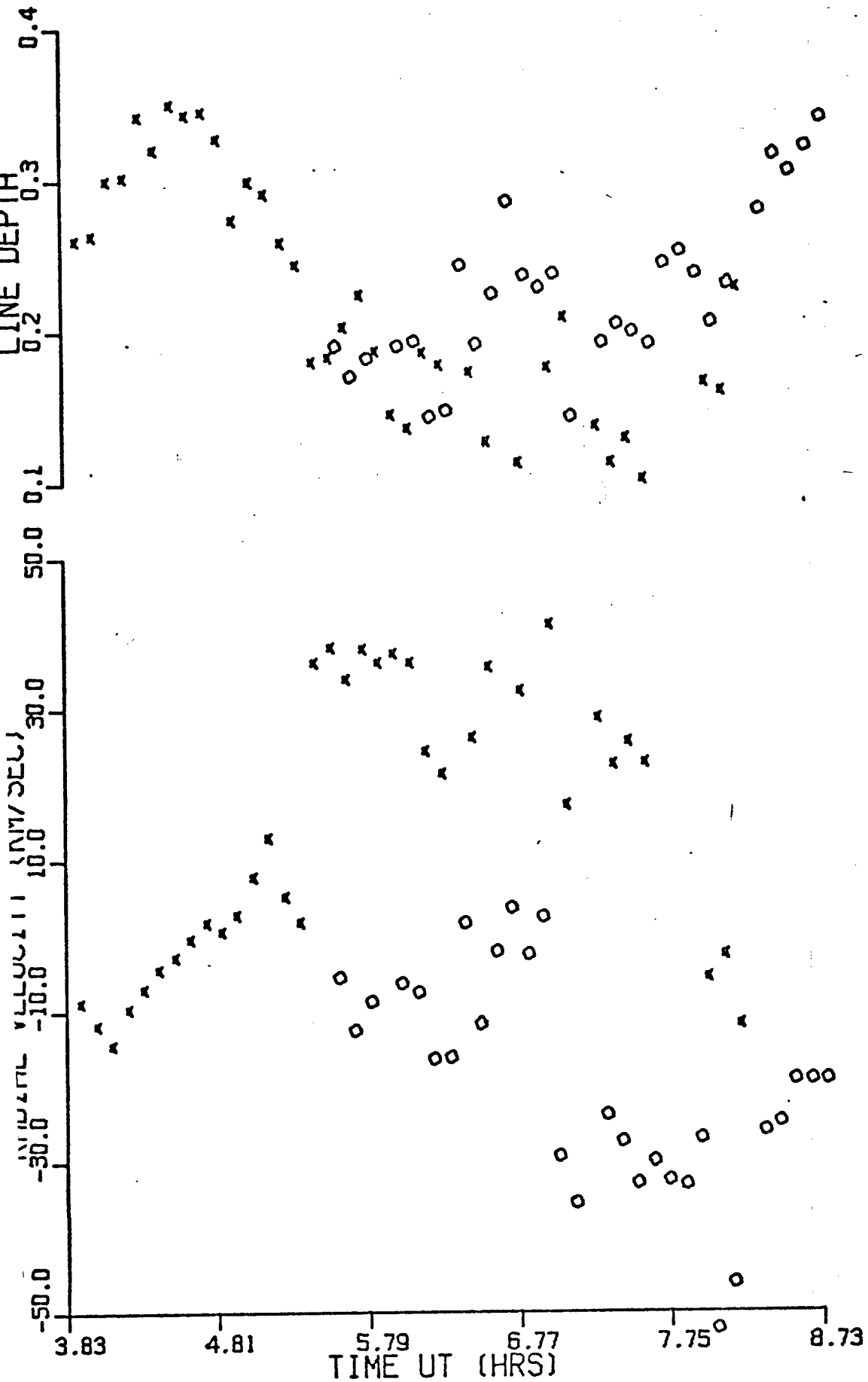

Figure 13(c). Radial velocity curve for Si III 4553 for Oct. 16.

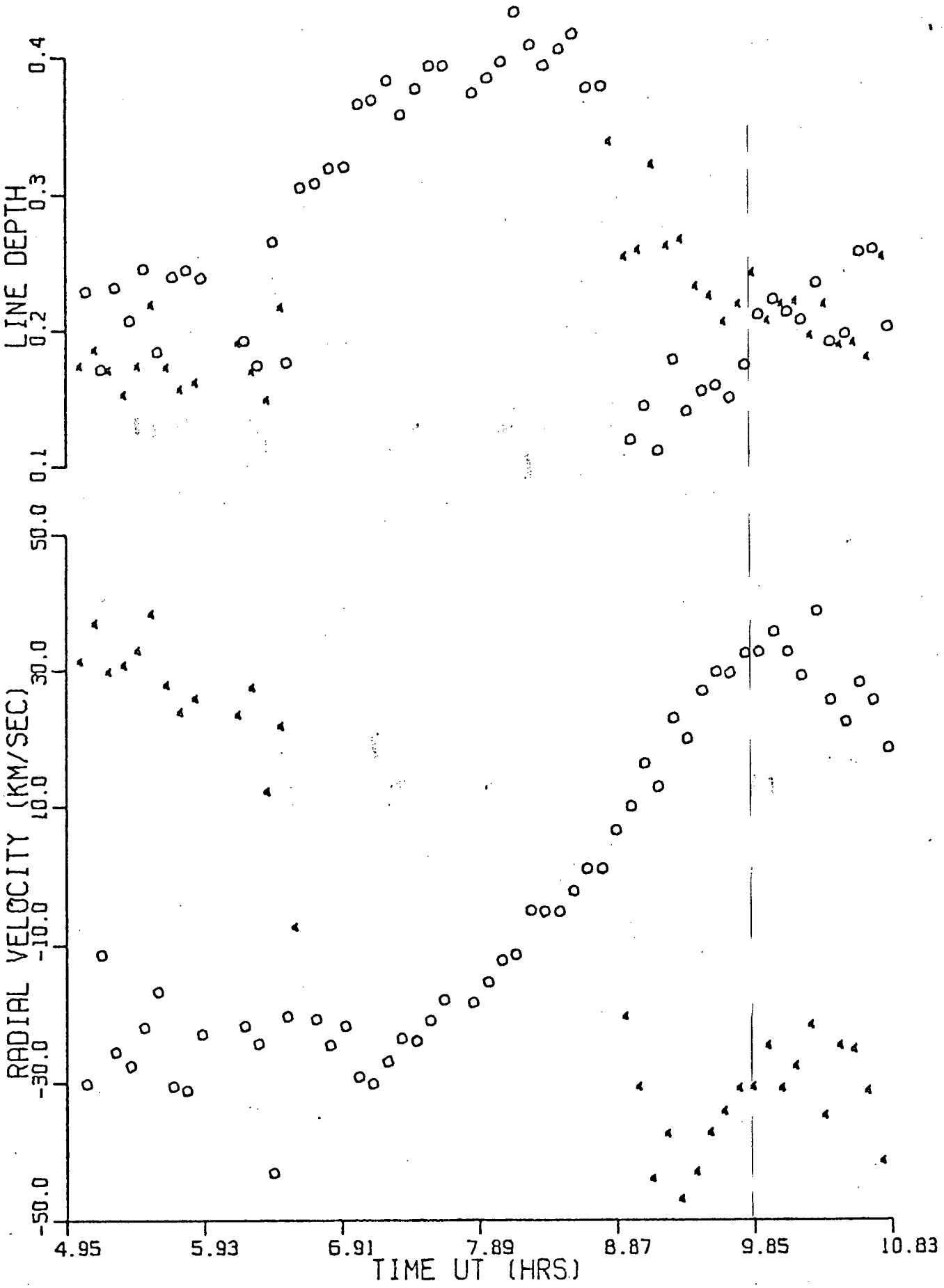

Figure 13(d). Radial velocity curve for Si III 4568 for Oct. 16.

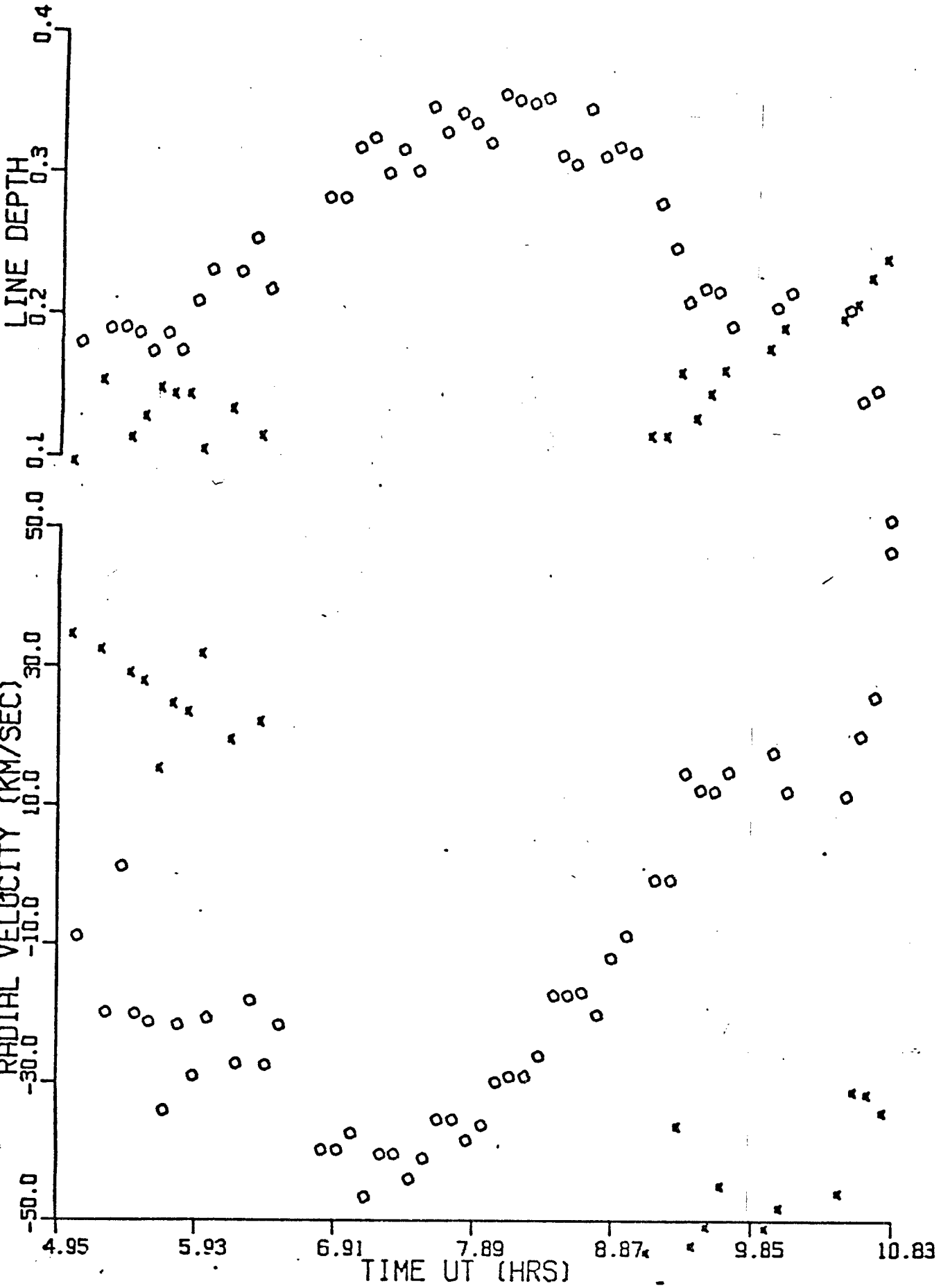

Figure 14(a). Gaussian fit to input data for block #10

Figure 5a. Si 111 4553

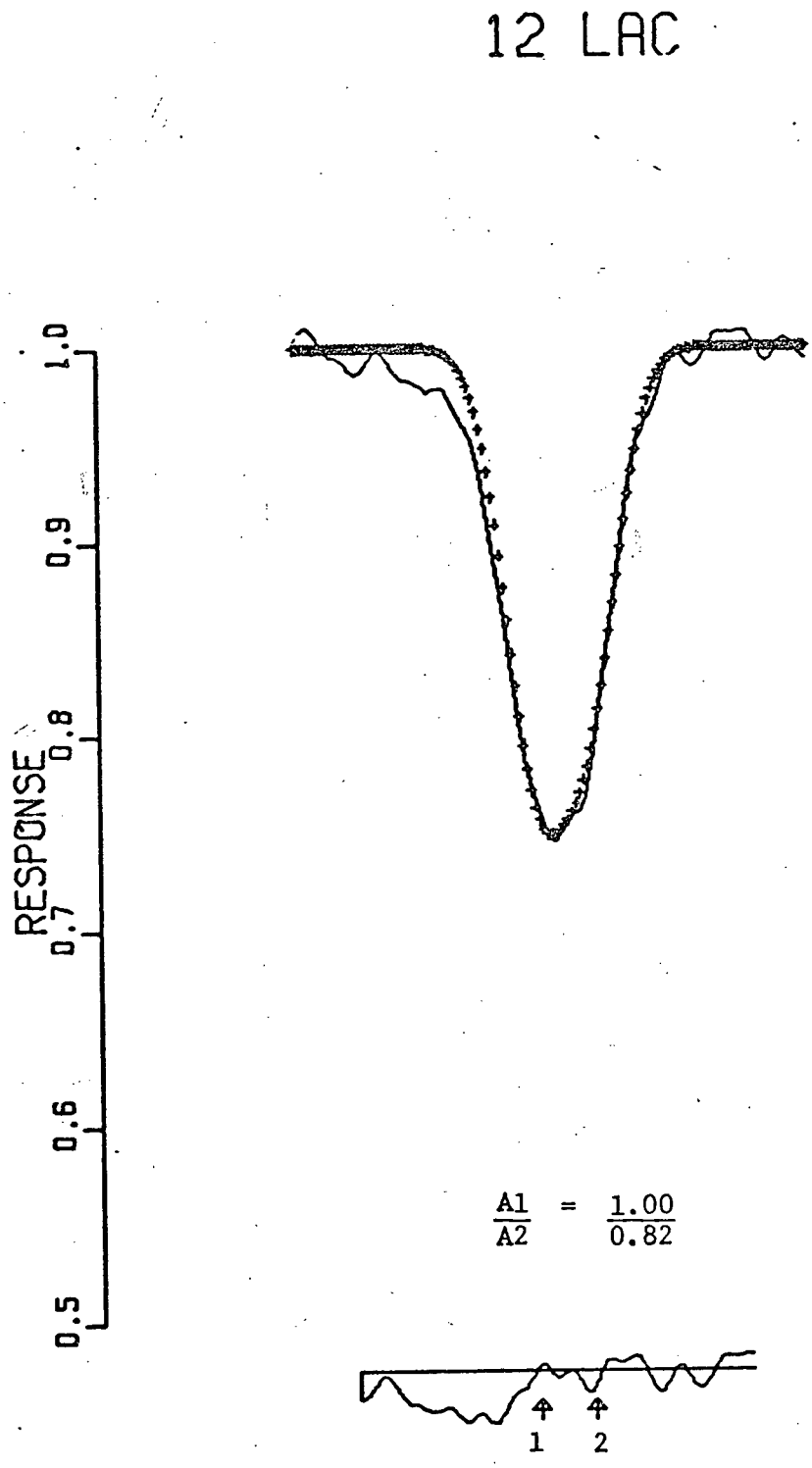

Figure 14(b). Gaussian fit to input data for block #10 of Figure 5b. Si 111 4553

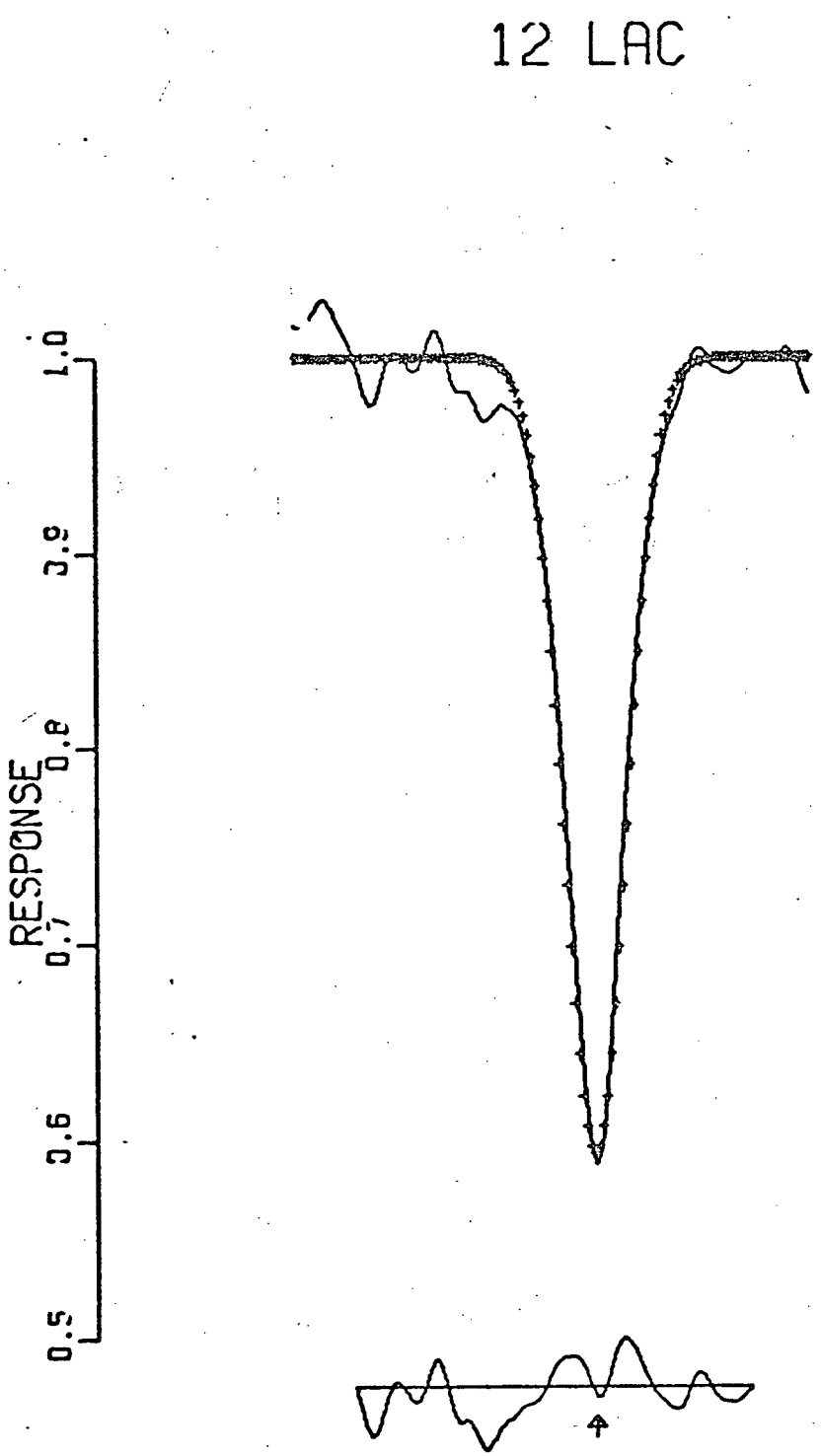

Figure 15(a). Radial velocity curve (centroid) for Si III 4553 for Oct. 15.

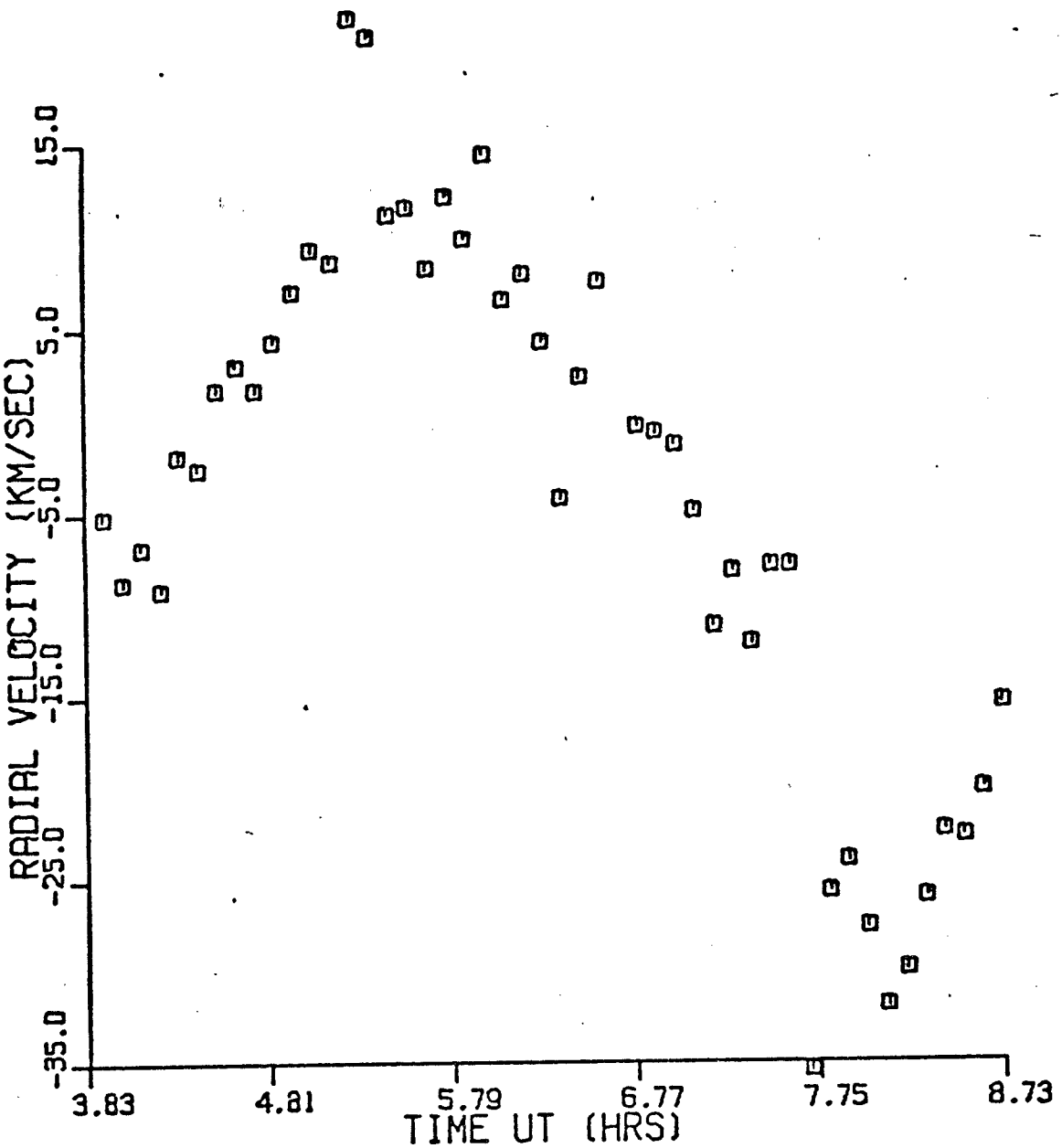

Figure 15(b). Radial velocity curve (centroid) for Si III 4553 for Oct. 16.

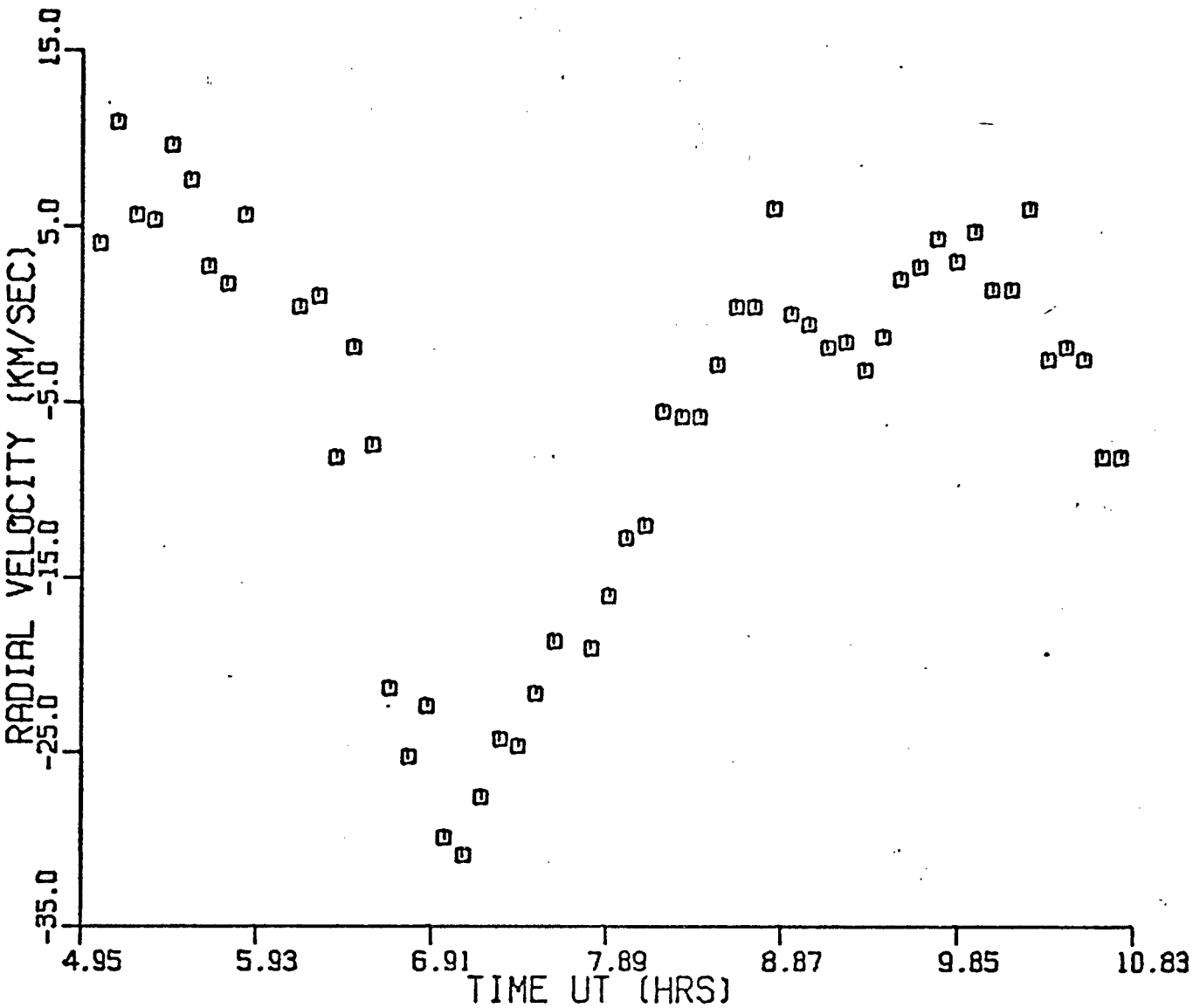

Discussion

Throughout this discussion I will use the velocity curve obtained by Bruce Goldberg (1973) for BW Vul for comparison. The two most prominent features of my observed velocity for 12 Lac are 1) its discontinuous nature and 2) evidence for a stillstand on the descending branch of the velocity curve. In BW Vul there is a period of ~40 minutes duration during which the radial velocity remains approximately constant. Because of the scatter in the data points it is not clear in the case of 12 Lac whether or not the velocity during 'stillstand' is really constant. Nevertheless as this feature is quite pronounced in BW Vul I will use the term 'stillstand' in my discussion.

In describing the various features of the velocity curves I will indicate in brackets [ ] which component I am referring to: x or o. Consider Figures 13(c) and 13(d):

1) The stillstand [o] first takes place at ~5 hrs U.T. The discontinuity preceding the stillstand results from the splitting of the line into two components.

2) There is evidence for a blue shift following stillstand [o] at ~6.5 hrs U.T. This effect is more obvious in Figure 13(d) for λ 4568. The 'flattening' of the velocity curve near the phase of maximum blue shift as observed in BW Vul is also quite evident in λ 4568. For λ 4568 the amplitude difference between maximum blue shift and the stillstand velocity is ~30 km/sec. For λ 4553 it is only half this amount. It is not clear from these observations whether this discrepency is intrinsic or

instrumental.

3) The rapid rise of one component [o] to maximum redshift is seen prior to a renewal of the cycle.

4) After the red-shifted component reaches a maximum velocity it seems to experience a blue shift before fading away. This is seen particularly in Figure 13(c) for [x] at $\simeq$ 6 hrs U.T. This effect is not seen in BW Vul, in fact the opposite occurs; it continues to be red-shifted. It is suspected that the blue shift is not real and that what really happens is that the first few points have been overcorrected for raster shift. This point is further explained in #6 below.

5) For this night we have more than one cycle of the pulsation and are able to see the discontinuity reappear (at $\simeq$9.5 hrs U.T.) as a component [x] develops having the stillstand velocity.

Consider Figures 13(a) and 13(b):

6) I might note that in Figure 13(a) the points at the beginning of observation at $\simeq$4 hrs. U.T. seem abnormally high (by $\simeq$10 km/sec). We are seeing just slightly more than one cycle of the pulsation and thus the velocities at the beginning of the cycle on the ascending branch should be the same (at least for consecutive cycles). The fiducial shift corrections were greater than 2 sample points only near the beginning of the observing run. In particular the correction for the first few blocks were on the order of 15 km/sec -ie. the uncorrected points were at $\simeq$ -25 km/sec. It is possible that the non-linear expansion of the camera reading beam might be more serious near

the start of observation on a particular object.

7) There seems to be evidence for a blue shift following stillstand [o] particularly in Figure 13(a) for λ 4553 at $\sim$-7.75 hrs as noted in point(2) for the other night's data.

8) The scatter in Figure 13(b) is very large.

A possible cause for the scatter in the radial velocity measurements is the profile shape assumed for one component. Perhaps the two components have different widths and/or the width of the components changes with time. The wavelength shifts determined by the deconvolution method would then be in error. In a few cases, the deconvolution technique yielded three components. This is most likely not a real physical situation but more a function of the profile shape assumed for the various components.

The line profile and radial velocity changes are directly correlated. Compare Figures 12 and 13. Consider Figures 12(a), 12(b), 13(a) and 13(b). At the beginning of the ascending branch of the velocity curve the lines are sharpest, deepest and essentially symmetrical. The deepest phase occurs at $\sim$-4 hrs. U.T. As the cycle progresses the lines become shallower and broader with an extended wing to the red. At $\sim$ 5.5 hrs. U.T. the lines begin to double as a component [o] develops having the stillstand velocity. This component increases in intensity while the redshifted component [x] fades away. During stillstand the lines become sharper and deeper again (shown very clearly in Figures 12(a) and 12(b) at $\sim$6.5 hrs. U.T.) but less

so than at the beginning of the ascending branch. During the blue shift following stillstand [o] there is an asymmetry showing an extended wing to the blue. The lines then get narrower and deeper prior to the renewal of the cycle. Much the same thing is seen for the data of October 16.

It is very interesting to compare Figures 13(a) and 15(a) and Figures 13(c) and 15(b). When the two components are of equal intensity, the velocities in Figure 15 are a straight average of the velocities for the separate components. As one component becomes stronger than the other, the resulting (centroid) velocity is weighted more towards the velocity of the stronger component. For Figure 13(a) the velocity amplitude is $\simeq$ 70 km/sec; for Figure 15(a) it is $\simeq$ 45 km/sec. The velocity amplitude determined from a curve showing the wavelength shifts from the centroid will thus be much less than the true value. There does not appear to be much evidence in Figures 15(a) and 15(b) for a stillstand on the descending branch of the velocity curve.

The whole question of the multiple periodicity of 12 Lac is very complex. Because of its importance I will present here a short summary of the period determinations in 12 Lac. In 1953 De Jager (De Jager, 1953) tried to explain the variability of the star by means of a sum of two independent oscillations with frequencies being not far from each other. His components with periods of 0.19308883 days(P1) and 0.197367 days(P2) give the beat period P=8.908 days. In consequence, one ought to expect

that the amplitudes of brightness and radial velocities, and the values of [O-C] calculated for maxima or minima of brightness and radial velocities from the period 0.19308883 or 0.197367 days should change according to the phase of the beat period. This did not occur, and in 1957 De Jager (De Jager, 1957) found the existence of the third oscillation in the star with a period of 0.15583 days. Rakosch (1960) confirmed the presence of the three independent oscillations but with slightly different values of the periods (0.19308997 days, 0.19737253 days and 0.15292 days). He also found a new period for colour index variations (0.118644 days). A large number of observations obtained during the "International Lacerta Weeks" compiled and published by De Jager (1963) were used by Barning (1963) for the determination of variability of 12 Lac. His result is four independent oscillations; two with previously known periods (0.19308883 days and 0.197358 days), and two additional ones with periods 0.182127 days and 25.85 days. The longest period found by Barning is probably not real because of the many uncertainties involved. Opolski and Ciurla (1961, 1962), Jerzykiewicz (1963) and Ciurla (1973) found that the short period (0.19308858 days) varies periodically with a period of 8.876 days. They suggest that the components of the light curve with the short periods P1 (0.19308883), P2 (0.197367) and P3 (0.15583) represent no more than a formal description of the observed variability of 12 Lac.

Any periods determined from previous radial velocity curves (such as Figures 15(a) and 15(b)) should be re-examined. The

velocity curve is clearly discontinuous and this splitting might influence any period determinations.

There have been a number of theoretical investigations undertaken towards explaining the line splitting at certain phases.

1) The double lines are formed in different parts of the star's disk (McNamara and Gebbie, 1961; Huang, 1955).

2) They arise from two layers, one above the other (Odgers, 1955; Goldberg, 1973).

3) They are the consequences of non-radial pulsation (Osaki, 1971).

As mentioned before, Huang (1955) found that the equivalent width in ν Sco did not vary throughout the cycle. He interpreted this to mean that the splitting of line profiles is due to macroscopic motion: the two streams must be moving in different parts of the star's disk instead of one above the other.

In (2) the motion is radial. The interpretation is based on the following picture: An atmosphere is ejected with high velocity which after travelling outwards for a time then falls back into the general stellar photosphere at high speed. For a time at the stillstand phase the stellar surface proper is visible and then another atmosphere is ejected, (Goldberg, 1973).

The paper by Heard et al (1976) mentions work by Watson and

Stanford that extends Osaki's work and shows that at moderate to large amplitude, non-radial pulsation can produce line splitting of the type observed in BW Vul and now seen in 12 Lac.

Both the non-radial and radial explanations offer a qualitative description of the line splitting. More work needs to be done to decide which is the correct interpretation.

Summary and Conclusions

The broadening of the line profiles at certain phases is seen to be due to the presence of two unresolved components. The discontinuity in the radial velocity curve preceding stillstand is due to the growth of a component at the stillstand velocity. The line splitting and consequent discontinuous velocity curve should prove a strong incentive for more theoretical and observational investigations.

There is one very significant difference between 12 Lac and BW Vul. BW Vul appears to be singly periodic. The line profile and radial velocity changes repeat from cycle to cycle. The amplitude of the velocity curve remains constant.

12 Lac has (supposedly) a number of periods. The radial velocity amplitude is variable. On Oct. 15 the total velocity amplitude is ~70 km/sec; on Oct. 16 it is ~ 80 km/sec. The radial velocity curves and line profile variations do not repeat from cycle to cycle. On Oct. 16 the velocity amplitude separation at stillstand between the components is much larger than that on Oct. 15. More observations should be undertaken to accurately determine the period(s) of radial velocity amplitude variation. In choosing between any radial or non-radial theory this difference in velocity amplitude must be considered.

An interesting side result of this investigation is that

though the velocity amplitude is greater on Oct. 16 resulting in broader lines, the line profiles at the sharp line phase (one component present) have the same width for both nights. The same Gaussian profile gave a satisfactory fit for both sets of data.

Another important result is that the amplitude of the radial velocity curve is much greater than what was previously obtained. Heard et al (1976) find that the amplitude of the velocity varies slightly from 43 km/sec to 35 km/sec. The splitting of the components shows that the true radial velocity amplitude is about twice that obtained previously.

With regards to 12 Lac it is proposed that a number of things be done:

1) As summarized in the Discussion section there has been a great amount of work done through the years, on examining the light and radial velocity curves for multiple periodicity. Any researcher who attempts to use these periods in a model explaining the line profile and radial velocity variations should keep in mind the line splitting and conseguent discontinuous velocity curve.

2) More observations should be undertaken at this high spectral and time resolution. If one had observations of a large number of cycles, one would have a clearer idea of whether the scatter (particularly at stillstand) was intrinsic or instrumental.

3) Lines of other elements should be observed; in particular He Iλ4471 and the hydrogen lines. Two possible motivations for

this line of investigation are: 1) the presence of emission lines in some β Cephei stars (Underhill, 1966) and 2) Struve and Zebergs (1955) have shown that the hydrogen lines lag on the descending branch of the velocity curve.

Observations of other β Cephei stars should most definitely be obtained at high spectral and time resolution in order tc see if any line splitting occurs. A complete list of the 18 classical β Cephei stars is given in Underhill (1966). All of the stars are very bright (>6th magnitude) and their periods are short (<6 hours). A complete cycle (or more) of the pulsation could be observed in one night of observation.

Bibliography

Adams, W.S. 1912, Ap.J., 35 , 179.

Aizenman, M.L., Cox, J.P. and Lesh, J.R. 1975, Ap.J., 197 , 399.

Barning, F.J.M. 1962, B.A.N., 17 , 22.

Beres, K. 1966, Acta Astr., 16 , 161.

Bevington, P.R. 1969, Data Reduction and Error Analysis for the Physical Sciences (McGraw-Hill).

Buchholz, V.L., Walker, G.A.H., Auman, J.R. and Isherwood, B.C. 1973, in Astronomical Observations with Television-type Sensors, ed. J.W. Glaspey and G.A.H. Walker (Univ. of British Columbia, Inst. of Astronomy and Space Science), p. 199.

Ciurla, T. 1973, Acta Astr., 23 , 367.

Clayton, R.W. and Ulrych, T.J. 1976, in preparation.

Cox, J.P. 1974, Reports on Progress in Physics, 37 , 563.

De Jager, C. 1953, B.A.N., 12 , 81.

----------. 1957, B.A.N., 13 , 149.

----------. 1963, B.A.N., 17 , 1.

Fahlman, G.G. and Glaspey, J.W. 1973, in Astronomical Observations with Television-type Sensors, ed. J.W. Glaspey and G.A.H. Walker (Univ. of British Columbia, Inst. of Astronomy and Space Science), p. 347.

Fath, E.A. 1938, Pop. Astr., 46 , 241.

Glaspey, J.W., Eilek, J.A., Fahlman, G.G. and Auman, J.R. 1976, Ap.J., 203 , 335.

Goldberg, B.A. 1973, PhD. Thesis, University of British Columbia.

Grabowski, B. 1966, Acta Astr., 16 , 309.

----------. 1969, Acta Astr., 19 , 23.

Heard, J.F., Hurkens, R.J., Percy, J.R. and Porco, M. 1976, to be published.

Hill, G. 1967, Ap.J. Suppl., 14 , 263.

Huang, S.S. 1955, P.A.S.P., 67 , 22.

Jerzykiewicz, M. 1963, Acta Astr., 13 , 253.

Kanasewich, E.R. 1973, Time Sequence Analysis in Geophysics (The University of Alberta Press).

Lesh, M.I. and Aizenman, J.R. 1973a, Astron. and Astrophys., 22 , 229.

----------. 1973b, Astron. and Astrophys., 26 , 1.

McNamara, D.H. and Gebbie, K.B. 1961, P.A.S.P., 73 , 56.

Odgers, G.J. 1955, Publ. D.A.O., 10 , No. 9, 215.

Opolski, A. and Ciurla, T. 1961, Acta Astr., 11 , 231.

----------. 1962, Acta Astr., 12 , 269.

Opolski, A. and Grabowski, B. 1966, 16 , 303.

Osaki, Y. 1971, Pub. Astr. Soc. Japan, 23 , 485.

--------. 1974, Ap.J., 189 , 469.

Percy, J.R. 1967, J.R.A.S.C., 61 , 117.

Rakosch, K. 1960, A.N., 285, 211.

Richardson, E.H. 1973, in Astronomical Observations with Television-type Sensors, ed. J.W. Glaspey and G.A.H. Walker (Univ. of British Columbia, Inst. of Astronomy and Space Science), p. 433.

Sato, N. 1973, Astrophys. and Space Sci., 24 , 215.

Struve, O. 1951, Ap.J., 113 , 589.

---------. 1955, P.A.S.P., 67 , 135.

Struve, O. and Zebergs, V. 1955, Ap.J., 122 , 134.

Thompson, I.B. 1974, M.Sc. Thesis, University of British Columbia.

Underhill, A.P. 1966, The Early Type Stars (Dordrecht, Holland: D. Reidel Co.).

Walker, G.A.H., Auman, J.R., Buchholz, V.L., Goldberg, B.A., Gower, A.C., Isherwood, B.C., Knight, R. and Wright, D. 1972, Advances in Electronics and Electron Physics, 33B , 819.

Watson, R.D. 1972, Ap.J. Suppl., 24 , 167.

Appendix A

In any method of deconvolution one of the requirements is that you have a knowledge of the profile shape of the components. A Gaussian profile which gave the best fit to a data profile at the sharpest line phase was used. The widths of the two components are assumed to be equal; as well the assumption is made that the components though they decrease/increase in intensity, still retain the same profile shape throughout the cycle.

The new method is essentially this:

1) The data is treated as a power spectrum.
2) The autocovariance function is obtained from this 'power spectrum'.
3) The autocovariance is weighted by the amplitude spectrum of the assumed profile shape for one component.
4) The Maximum Entropy Power spectrum is then obtained where the autocorrelation coefficients computed above are used directly to obtain the prediction-error coefficients.

One of the drawbacks of conventional deconvolution techniques which employ a smoothing of the autocorrelation function by a time domain window or a smoothing of the squared magnitude of the Fourier Transform is that they do not design a window which is based on the true spectrum. This leads to leakage of power through side lobes in the transfer function and also puts a limit on the resolution. The Maximum Entropy Method

estimator retains all the estimated lags without smoothing and uses Weiner optimum filter theory to design a prediction filter which will whiten the input power spectrum. From the whitened output power and the response of the prediction filter it is possible to compute the input power spectrum (Kanasewich, 1969).

The accuracy of the positions depends on the number of sinusoids in the autocorrelation function. It is estimated that the positions are determined to $\pm$ 1 sample point. Some results are shown in the following Figures. The data must be inverted to be considered as a power spectrum which accounts for the pseudo-emission line spectrum. The bottom graph is a plot of the input data. The middle plot shows the deconvolved spectrum. The top graph is the reconstructed profile. This is obtained by convolving the deconvolved spectrum with the assumed profile shape for one component. The data blocks considered are those of Figures 5(a) and 5(b) for λ 4553.

Figure A.1 Deconvolved spectrum for block # 3 of Figure 5a.

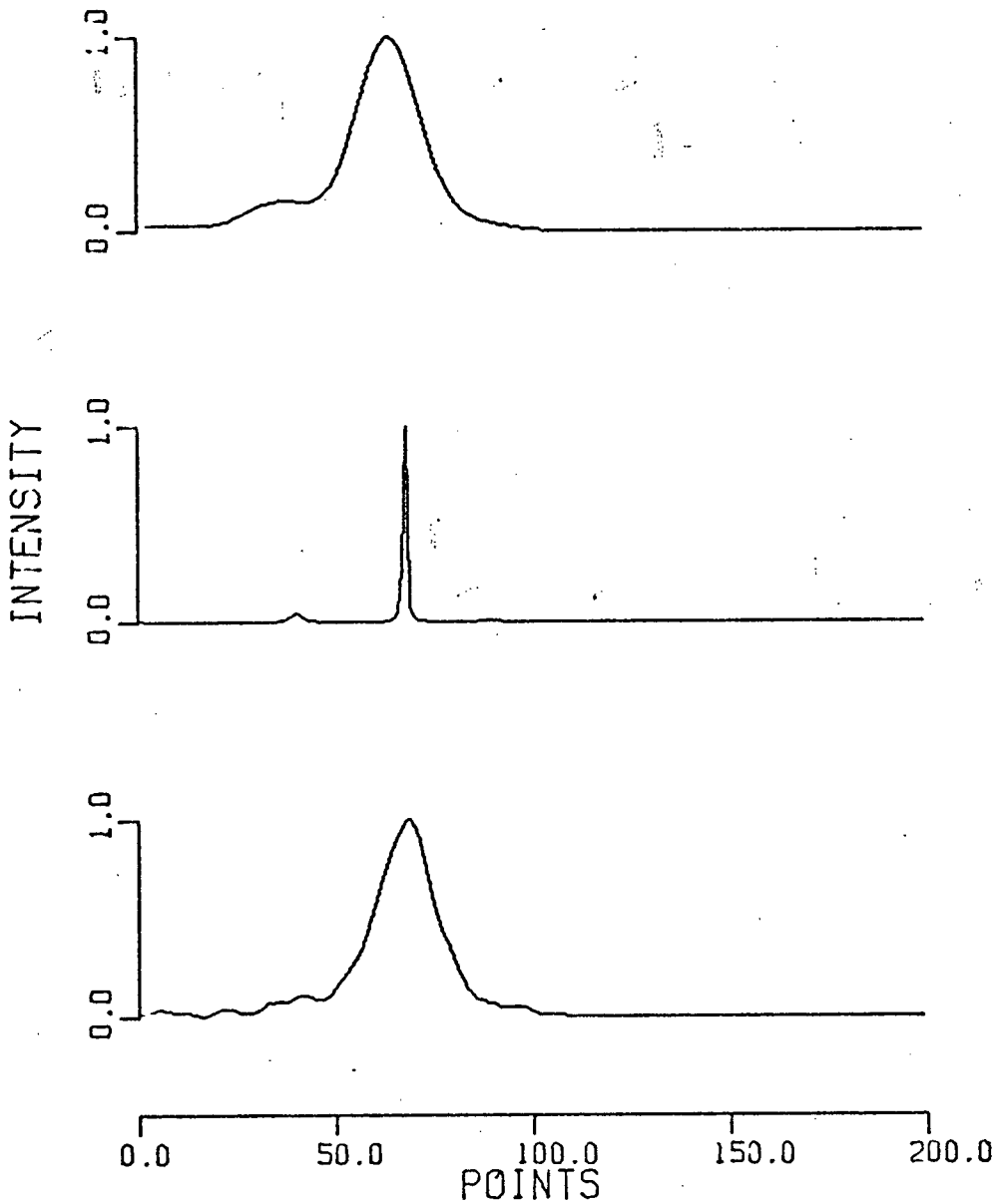

Figure A.2 Deconvolved spectrum for block # 9 of Figure 5a.

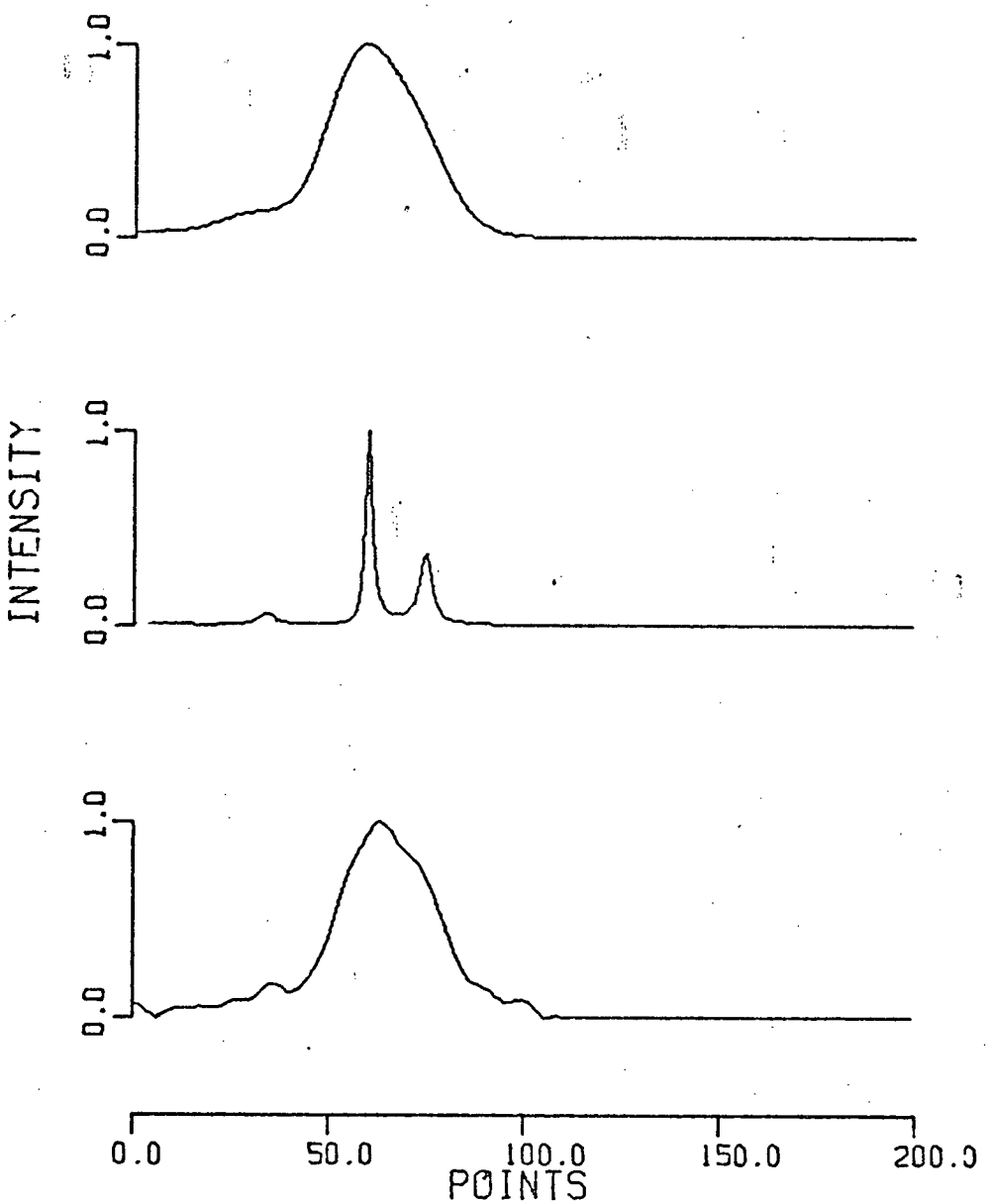

Figure A.3 Deconvolved spectrum for block # 10 of Figure 5a.

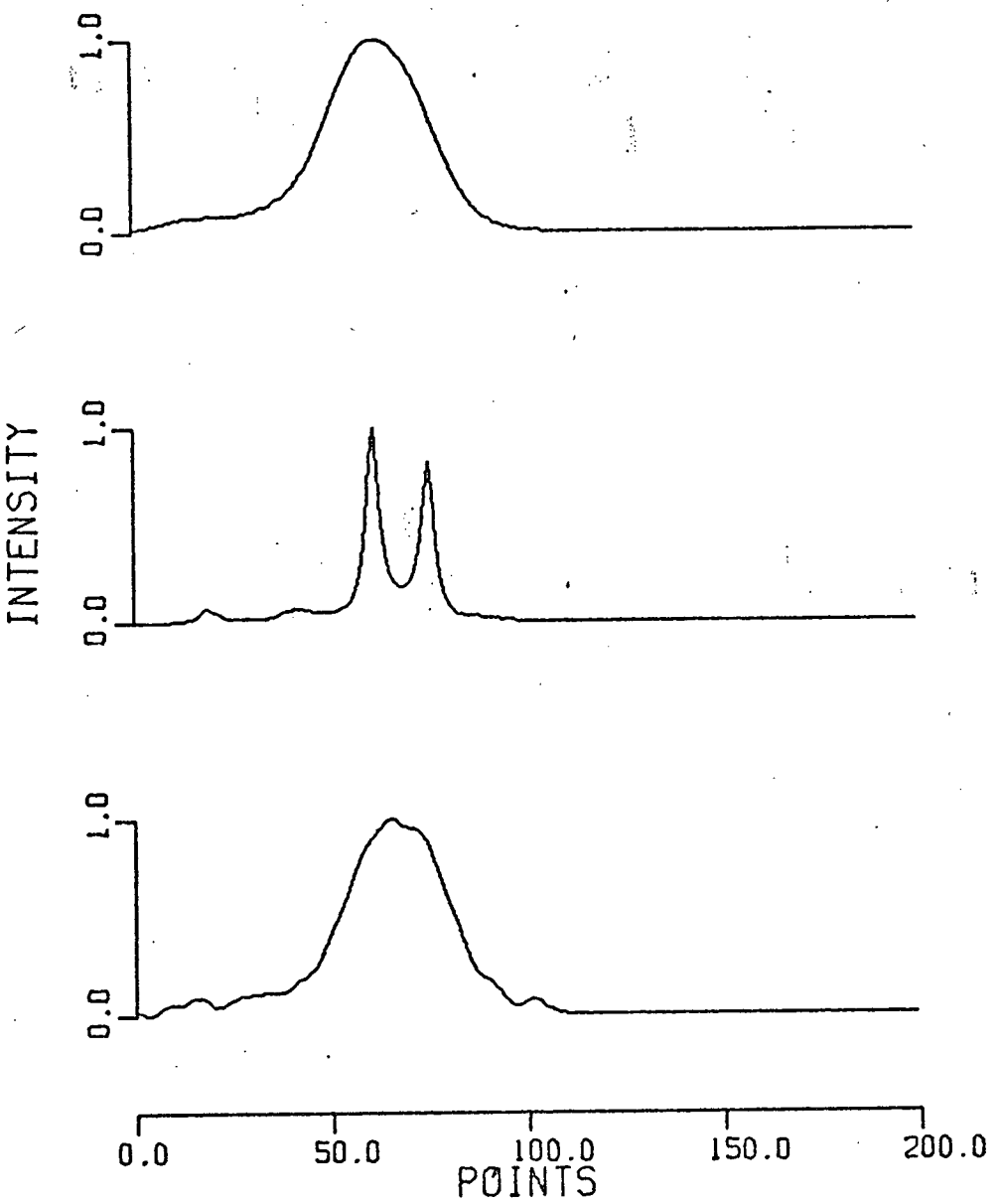

Figure A.4 Deconvolved spectrum for block # 12 of Figure 5a.

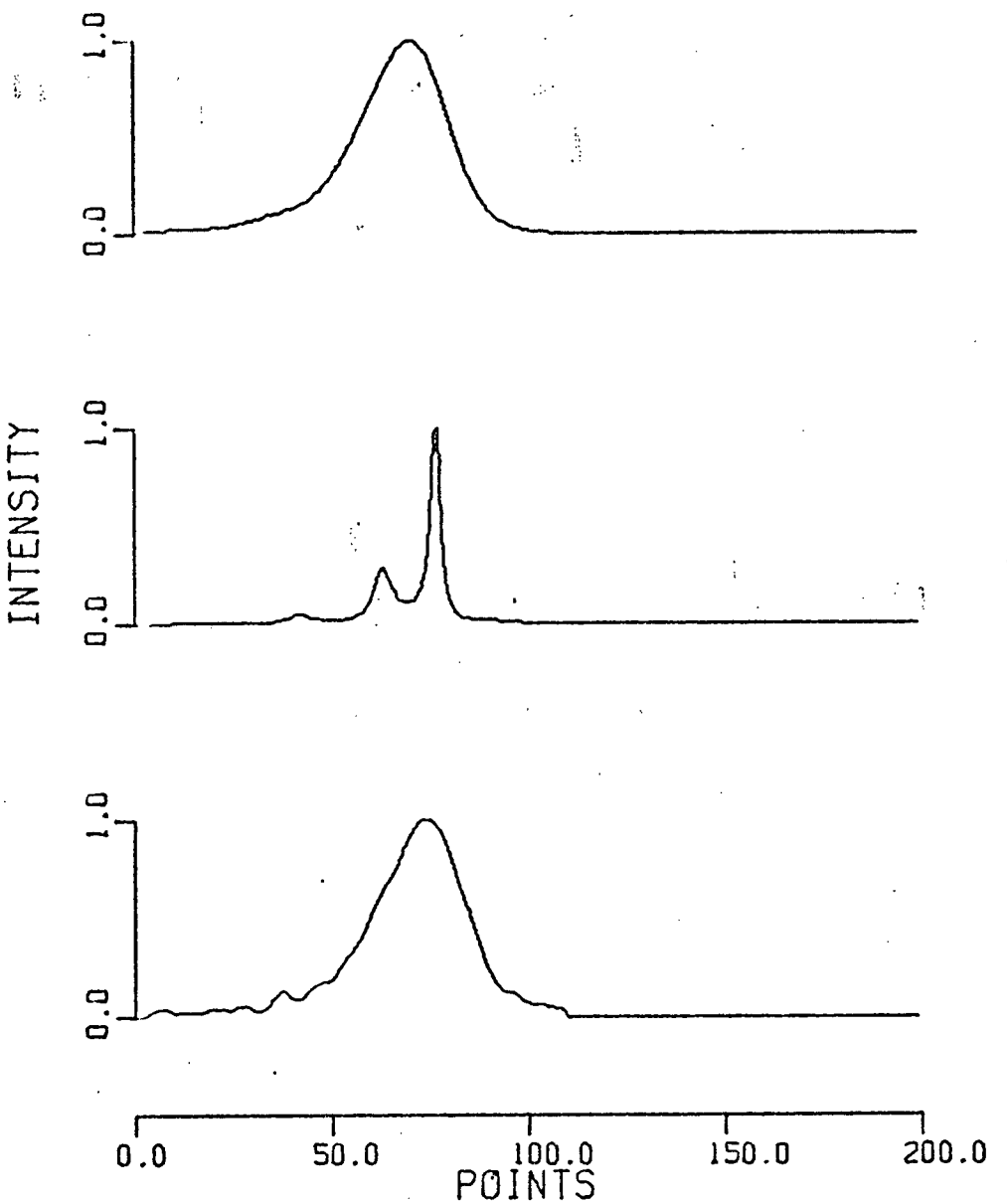

Figure A.5 Deconvolved spectrum for block # 1 of Figure 5b.

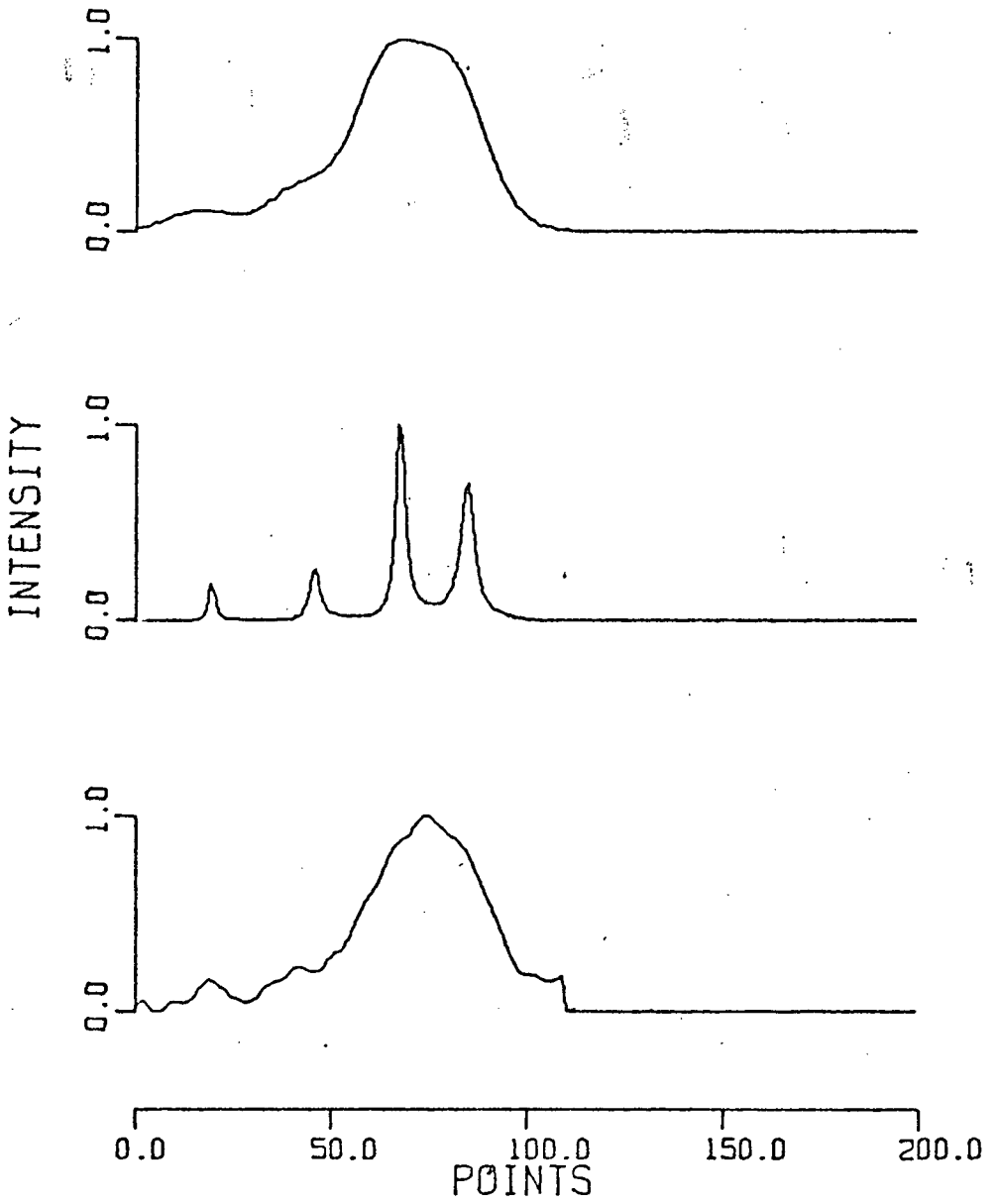

Figure A.6 Deconvolved spectrum for block # 3 of Figure 5b.

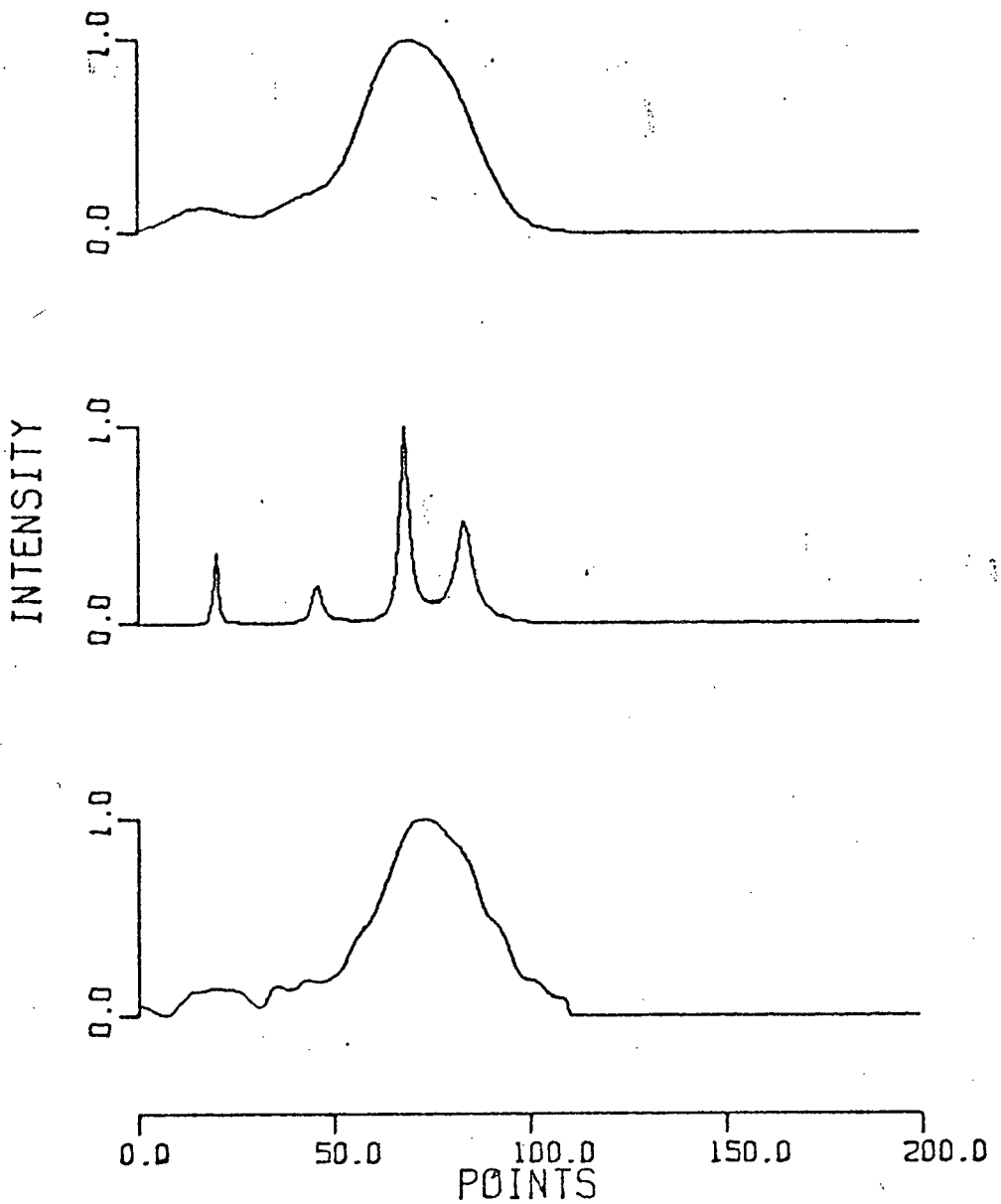

Figure A.7 Deconvolved spectrum for block # 5 of Figure 5b.

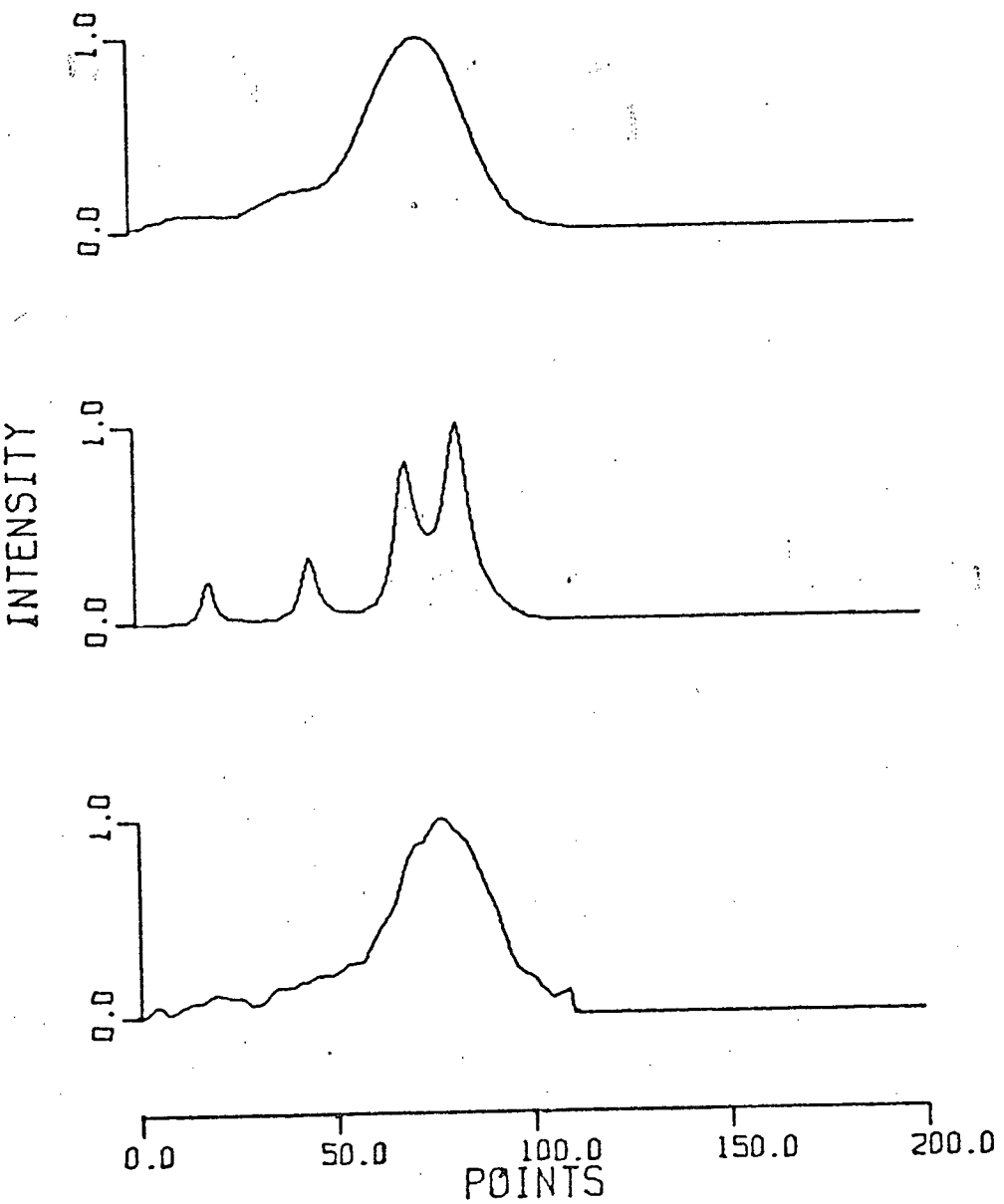

Figure A.8 Deconvolved spectrum for block # 13 of Figure 5b.

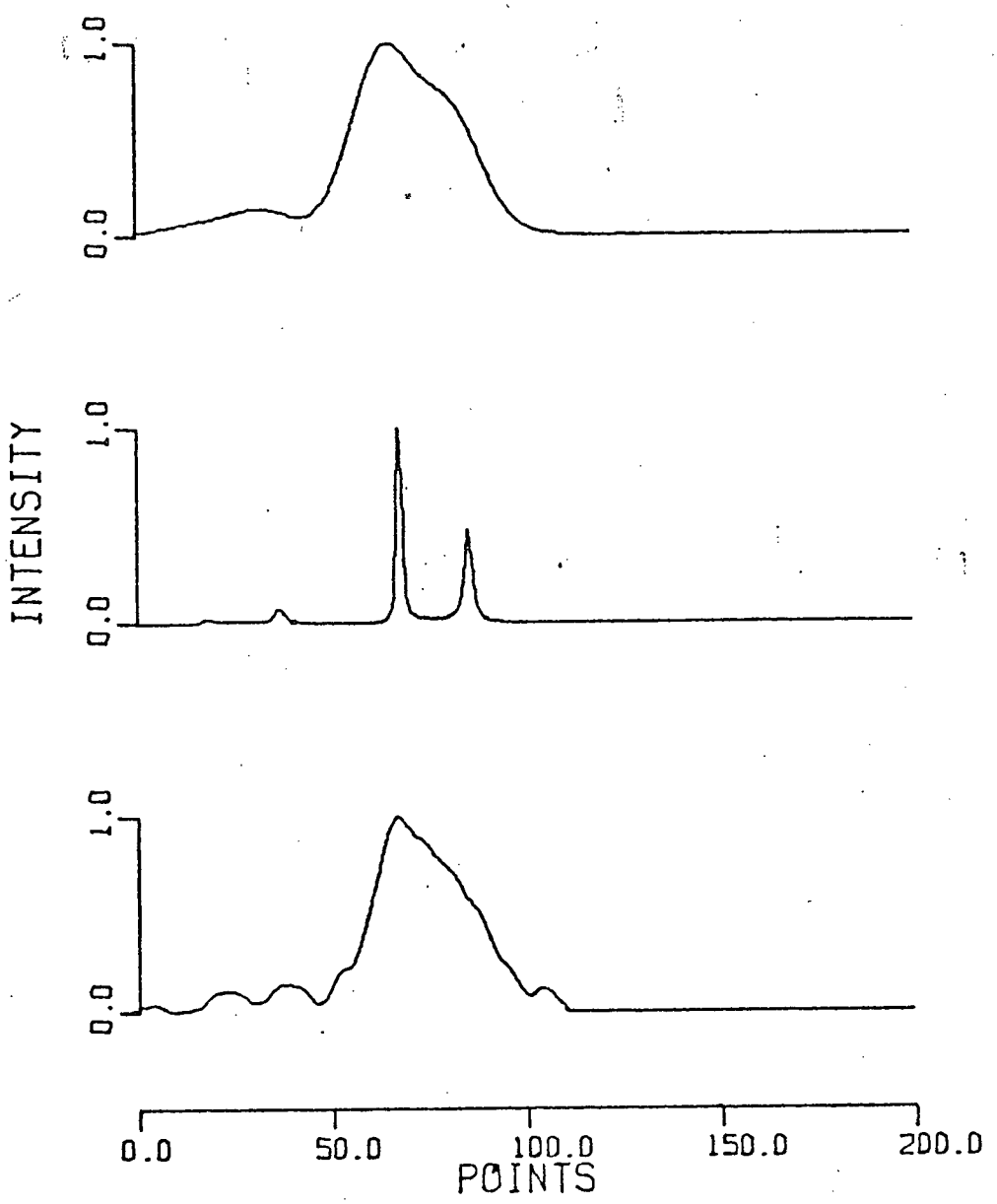

Figure A.9 Deconvolved spectrum for block # 14 of Figure 5b.

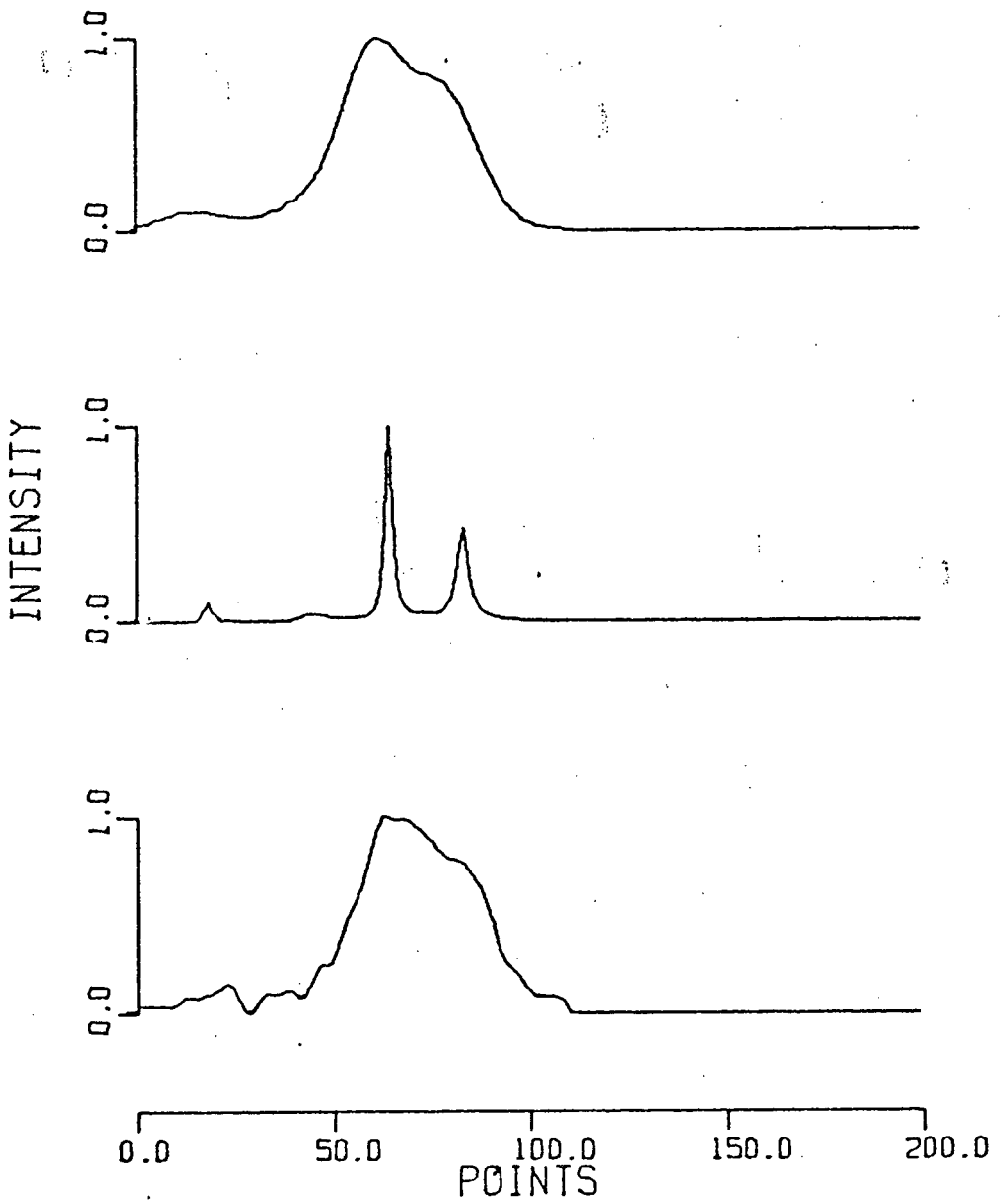

Figure A.10 Deconvolved spectrum for block # 15 of Figure 5b.